

**Optical Brighteners: PARAFAC analyses of EEM  
Fluorescence data for the conceptual design of field  
instrumentation and methods.**

**FINAL REPORT**



SUBMITTED TO:  
CHRISTOPHER J. ANASTASIOU  
SPECIAL PROJECTS  
FLORIDA DEPARTMENT OF ENVIRONMENTAL PROTECTION  
13051 N. TELECOM PARKWAY,  
TEMPLE TERRACE, FL 33637-0926 USA  
PHONE: (813) 632-7600 ext 285  
SUNCOM: 514-9155

SUBMITTED BY:  
L.K. DIXON  
MOTE MARINE LABORATORY  
1600 KEN THOMPSON PARKWAY  
SARASOTA, FLORIDA 34236  
(941) 388-4441

February 16, 2009

Mote Marine Laboratory Technical Report No. 1316  
*This document is printed on recycled paper*

# TABLE OF CONTENTS

<b>Acknowledgements</b> .....	<i>ii</i>
<b>Project Funding</b> .....	<i>ii</i>
<b>List of Figures</b> .....	<i>iii</i>
<b>List of Tables</b> .....	<i>v</i>
<b>Introduction</b> .....	<b>1</b>
<b>Background</b> .....	<b>2</b>
<b>Methods</b> .....	<b>2</b>
<i>Site Selection</i> .....	2
<i>Sampling</i> .....	2
<i>Calculation of Representative OSTDS Effluent</i> .....	3
<i>Detergents</i> .....	4
<i>Dilution Matrix</i> .....	4
<i>EEM and Absorption Analyses</i> .....	5
<i>EEM Post processing</i> .....	7
<i>PARAFAC Modeling</i> .....	8
<i>Optimized Field Method</i> .....	9
<b>Results</b> .....	<b>10</b>
<i>Absorption Correction</i> .....	10
<i>EEM Methodology Refinements</i> .....	13
<i>Detergents</i> .....	17
<i>Optimum PARAFAC Model</i> .....	18
<i>Conceptual Design of Field Instrumentation – Method 1</i> .....	32
<i>Conceptual Design of Field Instrumentation – Method 2</i> .....	36
<i>Application of Field Methods to EEM Data</i> .....	42
<i>Remote Sensing Considerations</i> .....	49
<b>Summary</b> .....	<b>51</b>
<b>Literature Cited</b> .....	<b>54</b>

## APPENDICES

<b>Appendix A</b>	Location of Ambient Samples
<b>Appendix B</b>	Project Data Quality Objectives
<b>Appendix C1</b>	Factor Loadings from PARAFAC Modeling for All Samples
<b>Appendix C2</b>	PF6 Factor Loads Converted to Approximate %OSTDS Effluent
<b>Appendix D</b>	Results of Proposed Filed Methods, Single and Dual Wave Length

### *Acknowledgements*

This project would not have been possible without the extensive contributions of Camia Buehler. In addition we would like to thank Katherine Lansdowne, Maya Dobrzeniecka, Dr. Ari Nissanka, Rusty Holmes, Jon Perry, Chris Anastasiou, Sarasota County (Water Quality Planning and Regulatory), and the owners of the WWTP, laundries, and OSTDS systems who graciously allowed access during both projects.

### *Project Funding*

This project and the preparation of this report was funded by the Clean Water Act Section 104(b)(3) (CFDA 66.475) Gulf of Mexico Program Grant from the U.S. Environmental Protection Agency (US EPA Gulf of Mexico Program Federal Grant Number MX96423005-4) through a contract with the Southwest District of the Florida Department of Environmental Protection. The total cost of the project was \$60,000 of which \$60,000 was provided by the US EPA.

## List of Figures

<b>Figure 1.</b>	Uncorrected and absorption corrected fluorescence data, 350/440 ex/em, together with the optical density (O.D.) of the sample dilution.....	11
<b>Figure 2.</b>	Noise reduction achieved for an undiluted sample with absorption correction (blue) relative to a sample diluted until absorption correction was unnecessary (red) but was then multiplied by the dilution factor.....	12
<b>Figure 3.</b>	Absorption correction factors applied to raw fluorescence data for an undiluted sample (upper) and a 1:20 dilution of the same sample. ....	12
<b>Figure 4.</b>	Dilution series of a sample corrected for dilution, but not absorption (upper), and corrected for dilution and absorption (lower). Dilutions were undiluted (heavy blue), 1:2 (cyan), 1:4 (green), 1:10 (red), and 1:20 (magenta). ....	13
<b>Figure 5.</b>	Spike recoveries of added detergent, relative to detergent fluorescence in deionized water, as a function of fluorescence amplitude at 350/440 ex/em. Note decline at fluorescence above 150-200 QSRF. ....	14
<b>Figure 6.</b>	Spike recoveries of added detergent, relative to detergent fluorescence in deionized water, as a function of turbidity. Maximum turbidity was 150 NTU. ....	14
<b>Figure 7.</b>	Dilution series of a turbid sample both with and without centrifugation for removal of particulates. Reducing turbidity allowed undiluted sample to produce acceptable values without dilution.....	16
<b>Figure 8.</b>	Filters capsules used to prefilter OSTDS samples for CDOM absorption determination illustrating the range in particulate color. ....	16
<b>Figure 9.</b>	Fluorescent EEMs of detergent mixture and selected detergents used as spiking solutions during analyses of OB recovery from various sample matrices. Left panels are of low excitation wavelengths and right panels are of higher excitation to capture amplitude differences between fluorescence regions.....	17
<b>Figure 10.</b>	Fluorescent EEMs of detergent mixture and selected detergents used as spiking solutions during analyses of OB recovery from various sample matrices. Left panels are of low excitation wavelengths and right panels are of higher excitation to capture amplitude differences between fluorescence regions.....	18
<b>Figure 11.</b>	Final PARAFAC model determined from 181 normalized initiating data of ambient samples, OSTDS, WWTP, laundries, and detergents. Spiked samples were not included in initiating data.....	19
<b>Figure 12.</b>	Spilt half analyses results in which 8 factor models were developed from random halves of initiating data. Agreement between first group (line) and second group(dotted) in both excitation (blue) and emission (red) modes indicate a robust model.....	20
<b>Figure 13.</b>	Spectral factors identified through PARAFAC modeling. Modeled range was 230-390 nm excitation and 272-600 nm emission.....	22
<b>Figure 14.</b>	Spike recovery of factor loads in matrix samples relative to loads in deionized water. No loading of PF6 and PF8 was present for Detergent I and so no spike recovery was calculated (circled areas).....	24

<b>Figure 15.</b>	Correlation of factor loads for PF2, PF6, and PF8 with CDOM absorption ( $a_{300}$ ) indicating PF2 exhibits a fluorescent response to CDOM absorption in addition to detergents. Ambient samples only.....	25
<b>Figure 16.</b>	Correlation of factor loads for PF2, PF6, and PF8 with CDOM absorption ( $a_{300}$ ) indicating PF2 exhibits a fluorescent response to CDOM absorption in addition to detergents. Ambient and OB source samples. ....	26
<b>Figure 17.</b>	Correlation of PF1 loads with absorption coefficients ( $a_{300}$ ) for ambient and OB source samples.....	28
<b>Figure 18.</b>	Correlation of PF1 loads with absorption coefficients ( $a_{300}$ ) for ambient samples illustrating some regional differences in the fluorescent portion of the CDOM pool. ....	28
<b>Figure 19.</b>	Distribution of PARAFAC factor loads, PF1 through PF8, by sample category.....	29
<b>Figure 20.</b>	Factor loads of PF6 and PF8 by sample category, at two different scales.....	30
<b>Figure 21.</b>	Factor loads of PF6 and PF8 by region for ambient samples, at two different scales. ....	31
<b>Figure 22.</b>	Overlap of the emission spectra of PARAFAC factors PF6 (red) and PF4 (blue). Arrows indicate a region of maximal response of PF6 with reduced influence of PF4. ....	33
<b>Figure 23.</b>	Corrected fluorescence emission spectra from 235 nm excitation of a Detergent A at 50% “typical” OSTDS (red dotted), moderate CDOM sample (blue), and sample spikes at 25% (green), and 50% “typical” OSTDS (red). ....	34
<b>Figure 24.</b>	Modeled PF6 factor loads as a function of fluorescence, 230/286 ex/em, both uncorrected and corrected for absorption, for ambient, source, and spiked samples. ....	34
<b>Figure 25.</b>	Compiled $r^2$ values of absorption coefficients at 250 nm ( $a_{250}$ ) as a function of fluorescence at individual wavelength pairs. Ambient samples only.....	35
<b>Figure 26.</b>	Absorption of ambient samples as a function of fluorescence at the most highly correlated ex/em wavelength pair. ....	35
<b>Figure 27.</b>	Correspondence of modeled and observed absorption coefficients at 300nm ( $a_{300}$ ) for all samples, using measured $a_{250}$ , a mean spectral slope of 0.0158, and a reference wavelength of 250nm. ....	37
<b>Figure 28.</b>	Examples of a fixed amount of OB (red) added to samples with varying CDOM (blue) to create a combined spectra (green). Arrows A and C are CDOM fluorescence, arrows B and D are fluorescence due to OB. Spectra are constructed from Gaussian functions for illustration.....	39
<b>Figure 29.</b>	Overlap of the emission spectra of PARAFAC factors PF1 (red) and PF2 (blue). Arrows indicate a region of maximal response of PF1 with reduced influence of PF2. ....	40
<b>Figure 30.</b>	Regions of excitation and emission for the dual wavelength method previously used (440 and 550nm, hatched bars) and the proposed method based on PARAFAC factor emission spectra (410 and 550 nm, gray bars). Regions A-primary Rayleigh, B-water Raman, and C-secondary Rayleigh. ....	40

<b>Figure 31.</b>	Relationship of raw and absorption corrected simple fluorescence ratios for 440/550 and 410/550 emissions. Slopes near unity indicate absorption correction can be neglected for the simple ratio approach. ....	41
<b>Figure 33.</b>	PARAFAC modeled PF6 loads as a function of simulated field data with 230-240 nm excitation, and an emission filter centered at 284 nm. Ambient samples (blue open circles); OB sources (green squares); and all samples including spikes (red points). At two different scales.....	43
<b>Figure 32.</b>	Relative intensity of deuterium lamp (blue), mercury vapor lamp (red), and bandpass of an example emission filters at 250 nm (green) used in simulation of field data from EEM data. ....	44
<b>Figure 34.</b>	Spike recovery from synthesized field data (230-240 / 284 ex/em) relative to fluorescence in deionized water. The UV peak was absent in Detergent I and so no spike recovery was calculated (circled area). ....	44
<b>Figure 35.</b>	Raw fluorescence at 550 and 410 nm as a function of absorption coefficient ( $a_{450}$ ). Ambient samples (blue open circles); OB sources (green squares); and spiked samples (red points).....	45
<b>Figure 36.</b>	OB computed with the corrected ratio method from 410/550 nm fluorescence as a function of absorption coefficient ( $a_{450}$ ). Ambient samples (blue open circles); OB sources (green squares); and spiked samples (red points). ....	46
<b>Figure 37.</b>	Spike recovery from synthesized field data using the corrected ratio method for 300-350 nm excitation and 410, 550 nm emissions, relative to fluorescence in deionized water.....	46
<b>Figure 38.</b>	Computed OB, as % typical OSTDS effluent, by the various dual wavelength adjusted ratio methods. Samples collected from Area D of Phillippi Creek. ....	48
<b>Figure 39.</b>	Loads of PF6 (OB-UV Peak) and PF2 (visible OB+CDOM) in individual detergents (where CDOM is absent) indicating the variety of manufacturer formulations.....	48
<b>Figure 40.</b>	Raw fluorescence (355 nm excitation) of a sample with low CDOM. Note water amplitude of Raman signal as a peak at 404 nm. ....	50
<b>Figure 41.</b>	Raw fluorescence (355 nm excitation) of samples with low (green), moderate (blue), and high (red) CDOM. Note water Raman signal in all samples as peak or shoulder at 404 nm.....	50

## List of Tables

<b>Table 1.</b>	Detergents evaluated for optical brighteners. ....	4
<b>Table 2.</b>	Median factor loads by sample category, including an estimated method detection limit (MDL), and the detergents used for routine spiking (at an estimated 100% OSTDS effluent level). ....	27

## Introduction

Optical brighteners (OB) are water-soluble dyes added to a number of manufactured products. By absorbing light in the ultraviolet (UV) region, the compounds are excited and subsequently emit light at a longer wavelength, fluorescing in the blue region of the visible spectrum. The dyes make white materials appear bluer or 'brighter'. Used extensively in paper manufacturing as well, the use of OB in laundry products imparts a specifically anthropogenic signal to resulting domestic wastes. Other classic waste tracers, excessive bacteria and nutrients, can have natural, wildlife, and agricultural sources in addition to human. As OB are rapidly absorbed by soils (Stoll et al., 1998; Mote Marine Laboratory, unpublished data), detection in the environment indicates either the relatively direct input of human wastes (typically consisting of sewage and grey water combined) or the presence of large quantities of wastes from which not all OB have been removed, as in waste water treatment plant (WWTP) effluents. Failing septic tanks (onsite sewage treatment and disposal systems - OSTDS) or OSTDS with inadequate filtration are also likely contributors. The sensitivity and rapidity of fluorescence techniques make detection of optical brighteners a useful surrogate of human wastes and could permit a rapid field screening method to identify problematic regions and to target the collection of more expensive analytical samples.

There are, however, natural fluorescent compounds, particularly in freshwater originating as surface drainage from wetlands. Dissolved humic and fulvic acids from soils and decomposing vegetation impart a coffee-colored tint to much of the freshwater of Florida and are collectively referred to as colored or chromophoric dissolved organic matter (CDOM). Humics and fulvics are also fluorescent compounds, similar to OB, with absorption in the UV and maximum fluorescent emission in the blue and green region of the spectrum. Any field screening or analytical method developed, particularly if for an estuarine area where a gradient of naturally occurring CDOM is expected, must be able to successfully separate OB from a potentially varying CDOM fluorescence. Other considerations are that the complex mixture of CDOM itself can have a wide range of fluorescent properties, depending on many factors including geographic variations in sources and photobleaching with age.

Excitation-emission matrix (EEM) fluorescence analysis is a laboratory technique in which sample fluorescence from multiple emission wavelengths is recorded for each of multiple excitation wavelengths. Although time consuming, the data developed can be used to depict a detailed, three dimensional picture of fluorescence. A statistical modeling technique, parallel factor analysis (PARAFAC), can then be used to identify, from a group of input data, the minimum number of three dimensional spectral shapes (factors) that, when combined, will adequately describe the vast majority of the samples. Each sample is then modeled as a mixture using varying amounts (loads) of the identified factors. The sample-specific factor loadings, when correlated with CDOM absorption and any known OB content, can be used to identify those samples with OB definitively present. The raw EEM data can be examined to select optimum wavelengths to reliably separate CDOM and OB fluorescence in a field screening method based on either flow-through fluorometry or a remotely sensed technique.

## **Background**

The project here reported was the second funded by the U.S. Environmental Protection Agency (EPA) Clean Water Act Section 104(b)(3)(CFDA 66.475) which granted funds to the Florida Department of Health, Bureau of Onsite Sewage Programs. Both projects were conducted with the Florida Department of Environmental Protection (FDEP) Southwest District performing sample collection and conventional analyses, and with Mote Marine Laboratory (MML) conducting EEM fluorescence and CDOM analyses, statistical modeling, data interpretation, and field method development. Sampling and site location assistance and funding of additional samples were also provided by Sarasota County, Water Quality Planning and Regulatory. Sampling and analyses were conducted under an EPA and DOH-approved Quality Assurance Project Plan (FDEP, 2006; FDEP, 2008). Both projects included the analysis of ambient samples as well as extensive dilution matrices in which various types of ambient water were combined with OB source waters and spiked with detergents (OB). Data from both efforts were analyzed under the most recent project.

## **Methods**

### *Site Selection*

Sampling in the first project targeted estuarine areas from Taylor to Sarasota Counties that were potentially impacted by OSTDS effluent. The most recent project attempted to collect a wide range of CDOM from regions with minimal OSTDS influence, targeting both spring fed systems, surface drainage systems, and surface drainage systems of varying size. Five OSTDS drain fields and two wastewater treatment plants (WWTP) were sampled during both efforts, and two commercial laundry effluents were sampled in the second effort. During the second effort the major sources (OSTDS, WWTP, and laundries) were each sampled twice to evaluate consistency of source fluorescence signature.

Station locations included those from Keaton Beach, Dekle Beach, and the Steinhatchee River in Taylor County, the Withlacoochee River along the border of Citrus County, the Chassahowitzka River in Citrus County, the Weeki Wachee River in Hernando County, the Manatee River in Manatee County, and Phillippi Creek (both at numerous locations in the main stem and along a selected small drainage area), South Creek within Oscar Scherer State Park, and along the Myakka River in Sarasota County. Wastewater treatment plants, OSTDS, and laundries were all located in Sarasota County. Appendix A, Figures A.1-A.11 illustrate the ambient sampling locations.

### *Sampling*

In the initial project, a total of 41 ambient samples plus field quality control samples (replicates and field blanks) were collected. Additionally, source samples were collected from OSTDS (five locations), a tertiary treatment and a secondary treatment wastewater plant in Sarasota County for a total of 48 field samples. The second project collected 15 ambient samples and 18 source samples. Samples for EEM and absorption measurements were collected by FDEP simultaneously with bacteriological and nutrient parameters, which were also analyzed by FDEP. Source samples were collected from WWTP permitted effluent streams, and from the discharges from individual laundry facilities. OSTDS samples

were collected by sinking shallow well points into the drainfield region of residential systems to avoid the high particulate levels expected in OSTDS reservoirs or distribution boxes.. Water tables varied and samples collected undoubtedly included a range of both groundwater and OSTDS effluent. The intent of the OSTDS samples was to determine if OB could be detected in drainfields and not to compute quantitative loading estimates.

Sample containers for EEM and absorption (125mL amber glass bottles with Teflon-lined caps) were acid washed (10% HCl, deionized water), capped with foil (10% methanol rinsed), and fired (450 °C) for 4 hours. Caps were rinsed with laboratory water, 10% methanol, and a final rinse of laboratory water. Sampling protocol was to obtain ambient water directly in sample bottles from near surface waters after an initial sample rinse that was discarded. Large non-representative particles (algal mats, vegetation) were avoided but moderate amounts of turbidity were acceptable in samples.

Samples were not filtered. Gloves were worn by sampling crew and contact of sample with plastics was minimized. Samples pumped from OSTDS did come in contact with a short length of silicone peristaltic tubing. All EEM samples were collected in duplicate. Along with the field samples collected, one replicate per sampling day was collected to assess system heterogeneity. Daily field equipment blanks and cleaning batch-specific container blanks were also processed. Samples were iced and maintained in the dark at 4 °C for transport back to MML within 24 hours and were initially processed for EEM and absorption within one week of collection.

#### *Calculation of Representative OSTDS Effluent*

Optical brighteners consist of a variety of compounds and laundry detergent formulations vary both by the specific OB compound(s) and the amount used. Laundry and WWTP effluents undoubtedly include a variety of OB due to the number of users. Single family OSTDS are more likely to contain OB from a single detergent manufacturer, but due the varying amounts and types of OB in different detergents, adjacent homes can have very different OB concentrations in OSTDS effluent, even if homeowner activities, water, and laundry usage are identical. There are other complications, as well. Some homeowners route laundry and other grey water through separate approved structures for landscape irrigation, thus bypassing the OSTDS. There may also be a diurnal or weekly variation in OB content due to the homeowner's timing of laundry tasks.

As a result, while average or 'typical' OB concentrations can be calculated for given detergents or detergent mixtures, and any OB detected in samples can be related to the 'typical' concentrations as a percentage of full strength OSTDS effluent, the range around the typical value is expected to be large. Also due to the range in potential OB loading from individual residences, quantitative amounts of OB detected do not form a precise loading estimate of OSTDS effluent to receiving waters. The presence of OB should be viewed as an indicator a direct OSTDS discharge rather than as a quantitative tool.

During both the analysis of ambient samples and analysis of the various sample combinations in the dilution matrices, samples were spiked with known amounts of detergent with OB to evaluate matrix effects on OB detection and recovery. In order to add meaningful

concentrations of OB and to place results in the context of a ‘typical’ OSTDS effluent, average detergent concentrations in septic effluent were calculated.

Detergent manufacturers recommend a certain amount to use per load of laundry. A medium sized load was estimated to be 61.7 L (16.3 gal, based on the average of four washing machine manufacturers). Wash water was defined as the recommended detergent amount per 61.7L average load size and ranged from 0.7-1.8 ml/L or 0.8-1.9g/L of detergent. Since a washing machine can use either a single or a two rinse cycle, 1.5 rinses were assumed. Laundry effluent was defined as the sum of wash and rinses waters or (1+1.5)\*61.7L. U.S. EPA (2002) data estimates an average wastewater production of 262.3 L (69.3 gal) per person per day on average, of which 56.8 L (15 gal) is from laundry (wash water and rinse water combined).

$$\frac{61.7 \text{ L wash water}}{(1+1.5) * 61.7 \text{ laundry effluent}} * \frac{56.8 \text{ L laundry effluent}}{262.3 \text{ L OSTDS effluent}} = \frac{86.6 \text{ ml wash water}}{\text{L OSTDS effluent}}$$

To minimize sample dilution in the spiking process, 5X concentrations of wash water were prepared of all individual detergents by using five times the manufacturer’s recommended detergent amounts in a 61.7 L medium-sized load. Samples spiked at 100% OSTDS level were therefore spiked with 86.6/5 ml or 17.3 ml/L of 5X wash water.

### *Detergents*

Over the course of both projects, the detergents in **Table 1** were evaluated for optical brighteners. For the first project, ten detergents were individually evaluated by EEM and equal volumes were combined for use as a consistent spiking solution. For the second project, 12 detergents were evaluated by EEM and five of the 12 used individually for spiking. Evaluating the EEM of individual detergents allowed the modeling effort to identify fluorescent peaks that may be unique to differing OB compounds. An OB reference compound, disodium 4,4’-bis(2-sulfostyryl)biphenyl (DSBP), was also evaluated, but was not found in any of the detergents evaluated.

**Table 1.** Detergents evaluated for optical brighteners.

All Stain Lifter	Arm and Hammer
Cheer with Colorguard	Colorbright Clorox2
Dreft	Fab Ultra 2X Spring Magic
Gain	OxyClean
Publix Tropical Scent	Purex
Surf	SA-8 (Amway)
Tide	Tide Free
Tide HE	

### *Dilution Matrix*

The preparation and analysis of a dilution matrix formed a large part of the effort in both projects and was used to expand the number of matrices evaluated. The recovery of OB added to the various matrices created was used to investigate the ability of the planned fluorescence data processing to reliably and quantitatively discriminate OB in the presence of varying quantities of naturally occurring fluorescent materials.

For the first project, the laboratory dilution series was limited to a number of mixtures of four source waters with two levels of OB spiking per mixture. Several were repeated over time to evaluate stability and reproducibility. Source waters were highly colored, low salinity water (HI CDOM), minimally colored saline water (LO CDOM), OSTDS effluent, and tertiary treatment WWTP effluent, collected in bulk from the same locations as the field samples. Absorption coefficients at 300 nm ( $a_{300}$ ) of the WWTP and OSTDS were  $11.3 \text{ m}^{-1}$  and  $49.3 \text{ m}^{-1}$ , respectively. The low CDOM sample was collected from saline waters of Sarasota Bay (33 PSU,  $a_{300} = 3.50 \text{ m}^{-1}$ ), the high CDOM sample was collected from the Myakkahatchee Creek tributary of the Myakka River (Salinity < 2 PSU,  $a_{300} = 45.1 \text{ m}^{-1}$ ). The high and low CDOM waters were also mixed to prepare intermediate CDOM water (MCDOM). Each of the three CDOM levels were then prepared as a dilution series with both WWTP and OSTDS waters, as 100:0, 50:50, and 0:100 mixtures for a total of 11 unique matrices. Absorption analyses of CDOM were performed on each of the mixtures. Each of the dilution matrix samples for evaluation was spiked with two concentrations of a detergent mixture, one to represent typical OSTDS concentrations (approximately 100% of OSTDS effluent) and another at half typical concentrations (50%).

The number of matrices evaluated was expanded significantly in the second project, with five ambient samples, five OSTDS, the 2 WWTP, the two laundries, and DI each combined into a total of 105 matrices for evaluation. The series was designed to investigate the recovery of a fixed amount of a single detergent from a wide variety of parent waters. An ambient sample of low salinity water from each of the five geographic regions sampled was successively mixed with DI, one of the WWTP samples, one of the laundry facility effluents, and one of the OSTDS samples in a randomized design. Absorption coefficients from samples in the second dilution matrix ranged as high as  $100 \text{ m}^{-1}$  at 400 nm. Each mixture was spiked with a single detergent.

#### *EEM and Absorption Analyses*

Quality criteria for EEM and absorption measurements from the most recent project are summarized in Appendix B and were generally the same for both efforts. For EEM analysis, samples were gently homogenized by inversion. Samples that were highly turbid were either centrifuged or diluted with laboratory deionized water during the determination of the limits of the method. Samples were not filtered prior to analysis as filtration has been demonstrated to remove OB from solution (MML, unpublished data). Subsequent analytical protocols were to centrifuge samples if turbidity exceeded 150 NTU. If subsequent maximum fluorescence of any sample exceeded 200 QSRF, then samples were diluted. All samples were scanned in a PTI QM-4 SE Spectrofluorometer, with excitation wavelengths of 220-455 nm (5nm increments) and emission wavelengths of 250-700nm (2nm increments). The instrument used a scanning fluorescence 75W Xenon arc lamp and spectral units were based on concave diffraction gratings. Excitation slit width was set at 5nm, emission slit width at 2nm and digital PMT slit width at 5nm.

Analyses for EEM included the daily EEM analysis of reference materials (quinine sulfate) to which fluorescence intensities were normalized to permit intercomparisons of data with other spectrofluorometric systems. Resulting data are presented in Quinine Sulfate Relative Fluorescence units (QSRF). Daily EEM of laboratory deionized water was used to evaluate

lamp intensity over time. Wavelength accuracy was confirmed at three locations using Raman emission maxima in water and agreement with literature values. Initial calibration verifications consisted of another preparation of quinine sulfate from an alternate source and were required to be within 90-110%. Continuing calibrations evaluated quinine sulfate fluorescence at a fixed excitation wavelength to confirm continuing instrumental response (85-115% required) and were repeated as a final calibration check at the completion of an analytical group. Spike recoveries of OB (minimum 1 per 20 samples, 85-115% recovery) were evaluated as fixed 350 nm excitation scans relative to identical OB preparations in laboratory deionized water. Duplicate precisions (minimum one per 10 samples,  $\leq 15\%$  RSD) were also evaluated at fixed excitation wavelengths.

Linear response of the fluorescence of quinine sulfate was evaluated between 0.02 to 400  $\mu\text{g/l}$ . Linearity for the instrumental conditions in use in this project began to degrade above 90  $\mu\text{g/l}$  ( $r^2 < 0.9995$ ), although  $r^2$  values still exceeded 0.999 for data as high as 200  $\mu\text{g/l}$  of quinine sulfate. Detection limits were determined to be 0.05  $\mu\text{g/l}$  of quinine sulfate.

During the initial project, turbidity and absorption coefficients of ambient samples were not as pronounced as the most recent effort and more turbid samples were generally diluted to less than 100NTU. Amounts of turbidity below this threshold were previously demonstrated not to cause interference. Most recently, the extreme turbidity in some OSTDS samples appeared to result in negative interferences. Turbid samples ( $>60\text{NTU}$ ) were therefore either centrifuged at 2100 rpm for 1 hour or diluted with laboratory deionized water. Both turbid and highly absorbing samples were successively diluted and analyzed as single excitation emission scans until agreement between successive dilutions (after correction for dilution and absorption) was greater than 95%. Absorption corrected spike recovery of the optimal dilution was confirmed to be within 85-115%, at which point the selected dilution of both sample and spike were analyzed as a full EEM.

Absorption was determined from 214-750 nm at 2 nm increments according to Ocean Optics Protocols for Satellite Ocean Color Sensor Validation (Mueller, *et al.*, 2003). A Perkin Elmer 650 spectrophotometer was used for the determination of full-spectrum absorption profiles. The instrument is a double beam, double monochromator, ratio recording UV/Vis spectrophotometer (tungsten-halogen sources). An all-reflecting optical system (SiO<sub>2</sub> coated) used a holographic grating (1440 lines/mm UV/Vis blazed at 240 nm) for wavelength selection and a R955 Photomultiplier sensitive in the 190 – 900 nm wavelength range for detection. The instrument is linear to 3.0A. All samples were filtered through 0.2  $\mu\text{m}$  Sterivex cartridges. Dilutions of highly absorbing samples were performed as needed. Analyses for absorption included instrumental zero on laboratory water, confirmation of zero stability with re-analysis of laboratory water as a sample, and measurement of solid standards (didymium glass and a 10% T filter) to confirm wavelength accuracy and instrument response within specified limits (90-110% of historical values). Duplicate precision (minimum 1 per 10 samples) was assessed at select wavelengths ( $<5\%$  RSD at 400 nm, 440 nm).

### *EEM Post processing*

Data processing began with data corrected for instrument-specific spectral lamp output, spectral grating efficiencies, and spectral photomultiplier sensitivity, all automatically applied with manufacturer's correction files. A daily emission wavelength correction was applied based on location of maximum Raman emission in laboratory DI water. Daily normalization for long term lamp and instrument drift was applied by multiplying by a Raman factor (RF), where:

$$RF = 80,000 / F_{275/303} \text{ of deionized water.}$$

It is essential that analyses include full-spectrum absorption profiles for correction of EEM data for both primary and secondary inner filter or self-absorption effects. In a highly absorbing sample, the energy reaching the sample volume viewed by the detector is much reduced, leading to less fluorescence being emitted. The reduced fluorescence is, in turn, subject to losses by absorption during the path to the detector. The losses are not spectrally neutral as there is a strong exponential shape to CDOM absorption. Failure to correct for self-absorption will result not only in reduced overall fluorescence amplitude, but in a false red shift of both excitation and emission maxima that could be interpreted as another substance. The false red-shift is proportional to the amount of CDOM present in a sample and so is particularly important to address when sampling across saline-freshwater gradients. A dilution series of humic substances will experience spurious spectral shifts which may be inappropriately attributed to changes in fluorescent components unless absorption effects are removed (Mobed, et al. 1996). The techniques of correction are varied (Lakowitz, 1983; Gauthier, et al., 1986; Puchalski, et al., 1991; Tucker, et al. 1992; MacDonald, et al., 1997; Mobed et al., 1996; McKnight, et al., 2001) both in model assumptions and level of complexity.

We chose a correction based on absorption of excitation and emission radiation as presented by Lakowitz (1983), using measured CDOM absorption coefficients applied across a 0.005 m path for the target volume of a 1 cm X 1 cm cell. Raw fluorescence data were multiplied by the resulting absorption correction factor, CF, which was:

$$CF_{em/ex} = 10^{(a_{em} + a_{ex}) * 0.005 / (2.303)}$$

where  $a_{ex}$  = absorption coefficient ( $m^{-1}$ ) of the excitation wavelength, and  
 $a_{em}$  = absorption coefficient ( $m^{-1}$ ) of the emission wavelength.

Data were normalized to quinine sulfate units to permit interlaboratory comparisons of EEM data by dividing by the slope of quinine response for the day;

$$QS \text{ Slope} = F_{QS-350/450} / [QS], \text{ where } [QS] = \text{quinine sulfate concentration in } \mu\text{g/L.}$$

Data were smoothed (MATLAB, Ver 6.0 R12) along the emission axis to reduce noise (negative values) at low fluorescence values. Primary and secondary Rayleigh and Raman emissions, data from any emission wavelengths shorter than excitation wavelengths, and any remaining negative data were set to missing (hard negative weighting; JiJi and Booksh, 2000) prior to analysis. Missing data are ignored for modeling purposes. All data were reviewed at

selected wavelengths for general efficacy of Rayleigh and Raman removal. Selected samples (generally OSTDS samples and mixtures) with high turbidity revealed inadequate removal of Rayleigh scattering effects and so the width of the Rayleigh mask was increased for those samples only.

Final data were in quinine sulfate relative fluorescence units (QSRF). For model development, samples were individually normalized to the maximum observed in a 230-440 nm excitation range and a 300-650 nm emission range. The normalization process minimized the range in amplitude between samples. Normalizing initiating data prevented a few highly fluorescing samples from prematurely accounting for the bulk of model variance and permitted the detection of relatively weaker fluorescing compounds. EEM were also corrected for dilution as necessary.

### *PARAFAC Modeling*

Parallel factor analysis (PARAFAC, PFTools for Matlab, Andersen and Bro, 2003) is the technique of linear unmixing, which, when used with EEM fluorescence data, generates the three dimensional spectral shapes (factors) of excitation and emission and the relative amounts of each factor (loads) needed to produce the observed initiating data. Model development was the process in which the optimum number of unique spectral shapes was identified to describe the initiating data set without subjecting the model to over-parameterization. In all cases, the model was constrained to only present nonnegative excitation and emission spectra, but both excitation and emission factors were allowed to be multimodal. The optimum valid model was considered to be that with the maximum number of factors, in which the residual sum of squares was minimized, the appearance of identified factors appeared reasonable (Andersen and Bro, 2003), and model development on random halves of the initiating data developed comparable factor spectral shapes (split-half analysis; Stedmon et al., 2003) indicating robustness of identified factors.

PARAFAC model development was applied to 181 samples of normalized EEM data. Data selected included 74 ambient samples (generally undiluted) from 11 separate geographic regions, 35 detergent samples of 14 individual detergents and the detergent mixture, 47 samples of the two dilution matrices (also unspiked), and 25 samples of WWTP, OSTDS, or laundry effluent. By eliminating spiked samples from model development, the recovery of spikes would not be biased by forcing model factors to accommodate the fluorescent profiles of spiked samples and spike recovery could be considered completely independent of model development.

The OB standard, DSBP, was not qualitatively observed in any detergent used or in any sample. Preliminary modeling efforts that included DSBP resulted in a factor which was almost exclusively present in the two DSBP samples. Rather than increasing the number of factors, the amount of noise in factor loading results, and the computational overhead, DSBP samples were removed from model development.

From four to ten model factors were evaluated by split-half analysis. In addition, the wavelength range of the modeling effort was varied to restrict regions of instrumental noise while retaining low-wavelength peaks determined to be of significance. The factors

identified in the optimum model were then associated with CDOM, OB, a combination of CDOM and OB, or other fluorescing compounds based on excitation-emission maxima, spectral appearance, correlation with CDOM absorption or OB added, similarity to detergent fluorescence or other samples of known origin, or literature values.

Lastly, the spectral shape of identified factors were applied to all non-normalized EEM results to arrive at quantitative amounts or loadings of each factor in individual samples. Robustness of computed loadings was evaluated by varying the order of factors applied to data, and by comparing loads determined on diluted samples and subsequently corrected for dilution with loads computed directly on data already corrected for dilution. Precision of duplicate analyses, replicate samples, agreement between diluted samples at various dilution factors, and spike recovery was assessed using the calculated factor loads generated by the final PARAFAC model.

The use of different detergents with differing amounts of OB resulted in a range of factor loads that could each represent a 100% OSTDS effluent. The percentage of OSTDS present in each sample was calculated relative to each individual detergent and then a mean value of %OSTDS was presented for assessment of ambient samples. A typical detection limit study evaluates the standard deviation of seven replicate samples of a specified but low concentration range, with all seven analyzed in one analytical group. An explicit detection limit study was not performed for factor loads due to the difficulty of assembling a surrogate sample with the required low concentration range for of all factors. Instead, detection limits, were approximated from the variation in all factor loads as computed from deionized water samples over the course of the project. As these were compiled over a number of months, the detection limit in factor load units is expected to be somewhat larger than a detection limit determined in the typical manner.

### *Optimized Field Method*

The ultimate outcome of the research here reported was to develop a rapid field survey method which could be used to qualitatively or quantitatively assess the role of OSTDS effluent in areas of suspected adverse impacts. One approach would be to develop a simplified fluorescence method using a minimum number of wavelengths, either for point assessment (a ‘dip-stick’ approach) or for mapping (a flow-thorough approach). More complex but also desirable would be a remotely sensed application, again with a minimized number of fluorescent emission wavelengths and utilizing either an active excitation source (such as laser) or relying on passive solar stimulated fluorescence.

Dual wavelength methods have been previously proposed and tested (Dixon and Julian, 2005; Dixon, et al., 2005) but were based on more limited fluorescence information and on fewer ambient samples with a narrower range of CDOM. The EEM data collected in these two projects were used to assess the strengths and weaknesses of the dual wavelength method (which was applied in the first project). Additionally, EEM data were screened to identify optimal wavelength pairs (excitation and emission) that could be used to approximate CDOM absorption (for performing real-time absorption correction algorithms of any subsequent field method), and that could best recreate the calculated factor loads and OB present as determined by PARAFAC modeling.

## Results

### *Absorption Correction*

Efficacy of absorption correction was demonstrated repeatedly in the single scan fluorescence work, evaluated as fluorescence intensity at the single wavelength pair of 350/440 ex/em. The following example was characteristic of most ambient samples (high CDOM, moderate to low turbidity) collected during the project. If no absorption correction was applied, a 1:2 or 50% dilution of a sample would generate a fluorescence value that was substantively greater than half of the original, undiluted sample fluorescence. Increasing dilutions of the sample continued the trend, until expected fluorescence values were achieved with additional dilution only at very high dilution values. Once the appropriate dilution factors were applied to the data, the value for sample fluorescence was only approached asymptotically with increasing dilution. Sample dilution is a common approach to addressing highly absorbing samples (Baker, 2002b) and some protocols have a recommended upper limit of absorbance or optical density (O.D.) at the excitation wavelength (Komada, et al. 2002).

Absorption corrections, however, generated equivalent fluorescence values for all dilutions, including the undiluted sample. Absorption corrected data remain in quinine sulfate relative fluorescent units (QSRF). **Figure 1** illustrates both absorption uncorrected and absorption corrected fluorescence data, together with the O.D. of the sample dilution. Uncorrected data did not approach 95% of the true sample value (taken as the fluorescence of the most diluted sample times the dilution factor) until dilution was ~1:10, with ~ 0.03 O.D., while the undiluted samples exhibited fluorescence that was only 63% of the true value. To achieve 98% of true values, an estimated 1:70 dilution would be required, and given the exponential nature of CDOM absorption in natural samples, much higher dilutions would be required in order to work in the UV range. In contrast, data with absorption corrections applied averaged over 98.7% of the true value for all dilutions and the undiluted sample was 97.2% of the true value. The undiluted sample absorbance was >0.3 O.D., over a 10-fold increase in the dynamic range. Spike recoveries of selected detergents were similarly improved with absorption correction, from an average of 93%, 10.7 s.d., to an average of 98.0%, 8.0 s.d. **Figure 2** illustrates the noise reduction achieved when using an absorption corrected but undiluted sample, relative to a diluted sample.

The successful absorption correction is further demonstrated in the following figures of fluorescence scan data. One of the highest absorption ambient samples (Myakka River) was diluted in a series of 1:1, 1:2, 1:4, 1:10, and 1:20. If no correction for absorption were to be applied, then the fluorescence of the most dilute sample (corrected for dilution) would be the most representative of the ambient sample, but the noise of the low fluorescence sample (times the dilution factor) would be expected to be substantial.

The calculated absorption correction factor (**Figure 3**) ranged as high as 20 for the UV region of the undiluted sample, and only slightly over 1.15 for the 1:20 dilution. **Figure 4** illustrates the emission profiles of the dilution series at a 350nm excitation. The upper panel illustrates the various sample aliquots, uncorrected for absorption, but corrected for dilution. The heaviest line is the fluorescence of the undiluted sample. Increasing dilutions result in

higher fluorescence amplitudes, with values approaching but not reaching convergence. The lower panel illustrates fluorescence with both absorption and dilution correction applied. Agreement between these dilutions is excellent, with deviations of 3% RSD or less, and is better than expected of duplicate analyses.

As a result of absorption correction, the linear range of fluorescence was substantially extended, signal to noise ratios were improved, and more concentrated samples could be analyzed. The result is particularly relevant for the development of a field method where the field dilution of samples or a sample stream is not desirable.

The absorption correction is based on accounting for the absorption and reduction of excitation energy reaching the sample volume and the subsequent reduction in emission energy due to the absorption of sample fluorescence. The Beer-Lambert Law is used to compute the fractional energy reduction and thus the factor by which the resulting observed fluorescence should be increased. Limitations on the applications of the Beer-Lambert Law would therefore be expected to apply to the use of the absorption correction, particularly that solutions are dilute enough to where single interactions can be assumed, and that scattering (which would increase the effective path length and opportunities for absorption) is minimal. The limitation on scattering is important to define the maximum turbidity at which fluorescence measurements and absorption corrections can be considered useful. It should be kept in mind that absorption coefficients were determined on filtered samples, and to the extent that sample particulates result in additional absorption and/or scattering, the derived absorption correction represents a minimal value and possibly an undercorrection.

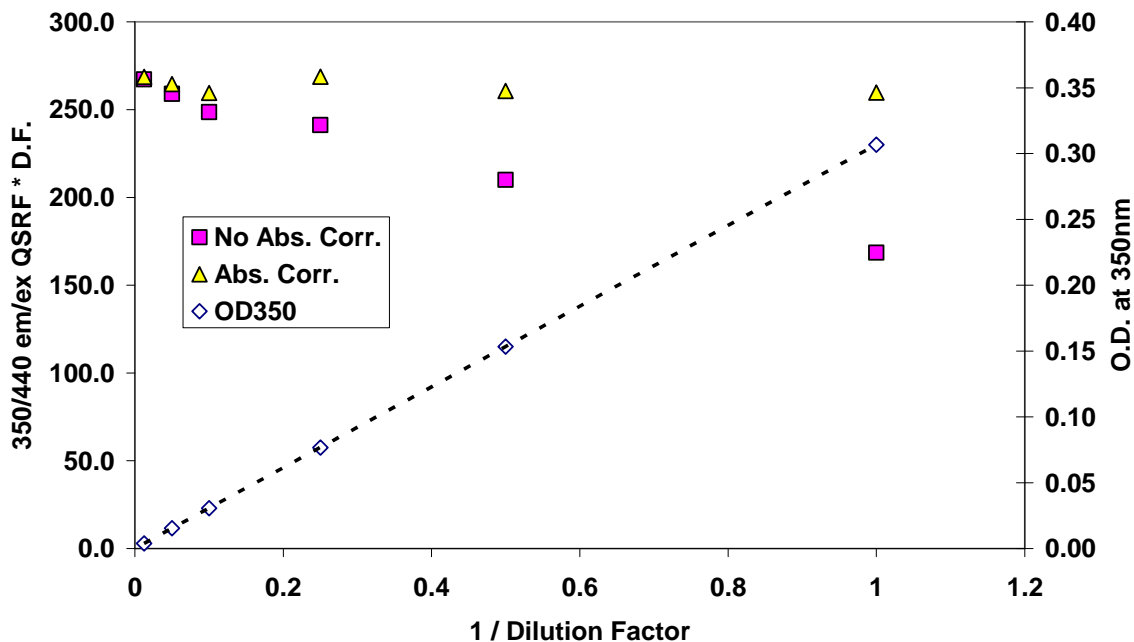


**Figure 1.** Uncorrected and absorption corrected fluorescence data, 350/440 ex/em, together with the optical density (O.D.) of the sample dilution.

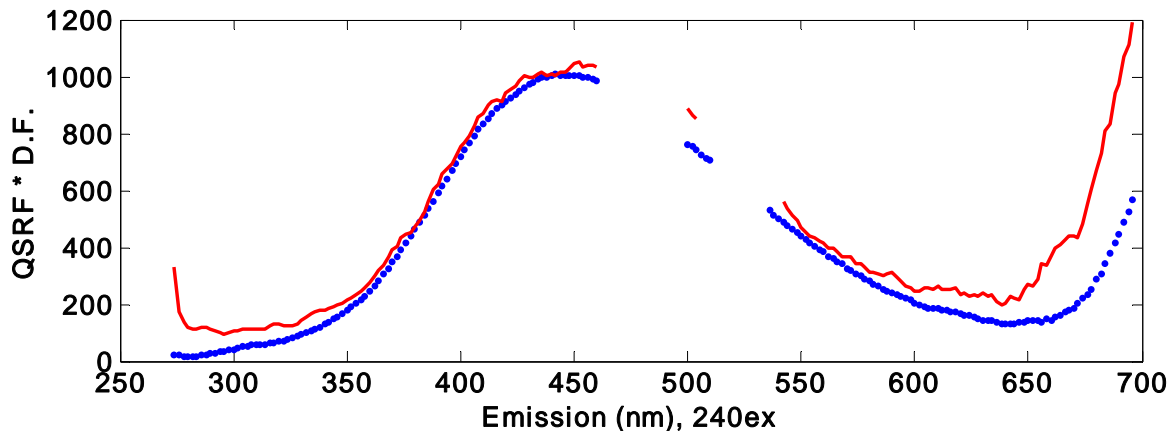


**Figure 2.** Noise reduction achieved for an undiluted sample with absorption correction (blue) relative to a sample diluted until absorption correction was unnecessary (red) but was then multiplied by the dilution factor.

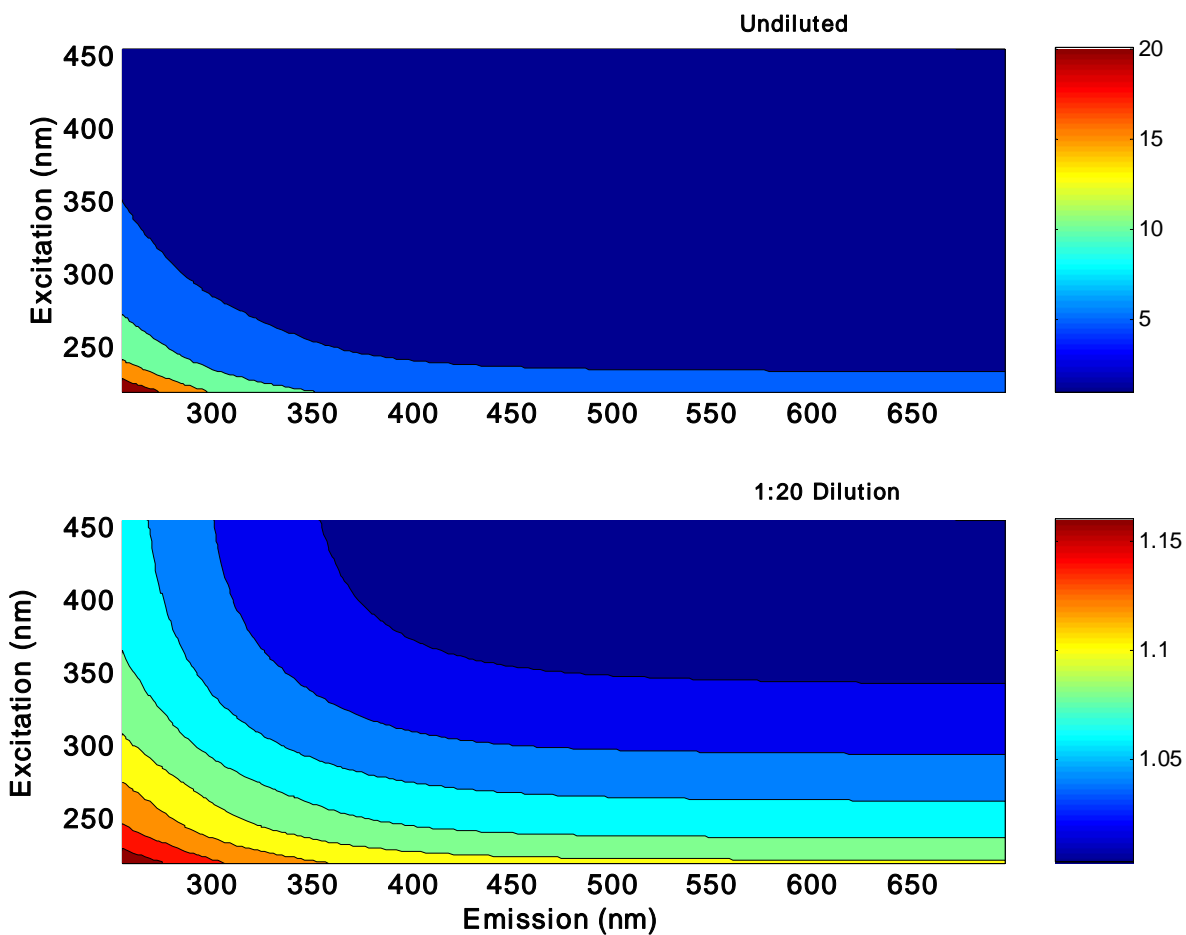


**Figure 3.** Absorption correction factors applied to raw fluorescence data for an undiluted sample (upper) and a 1:20 dilution of the same sample.

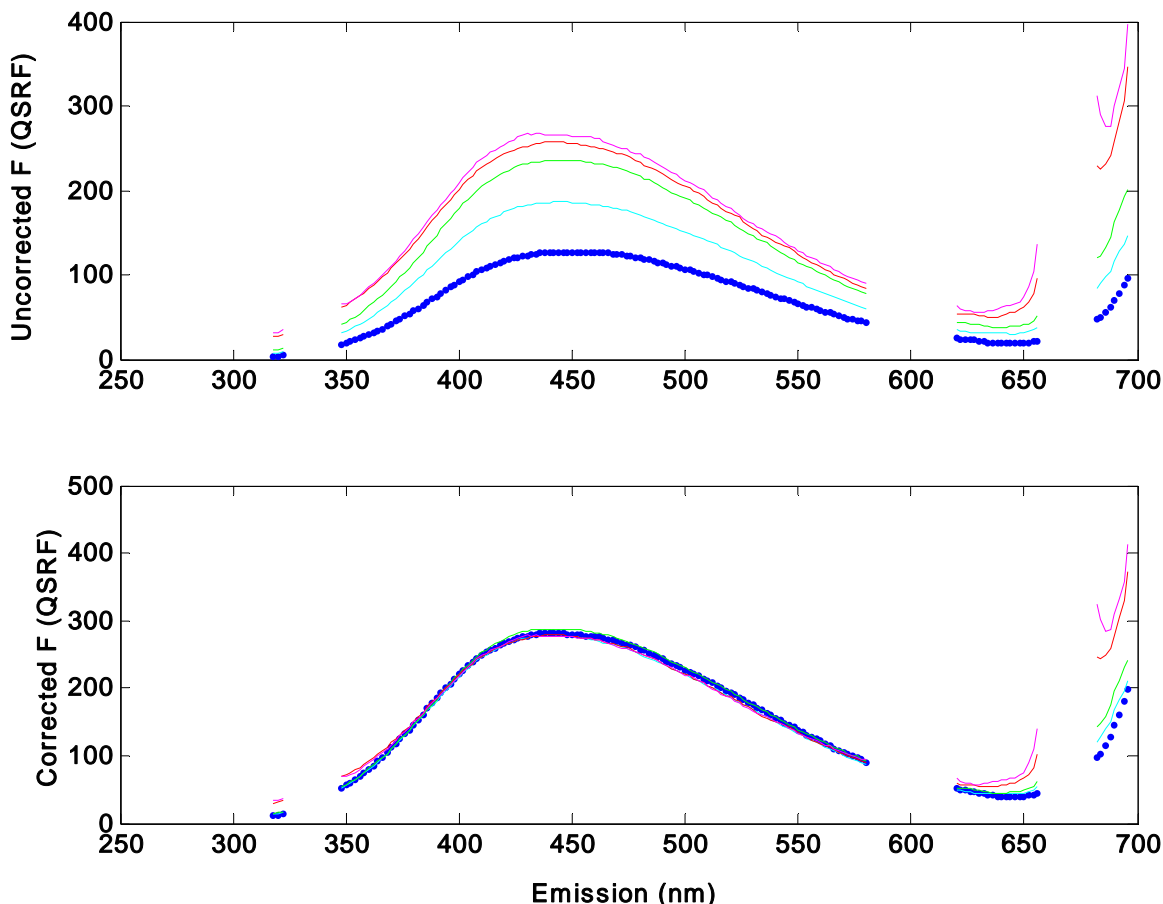


**Figure 4.** Dilution series of a sample corrected for dilution, but not absorption (upper), and corrected for dilution and absorption (lower). Dilutions were undiluted (heavy blue), 1:2 (cyan), 1:4 (green), 1:10 (red), and 1:20 (magenta).

#### *EEM Methodology Refinements*

In many literature reports, fluorescence EEM data are typically gathered on filtered samples to reduce Rayleigh emissions and to avoid anomalous signals from phytoplankton. The emphasis on the development of a field instrument from this work and the absorption of OB onto some filter media led us to pursue the limits of the method when applied to unfiltered samples. During the initial project, the  $a_{300}$  of almost all samples were less than  $100 \text{ m}^{-1}$  ( $\sim 0.43$  O.D. for a 1cm path). The wetter conditions that prevailed during the second project resulted in some samples with  $a_{300}$  approximately  $150 \text{ m}^{-1}$  ( $\sim 0.65$  O.D.). In addition, the extremely high levels of turbidity observed in the most recent OSTDS samples ( $>1000$  NTU) forced a re-evaluation of the limits of potential interferences in EEM and OB analyses.

A spike recovery analysis of detergent fluorescence at the 350/440 ex/em wavelength pair was performed on multiple dilutions of a several extreme samples. **Figure 5** indicated that when fluorescence (corrected for absorption and converted to quinine sulfate units) exceeded 200 QSRF, that spike recoveries declined, and that the best recoveries were when the spiked sample fluorescence was less than 150 QSRF. This result was consistent with the linearity studies of quinine sulfate and it is therefore likely that fluorescence becomes non-linear due to instrumental limitations. (If due to instrumental limitations through photomultiplier saturation, then range extensions might be accomplished by reducing excitation slit width and total energy.)

When samples were restricted to fluorescence values below the 200 QSRF threshold, spike recovery as a function of turbidity (**Figure 6**) indicated that OSTDS turbidity as high as 150 NTU did not interfere with spike recovery of detergents. That the absorption correction remained sufficient at these high turbidities implied that the scattering alone did not substantively increase the path length of the light through the sample cell. As a result, samples for EEM analysis were processed to remove particulates until turbidity was less than 150 NTU.

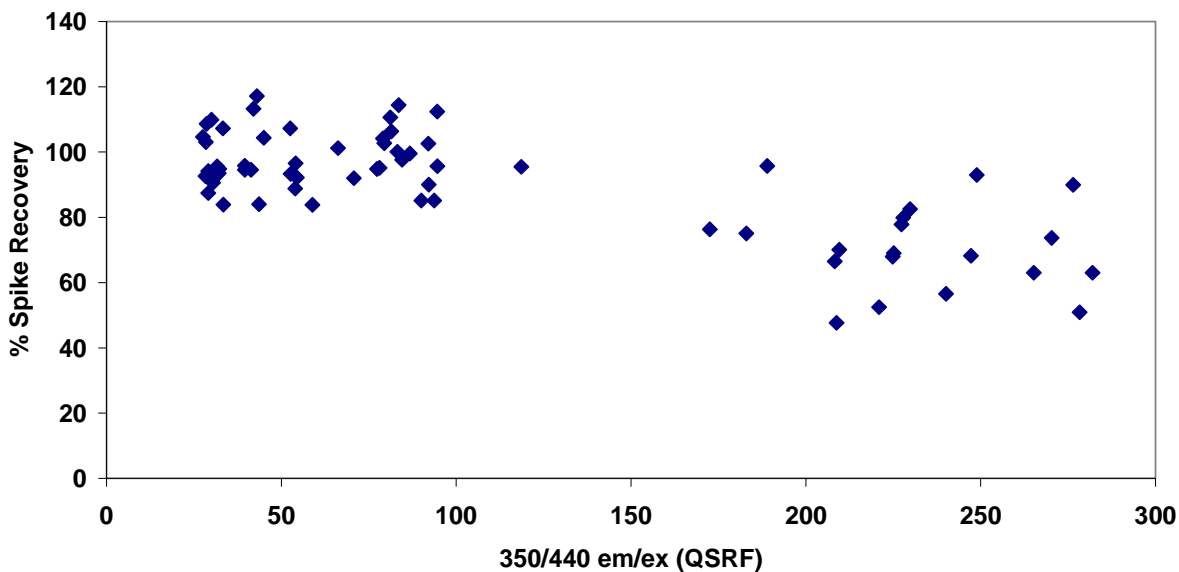


**Figure 5.** Spike recoveries of added detergent, relative to detergent fluorescence in deionized water, as a function of fluorescence amplitude at 350/440 ex/em. Note decline at fluorescence above 150-200 QSRF.

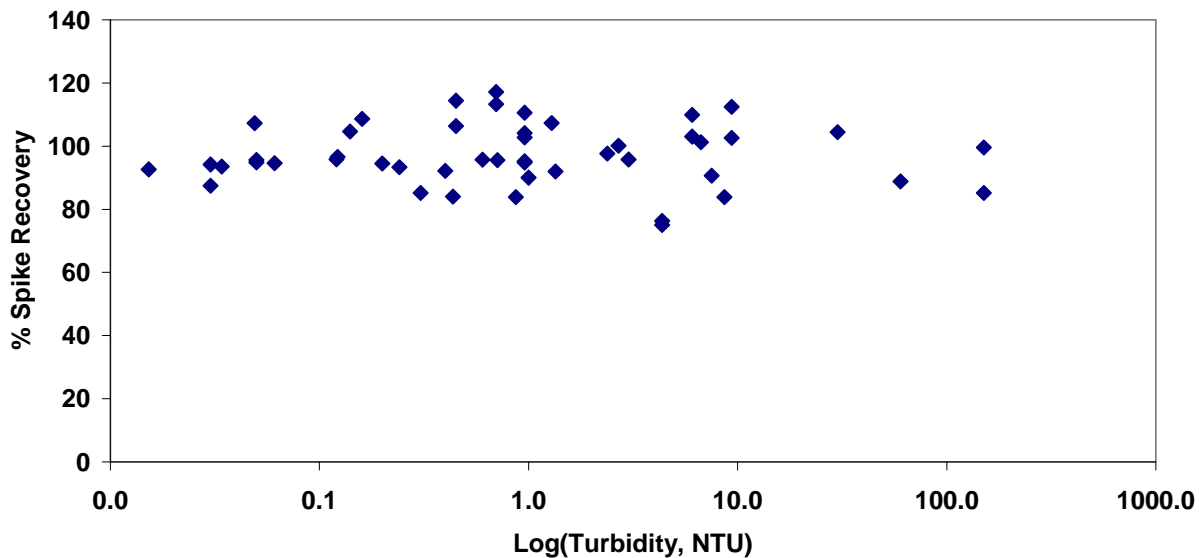


**Figure 6.** Spike recoveries of added detergent, relative to detergent fluorescence in deionized water, as a function of turbidity. Maximum turbidity was 150 NTU.

For samples with turbidity higher than 150 NTU, filtration (through a 0.45 $\mu$ m nylon membrane and glass fiber prefilter) was demonstrated to remove fluorescence. Since centrifugation of samples in most cases generated comparable results to raw samples, the fluorescent reduction of filtered samples was assumed to be the result of retention of dissolved fluorescent material onto the filter media, rather than the removal of fluorescent particulates. Centrifugation of ambient samples of moderate to low turbidity had little effect, and dilution series demonstrated that absorption corrections provided equivalent final fluorescence values from both undiluted and diluted samples. A higher turbidity sample from one OSTDS also illustrated that fluorescence was not necessarily associated with particulates. The undiluted raw and centrifuged sample (131 and 0.8 NTU respectively) generated 350/440 ex/em fluorescence of 136 and 142 QSRF, or within duplicate precision.

Other OSTDS, however, with a turbidity of over 600 NTU, displayed depressed fluorescence (**Figure 7**) in the raw sample relative to the centrifuged sample or to subsequent dilutions of either raw or centrifuged sample. Fluorescence of the turbid sample was depressed until turbidity had been reduced to ~150 NTU. The centrifuged sample (4 NTU), however, demonstrated constant fluorescence with dilution. Visual inspection of the sample indicated that particulates were dark, relative to other OSTDS. (Darker particulates could be a function of soil type for OSTDS samples or weather conditions for ambient samples, if sediments are organic in nature and are re-suspended by currents or wave action.) If particulates are absorbing, then the absorption correction applied for dissolved CDOM has accounted for only part of the loss in energy as the light beam transits the sample cell. A range of particulate colors obtained from OSTDS is illustrated in **Figure 8**.

For successful laboratory evaluations, absorption corrections were demonstrated to be effective at least up to 0.65 O.D.. For turbid samples, particulate influence can either be minimized (centrifuged to be relatively free of particulates, or diluted until turbidity is less than 150 NTU).

Absorbing particulates were not specifically accounted for in the EEM analytical protocol or the current absorption correction and could be problematic under some anticipated extreme field conditions. Determination of particulate absorption is possible with the spectral analysis of particles collected on a glass fiber filter (Yentsch, 1962; Bricaud and Stramski, 1990; Cleveland and Wiedemann, 1993), but is time consuming and unsuitable for a field method. A standard determination of CDOM on an unfiltered sample would be inappropriate as the observed energy reduction is due to both absorption and scattering from the sample cell, and would result in a significant overcorrection that would increase with increasing turbidity. For a field instrument which could operate over a wide range of turbidity, the most rigorous approach would be to incorporate an absorption measurement performed in an internally reflecting sample cell (similar to the 'a' channel of an 'ac-9' instrument, WetLabs, Inc.) which would minimize scattering contribution to a determination of absorption on a raw sample. Alternatively, a dilution loop could be incorporated into a field instrument which could be used if ambient turbidity warranted.

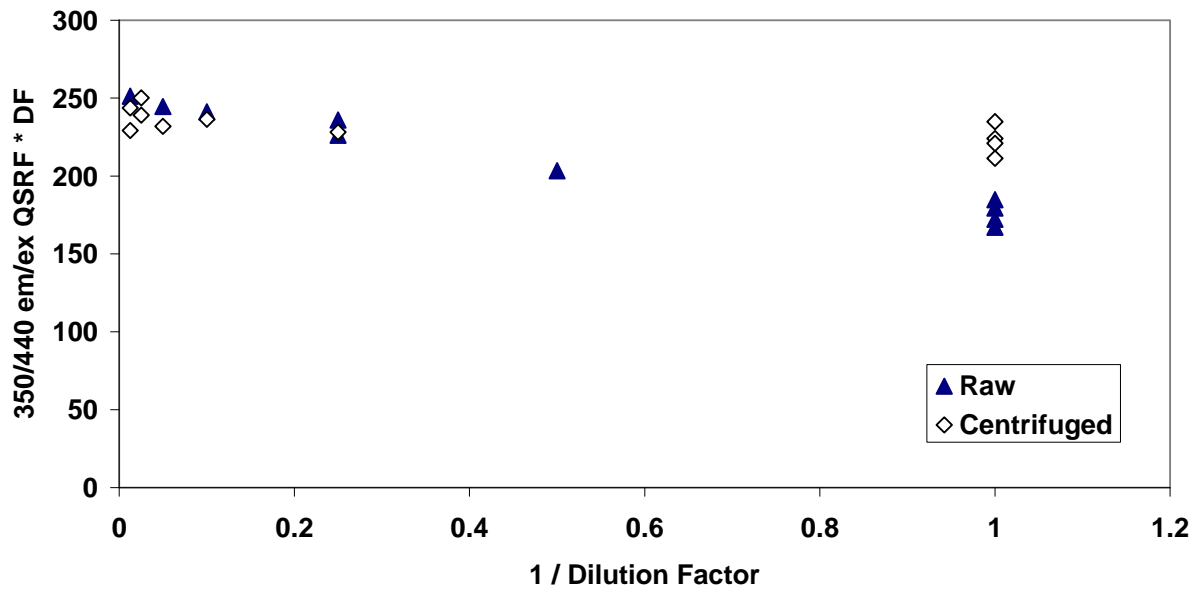


**Figure 7.** Dilution series of a turbid sample both with and without centrifugation for removal of particulates. Reducing turbidity allowed undiluted sample to produce acceptable values without dilution.



**Figure 8.** Filters capsules used to prefilter OSTDS samples for CDOM absorption determination illustrating the range in particulate color.

## Detergents

EEM spectra of the individual detergents used for spiking ambient samples and matrix dilutions appear in **Figures 9** and **10**. The EEM data are plotted in two wavelength ranges to accommodate the range in fluorescent intensity between spectral regions. Fluorescence of all detergents generally fell into one of three categories. Most, 11 of 14, exhibited a maximum emission in the UV excitation and emission range, similar to the detergent mixture, A, C, E, and J. For the same preparation of ‘typical’ OSTDS effluent, however, the relative fluorescent intensity of the UV peak varied substantially between detergents, indicating the varying formulations of the individual detergents. Regardless of wavelength, the maximum fluorescence was greatest overall for these 4 detergents. Three of the detergents were dominated by a peak in the expected OB region, with a predominantly UV excitation and a maximum emission between 400 and 450 nm, similar to detergent I. Much reduced amounts of this peak appear in many of the other detergents as well. One of the detergents tested had neither peak present and very low fluorescence overall.

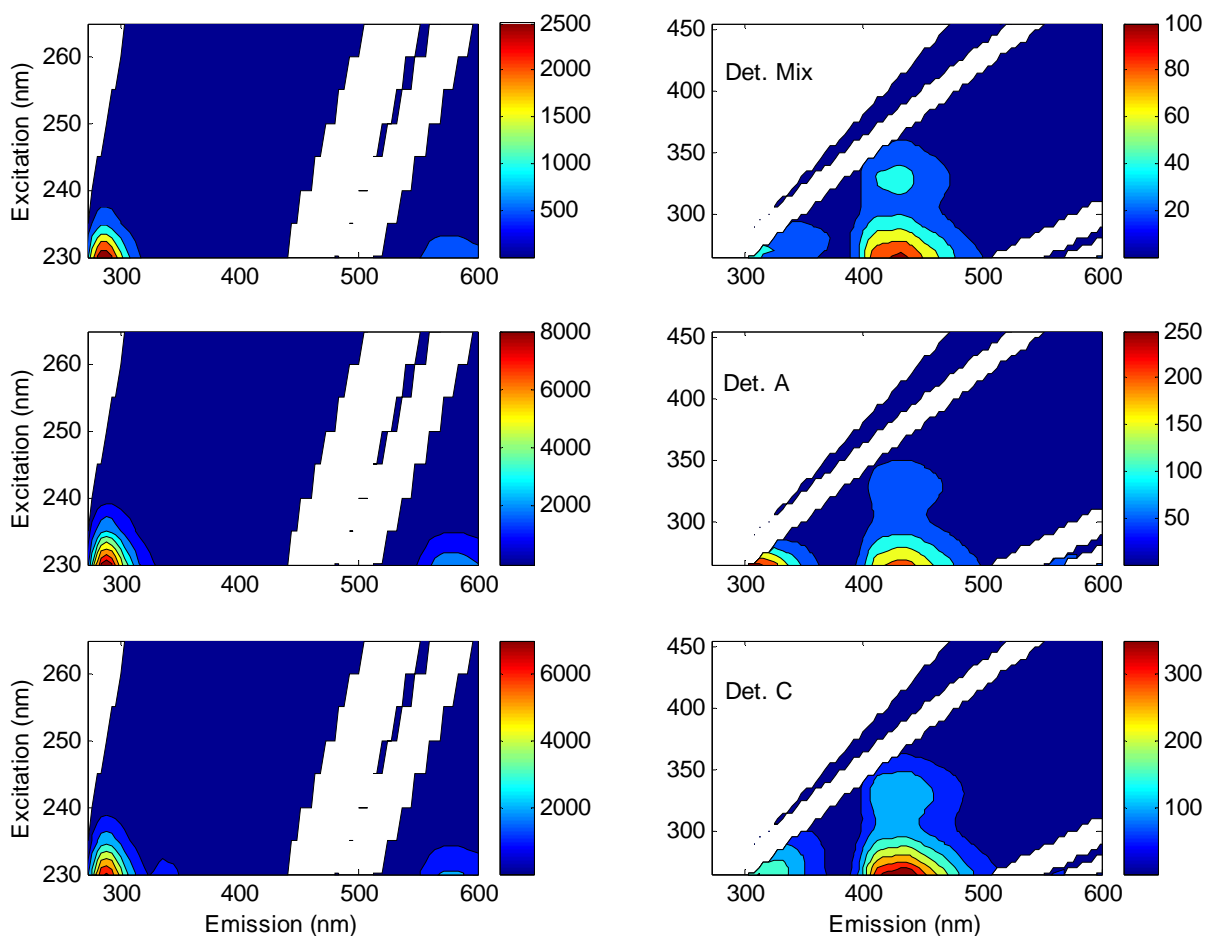


**Figure 9.** Fluorescent EEMs of detergent mixture and selected detergents used as spiking solutions during analyses of OB recovery from various sample matrices. Left panels are of low excitation wavelengths and right panels are of higher excitation to capture amplitude differences between fluorescence regions.

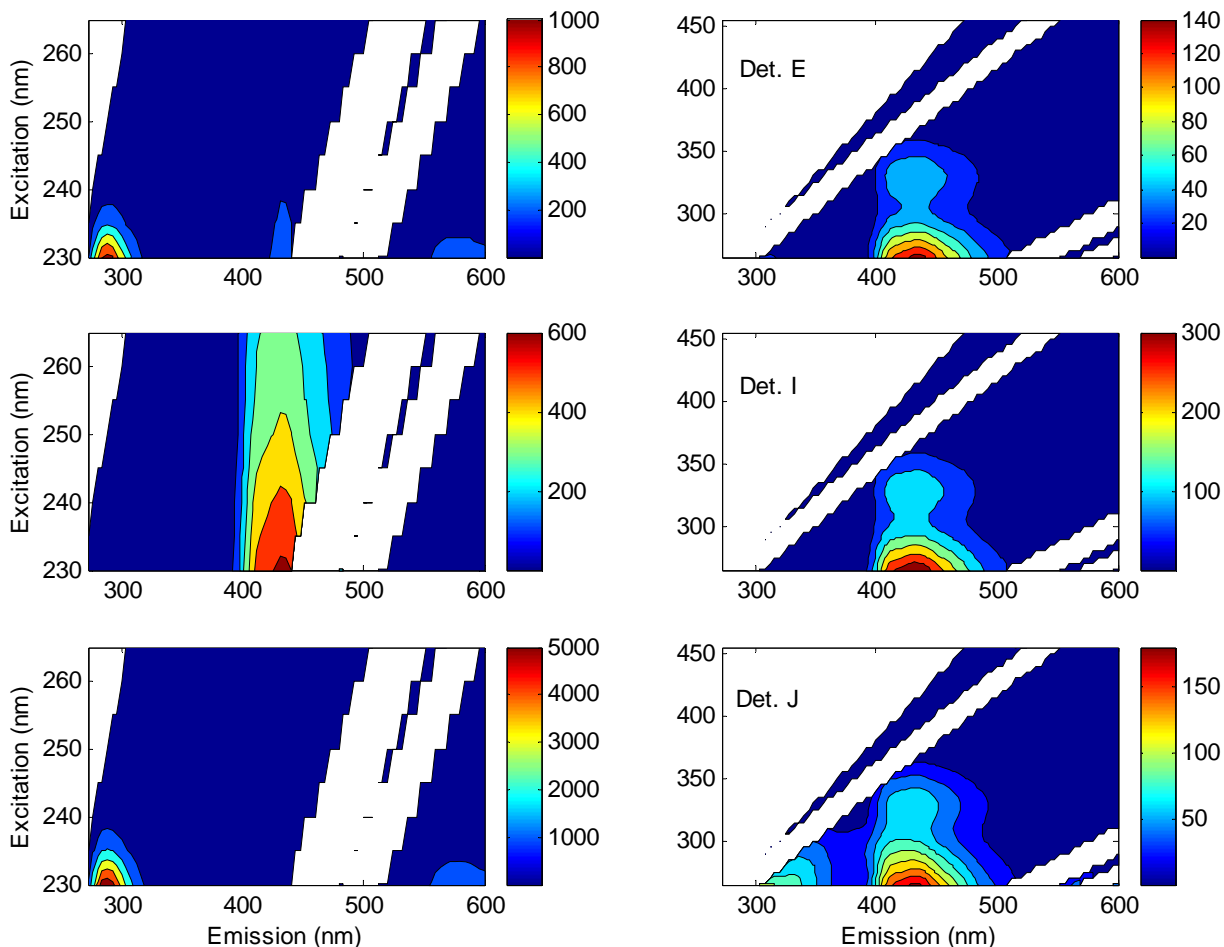


**Figure 10.** Fluorescent EEMs of detergent mixture and selected detergents used as spiking solutions during analyses of OB recovery from various sample matrices. Left panels are of low excitation wavelengths and right panels are of higher excitation to capture amplitude differences between fluorescence regions.

#### *Optimum PARAFAC Model*

Modeling was conducted with the normalized EEM data of the least dilute ambient samples available, unspiked matrix mixtures, WWTPs, OSTDSs, laundries, a detergent mixture and individual detergents (n=181). The optimum description of fluorescence components determined via PARAFAC proved to be an 8 factor model (**Figure 11**), based on the agreement between factors determined from a randomly selected half of the initiating data (**Figure 12**), or a split-half analysis (Stedmon and Markager, 2005). Excitation and emission ranges of the EEM data were trimmed to minimize noisy regions of EEM spectra and eliminate regions with little information, while maintaining UV peaks that were previously identified as helpful for detecting a mixed detergent spike. Final wavelength ranges were 230-390 nm excitation and 272-600 nm emission. Modeling was conducted on every other emission wavelength, i.e. every 4 nm, to minimize computational overhead. A smaller number of representative samples were used to confirm that comparable factors were generated whether emissions modeled were every 2 nm or every 4 nm, and that resulting factor spectra were relatively insensitive to the inclusion of selected extreme samples. Factor loadings were then computed for all samples using non-normalized EEMs and corrected for dilution as needed.

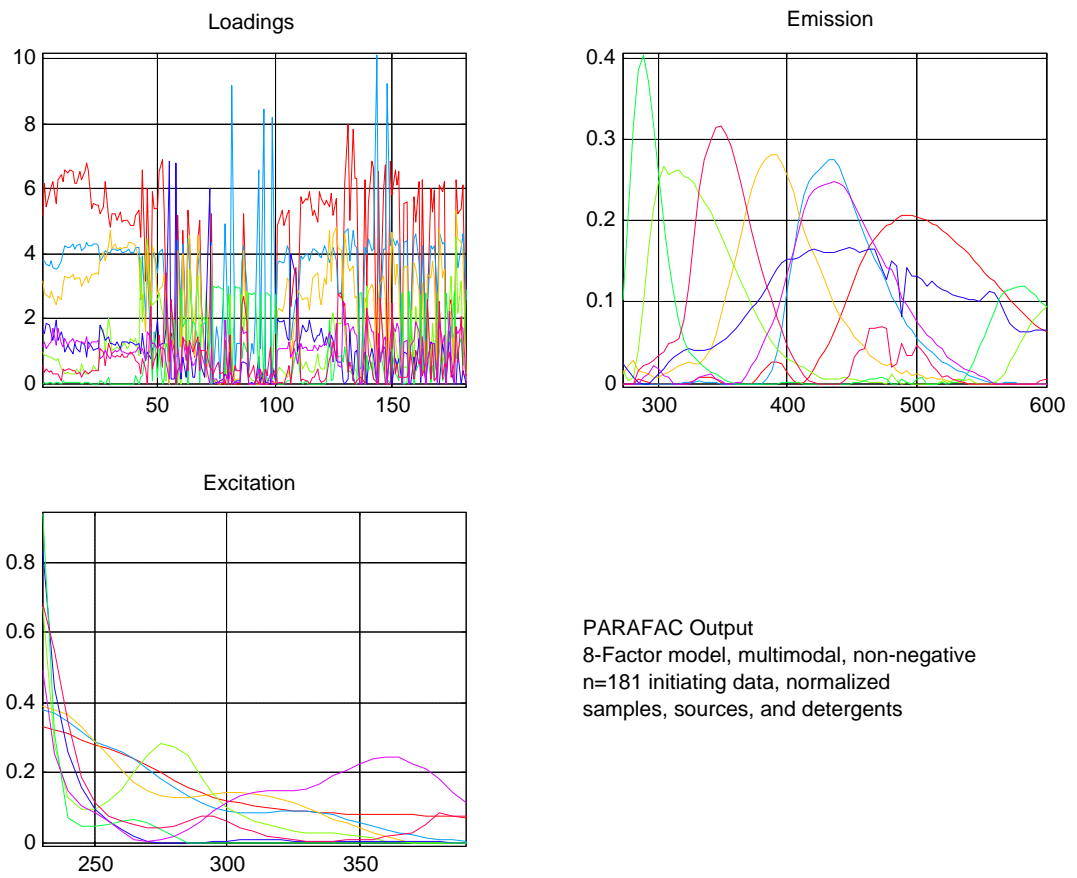


**Figure 11.** Final PARAFAC model determined from 181 normalized initiating data of ambient samples, OSTDS, WWTP, laundries, and detergents. Spiked samples were not included in initiating data.

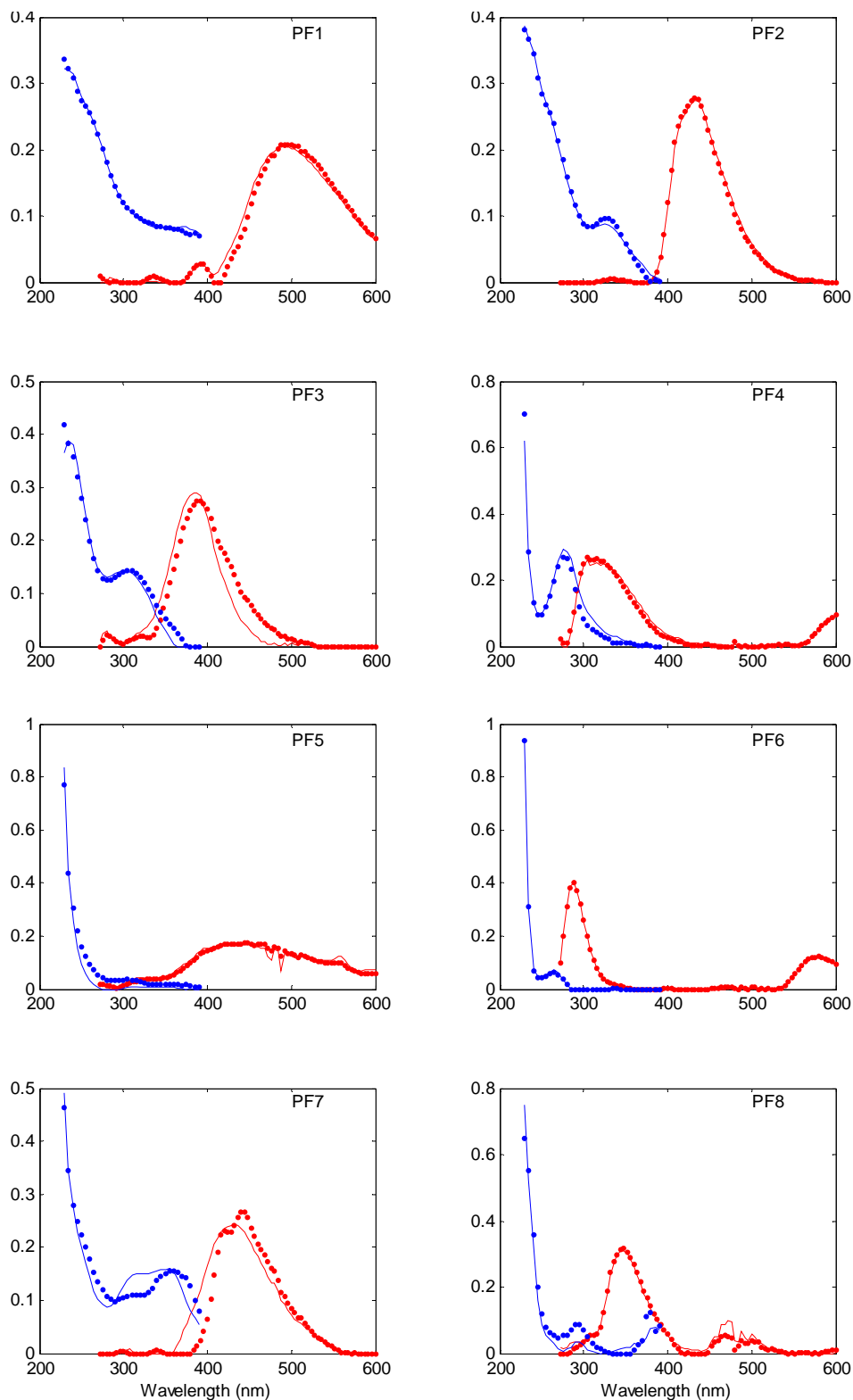


**Figure 12.** Split half analyses results in which 8 factor models were developed from random halves of initiating data. Agreement between first group (line) and second group (dotted) in both excitation (blue) and emission (red) modes indicate a robust model.

Identified factors are illustrated in **Figure 13**, and summarized according to the following discussion in **Table 2**, below. Excitation and emission spectra reported here may well be significantly blue-shifted relative to literature values, depending on absorbance of samples and whether absorption corrections were applied. The order and numbering of factors is an artifact of the model and reflects only the order of the most dominant features in the initiating and normalized data.

Factors identified were generally analogous to fluorescent landscapes reported in the literature, whether identified visually or through PARAFAC analyses. Factor PF1 was a broad emission peak most similar to fluorescence identified as terrestrially-derived humic and fulvic acids (Component 2, Stedmon and Markager, 2005; Component 3, Stedmon, et al., 2003; and Peak “H”, Baker et al., 2002). PF2 fluorescence was attributed to humics and fulvics from both natural and agricultural basins (Peaks “A”, Coble, et al. 1998; Component 4, Stedmon, et al., 2003; Components 5, Stedmon and Markager, 2005), but could also overlap the OB regions identified by Westerhoff (2001) and Baker (2002a). PF3 was most analogous to other humic peaks (Peak “M”, Coble, et al., 1998; Component 6, Stedmon and Markager, 2005). All three factors, PF1, PF2, and PF3, exhibited strong UV excitation maxima and some degree of correlation.

The spectral appearance of factors PF4 and PF8 was consistent with the numerous reported occurrences of the fluorescent amino acids tyrosine and tryptophan, respectively (Coble et al. 1998, Yamashita and Tanoue, 2003; Mopper and Shultz, 1993; Mayer, et al., 1999; Baker, 2002c; Baker, et al., 2004; Ohno and Bro, 2006). A range of wavelengths (+/- 10-20 nm) for the precise maximum of excitation and emission is present due to variations in solvent polarity, pH, and the degree of sequestration by protein structure. High levels of tryptophan, in particular, have been attributed to the presence of sewage or agricultural wastes (Baker 2002b, Stedmon, et al., 2003; Baker and Inverarity, 2004) or high levels of biological activity (Mopper and Shultz, 1993) and both tryptophan and tyrosine are also found in domestic wastes after tertiary treatment (Stedmon and Markager, 2005).

The factor PF5 exhibited a dominant UV excitation with a very broad and non-specific emission. The short wavelength excitation is consistent with reduced aromaticity of fulvic compounds (Senesi, et al., 1991), and it is attributed to either photobleached or otherwise highly degraded humic materials. PARAFAC factor 6 (PF6) was the UV peak associated with detergents and OB during the initial project although it is not a feature that has been reported in other work of CDOM fingerprinting for marine, riverine, lacustrine, estuarine, or domestic or agricultural waste environments (Coble, 1996; Baker, et al., 2004; Ohno and Bro, 2006; Baker, 2002; Stedmon, et al., 2003; Mayer, et al., 1999; Baker, 2002; McKnight, et al., 2001; Stedmon and Markager, 2005). Factor PF6 would not technically be defined as an OB compound based on the UV emission peak since the human eye is not sensitive in the 280-290 nm region. (There is a secondary emission near 570-580 nm, in the yellow region of the spectrum, that would not achieve desired whitening.) Reports of fluorescent peaks attributed to optical brighteners have previously emphasized a 340/~430 ex/em and a secondary peak of <250/~430 ex/em (Baker, 2002a) 260/430, 260/540, and 400/460 ex/em (Westerhoff, et al., 2001), and 345/430 ex/em (Takahashi and Kawamura, 2007).

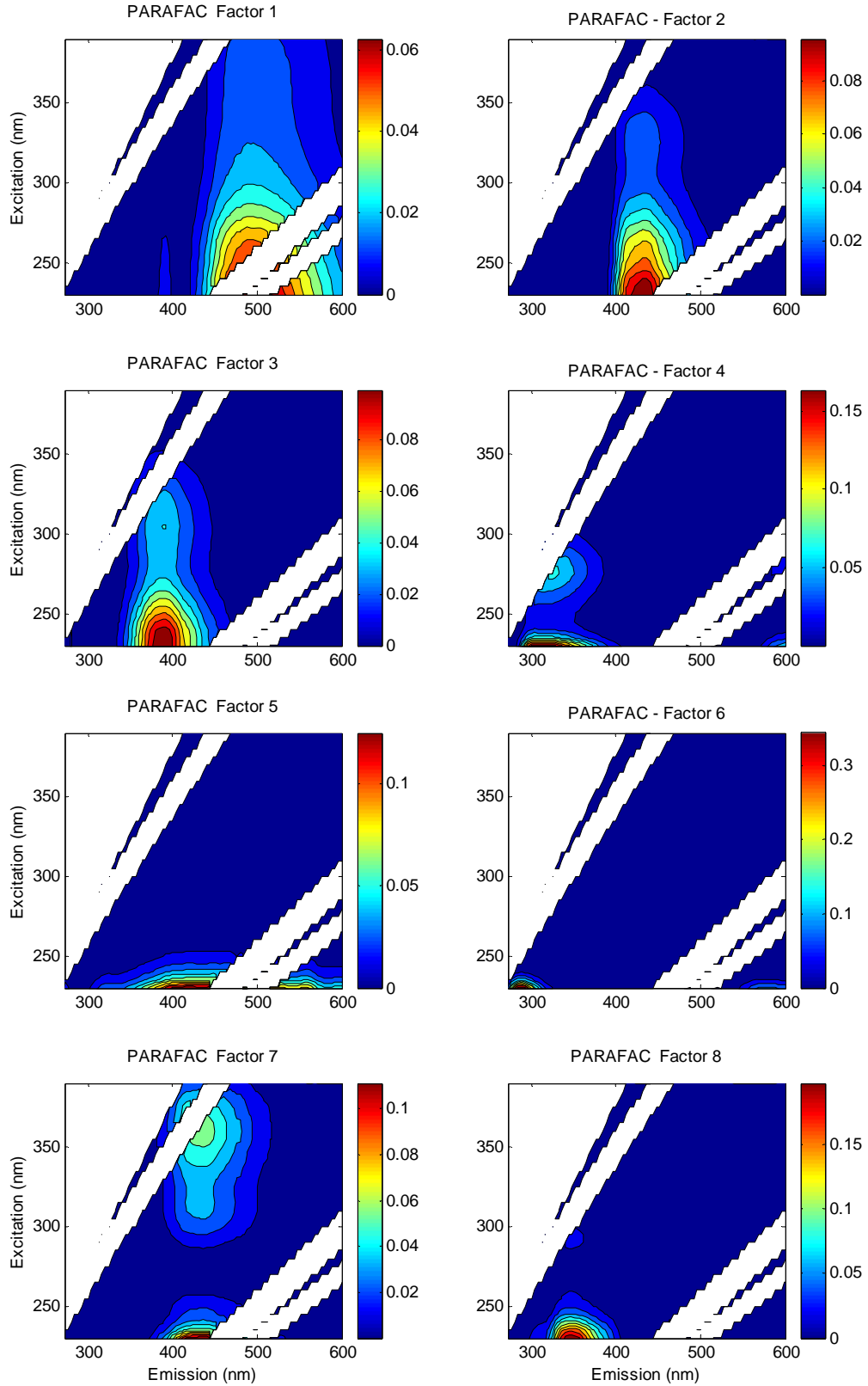


**Figure 13.** Spectral factors identified through PARAFAC modeling. Modeled range was 230-390 nm excitation and 272-600 nm emission.

Peak “C” of the literature (Coble, et al., 1998; Component 3, Stedmon, et al., 2003; Component 4, Stedmon and Markager, 2005) is most consistent with PF7 of this study, and Ohno and Bro (2006) identified a similar shape with freshly extracted wetland plants and crops. In contrast, Baker (2002a) attributed fluorescence from the same general region as PF7 to OB from a paper tissue mill. Our work indicated that PF7 also described one of the two most common OB (Hagedorn, et al., 2005), distyrylbiphenyl (DSBP) reasonably well, although both excitation and emission for DSBP were blue shifted by some 10nm relative to PF7. Of the detergents used for routine spiking, however, neither DSBP nor PF7 was substantively present in Detergent A, C, E, I, or J and was present in only one other detergent tested. The association of PF7 with OB must be considered as possible but unclear.

In order to identify the factor(s) with a quantitative fluorescent response to detergents or OB, loads were used to calculate spike recovery of samples with added detergent relative to factor loads computed for detergents in deionized water. Of the eight factors, PF2, PF6, and PF8 were potentially useful (**Figure 14**), although Detergent I had essentially no PF6 or PF8 loading and spike recoveries were not calculated for this detergent-factor load combination. Spike recoveries from the dilution matrix in the initial project (left portion of the panels in Figure 14, above) fell into two distinct categories, with the lower recoveries associated with samples that were composed of half or more OSTDS. As turbidities were within the 150 NTU maxima, and observations were within the 150 QSRF of linearity, the low recoveries were attributed to absorbing particulates and an inadequate absorption correction. Inadequate absorption correction would particularly result in low recoveries for the UV peak of PF6 due to the spectral shape of particulate absorption, which is quite similar to that of CDOM. During the second project, particulates were more strictly controlled and the spike recoveries were less distributed with mean spike recoveries of 98%, 97%, and 109% for PF2, PF6, and PF8, respectively. Of the three factors, the relative loading intensity of PF2:PF6:PF8 (as a factor loading) was approximately 2:5:1, indicating the largest detergent response in PF6. Decreased signal amplitude likely accounted for the increased scatter in spike recoveries noted for PF8.

The factors identified as quantitative for detergents and/or OB were evaluated for the influence of CDOM on factor loads using  $a_{300}$  (**Figure 15**) and restricting data to the ambient samples only. A significant correlation of supposedly “OB” factor loads with CDOM absorption would indicate that while a factor may respond quantitatively to added detergent, any CDOM in the sample could also be identified as detergent or OB. Loads of factor PF2 were significantly correlated with absorption, while PF6 and PF8 were not. The relationship was maintained when samples with OSTDS, Laundry, and WWTP components were included (**Figure 16**). PARAFAC modeling was not successful at identifying a factor which was uniquely associated with OB fluorescence in the visible range.

Response to added detergents was visible in PF2, PF6 and PF8. Of these factors, PF2 displayed correlation with absorption and therefore was also a function of CDOM. This result was consistent with close similarity in the literature values of Peaks “A”, “C”, and that of optical brightener (Coble, 1996; Coble, et al., 1998; Westerhoff, et al., 2001, Baker, 2002a). PF8, while quantitative for detergents, and uncorrelated with CDOM, was almost identical to reported fluorescence peak positions for tryptophan and has the potential to provide false positives for detergents if a highly proteinaceous sample is encountered.

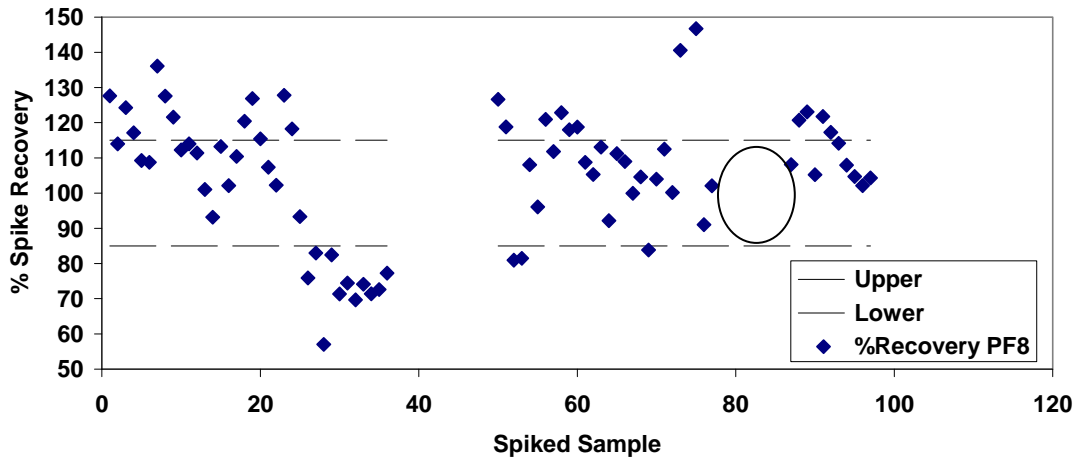
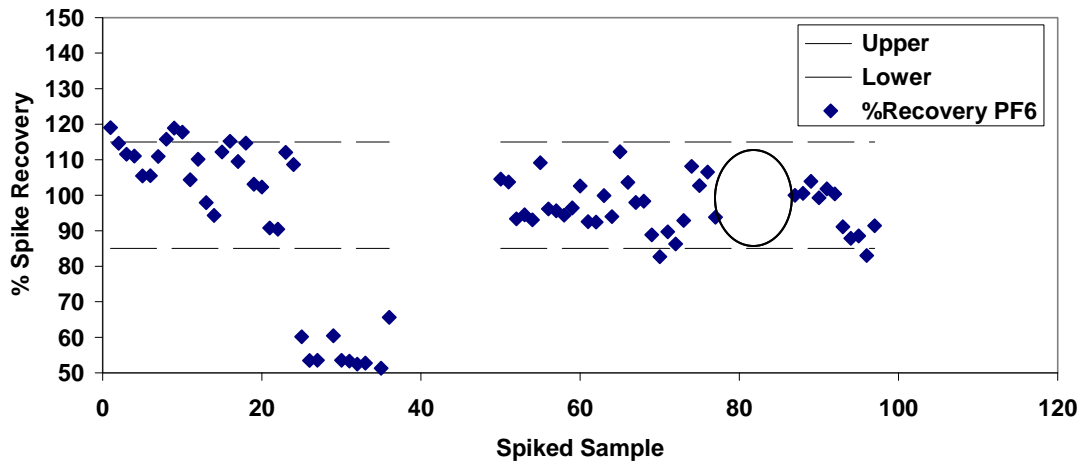
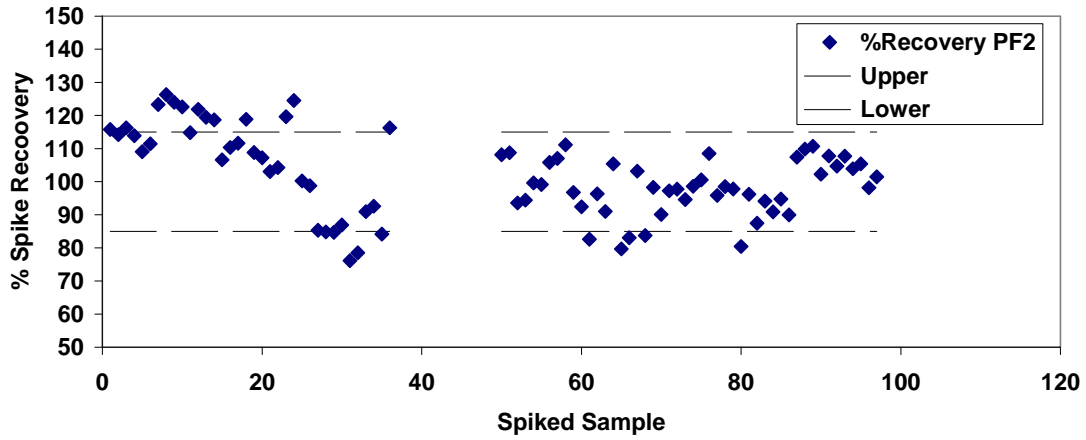


**Figure 14.** Spike recovery of factor loads in matrix samples relative to loads in deionized water. No loading of PF6 and PF8 was present for Detergent I and so no spike recovery was calculated (circled areas).

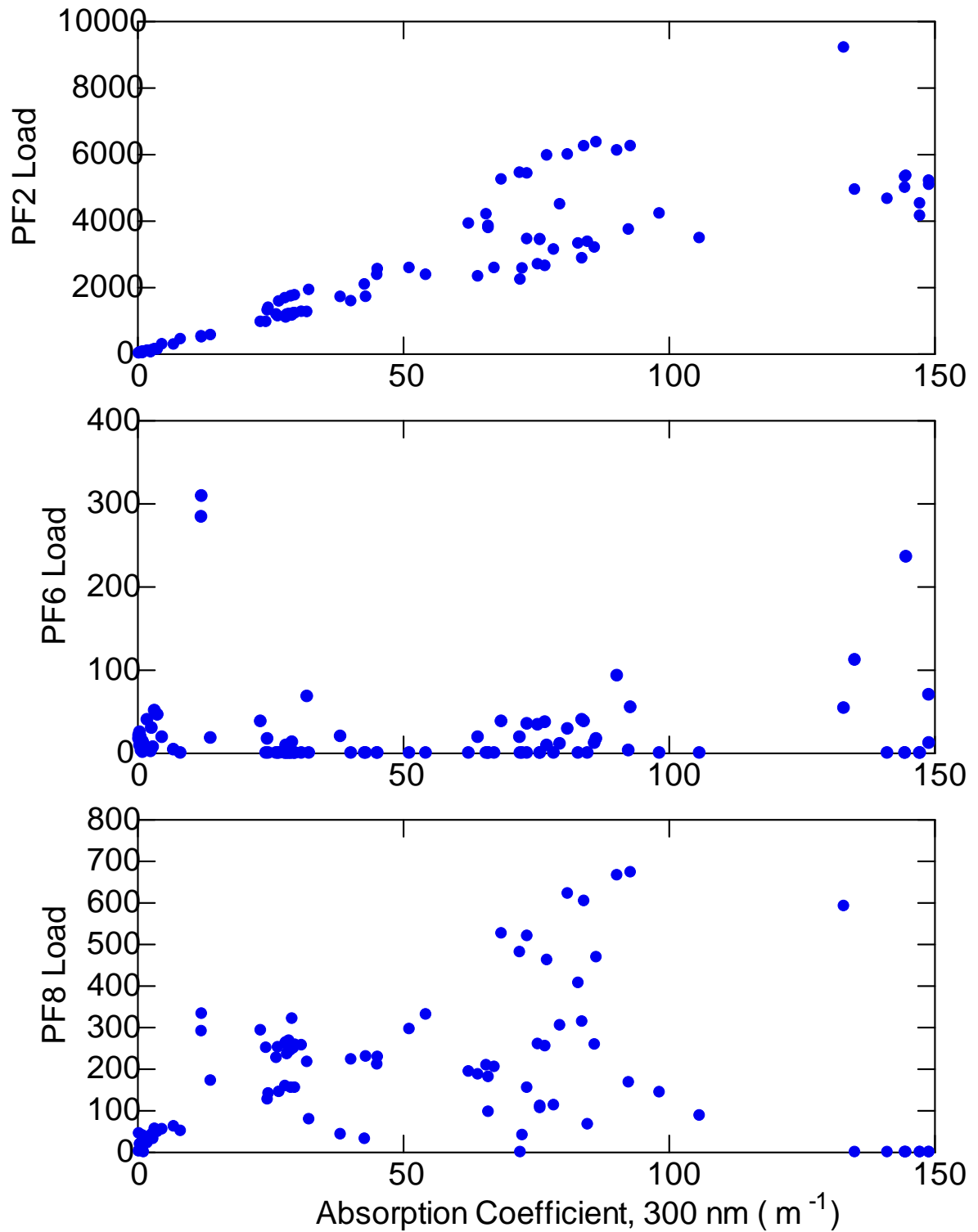


**Figure 15.** Correlation of factor loads for PF2, PF6, and PF8 with CDOM absorption ( $a_{300}$ ) indicating PF2 exhibits a fluorescent response to CDOM absorption in addition to detergents. Ambient samples only.

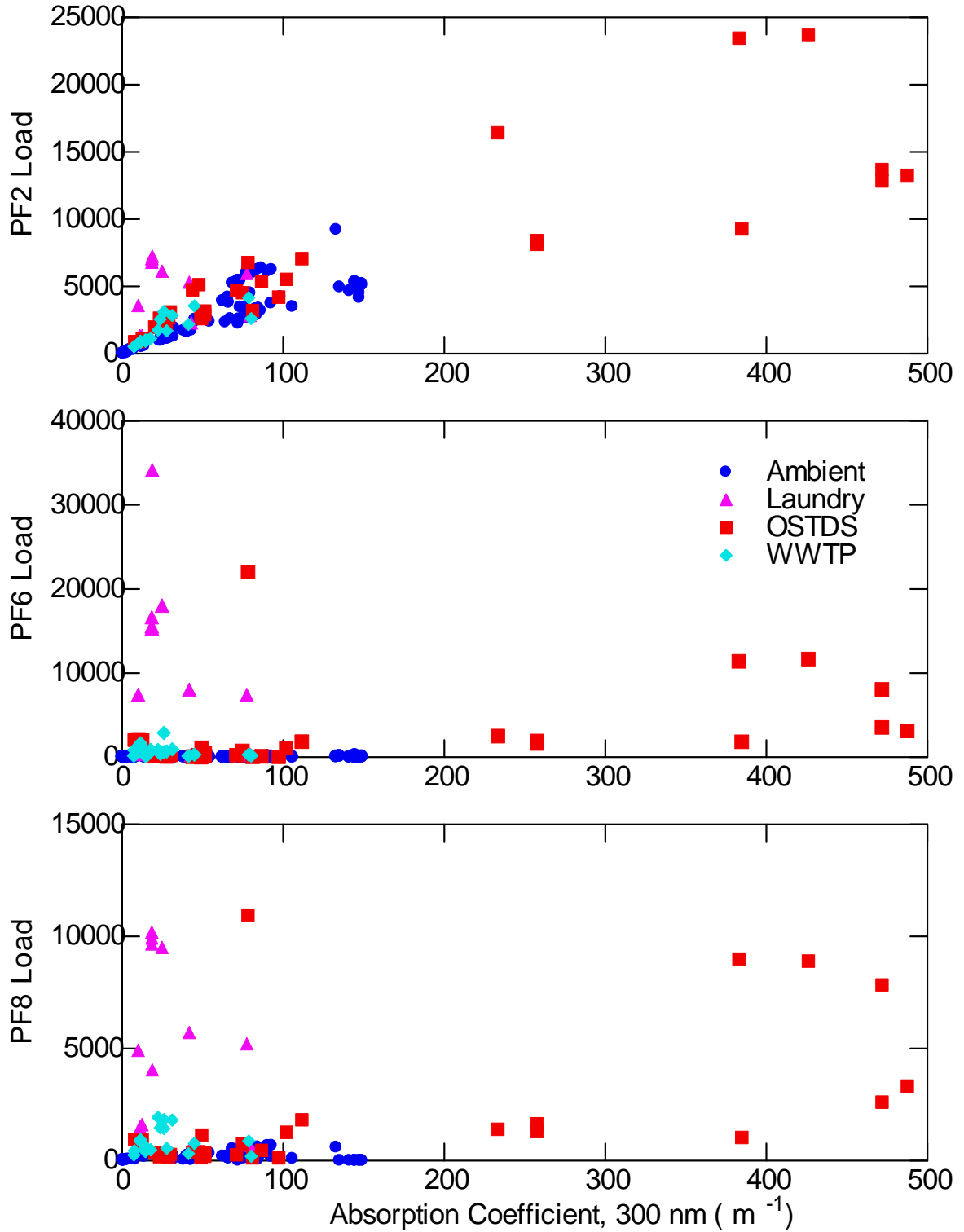


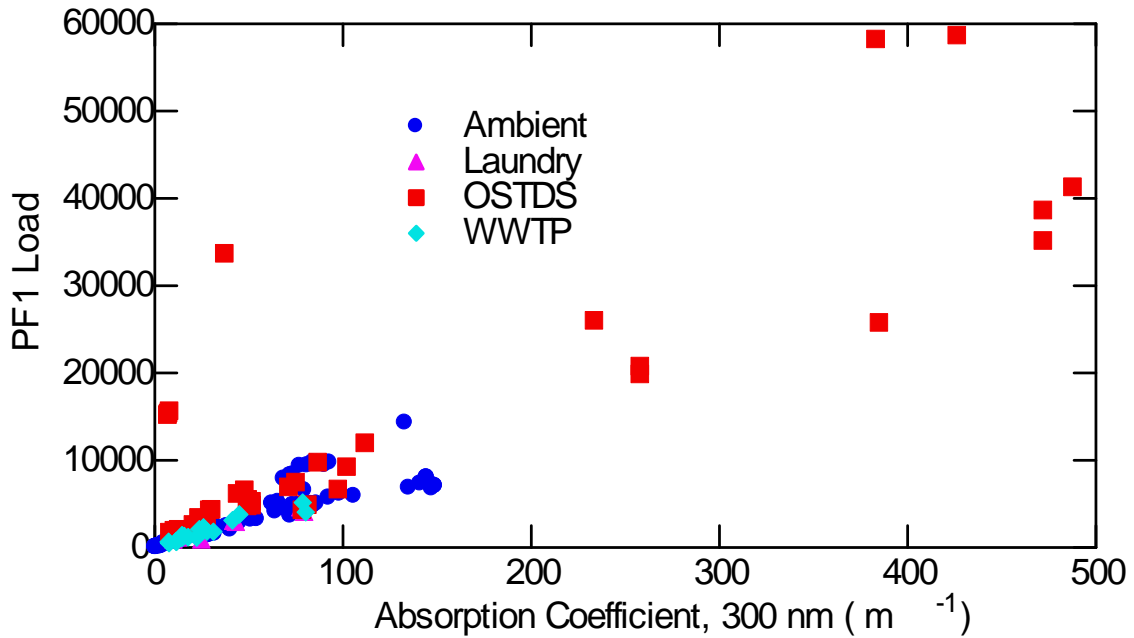
**Figure 16.** Correlation of factor loads for PF2, PF6, and PF8 with CDOM absorption ( $a_{300}$ ) indicating PF2 exhibits a fluorescent response to CDOM absorption in addition to detergents. Ambient and OB source samples.

The remaining factor loads which did not respond to added detergents or OB also displayed at least some dependence on absorption. Of the non-detergent factors, PF1 loads exhibited the most response for the range of absorption observed (**Figure 17**) and further exhibited some interesting regional differences in the ambient samples (**Figure 18**). Comparison of PF1 loads for sample and detergent spiked sample pairs also demonstrated a precision that was generally less than 15% or comparable with duplicate precision, further confirming the low sensitivity of PF1 to detergents. Factors PF2, PF3, and PF7, while all significantly correlated with absorption, displayed increasingly smaller slopes of loads as a function of absorption. In the ambient samples, loads of factors PF1, PF2, PF3 (and to a lesser extent PF7) were all highly correlated.

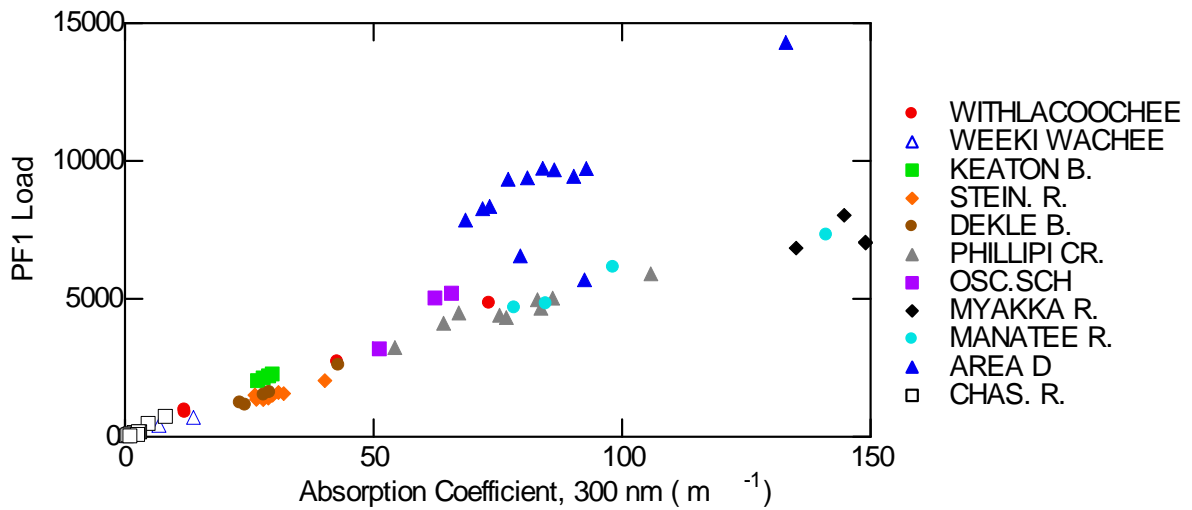
Including both ambient samples, source samples and unspiked dilution matrix samples, median factor loads by sample category appear in **Table 2**, together with a detection limit (MDL) in loading units estimated from the variation in factor loads observed for DI samples, and median loads of the various detergents. Distributions are illustrated in **Figure 19** by sample type and illustrate that the OSTDS samples and laundry samples are highly variable. The humic components PF1, PF2 and PF3 have roughly similar proportions for both ambient samples and OSTDS samples, but differ for the other categories. Laundry samples were marked by high levels of PF2 (humic and OB) and PF4 (tyrosine-like), PF6 (UV-OB), PF7 (older humics, or OB) and PF8 (tryptophan-like and OB). The low amounts of PF1 in laundry samples, relative to the observed absorption coefficients (Figure 17, above) indicated that the bulk of the PF2 in laundry samples represented detergents and OB rather than humics. WWTP samples were also noted as having lower amounts of humic fluorescence (PF1, PF2, PF3) than the ambient samples, and often higher amounts of PF4 (tyrosine-like), PF7 (older humics and OB), and PF8 (tryptophan and OB). OSTDS samples, in addition to the wide variability, were noted for often high loadings of humics (PF1, PF2, and PF3), PF4 (tyrosine-like) and PF5 (degraded material). OSTDS levels of PF6 (UV-OB), PF7 (older humics or OB), and PF8 (tryptophan-like and OB) were less than laundry samples but greater than ambient or WWTP loadings. Detergents used were primarily dominated by PF2, PF6 and PF8 loadings.

**Table 2.** Median factor loads by sample category, including an estimated method detection limit (MDL), and the detergents used for routine spiking (at an estimated 100% OSTDS effluent level).

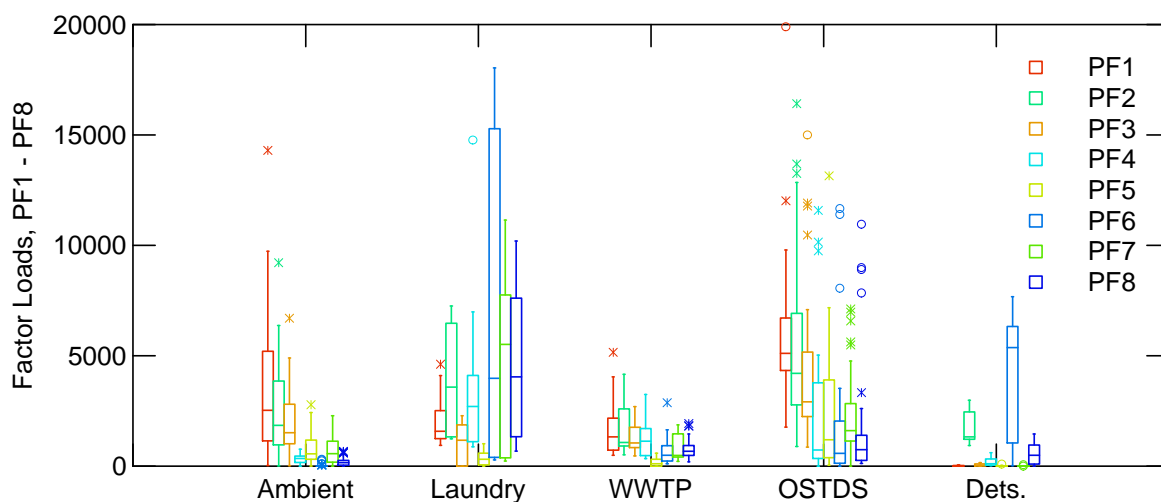
Median n=	MDL	Ambient 94	Laundry 15	WWTP 22	OSTDS 38	Detergents
PF1, Humic	7	2,530	1,579	1,327	6,836	26
PF2, Humic/OB	6	1,846	3,581	1,070	4,935	2,654
PF3, Humic	12	1,513	1,173	1,051	3,651	92
PF4, Tyrosine	53	347	2,705	1,128	1,348	210
PF5, degraded	11	561	314	111	3,608	0
PF6, UV-OB	29	3	7,379	494	1,364	10,744
PF7, Humic/OB?	2	565	5,513	488	1,754	0
PF8, Tryptophan/OB	2	157	4,046	673	932	992



**Figure 17.** Correlation of PF1 loads with absorption coefficients ( $a_{300}$ ) for ambient and OB source samples.



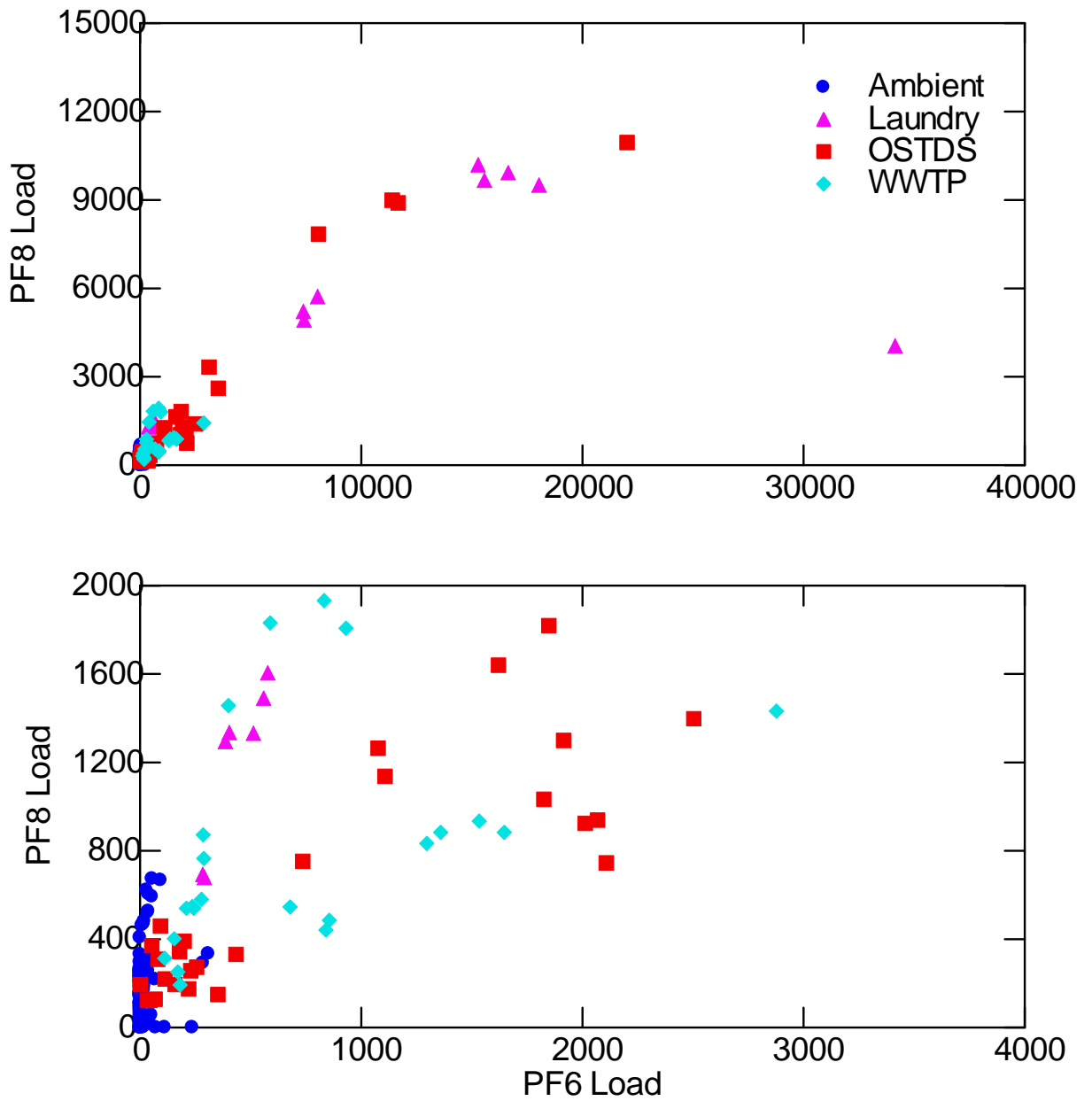
**Figure 18.** Correlation of PF1 loads with absorption coefficients ( $a_{300}$ ) for ambient samples illustrating some regional differences in the fluorescent portion of the CDOM pool.



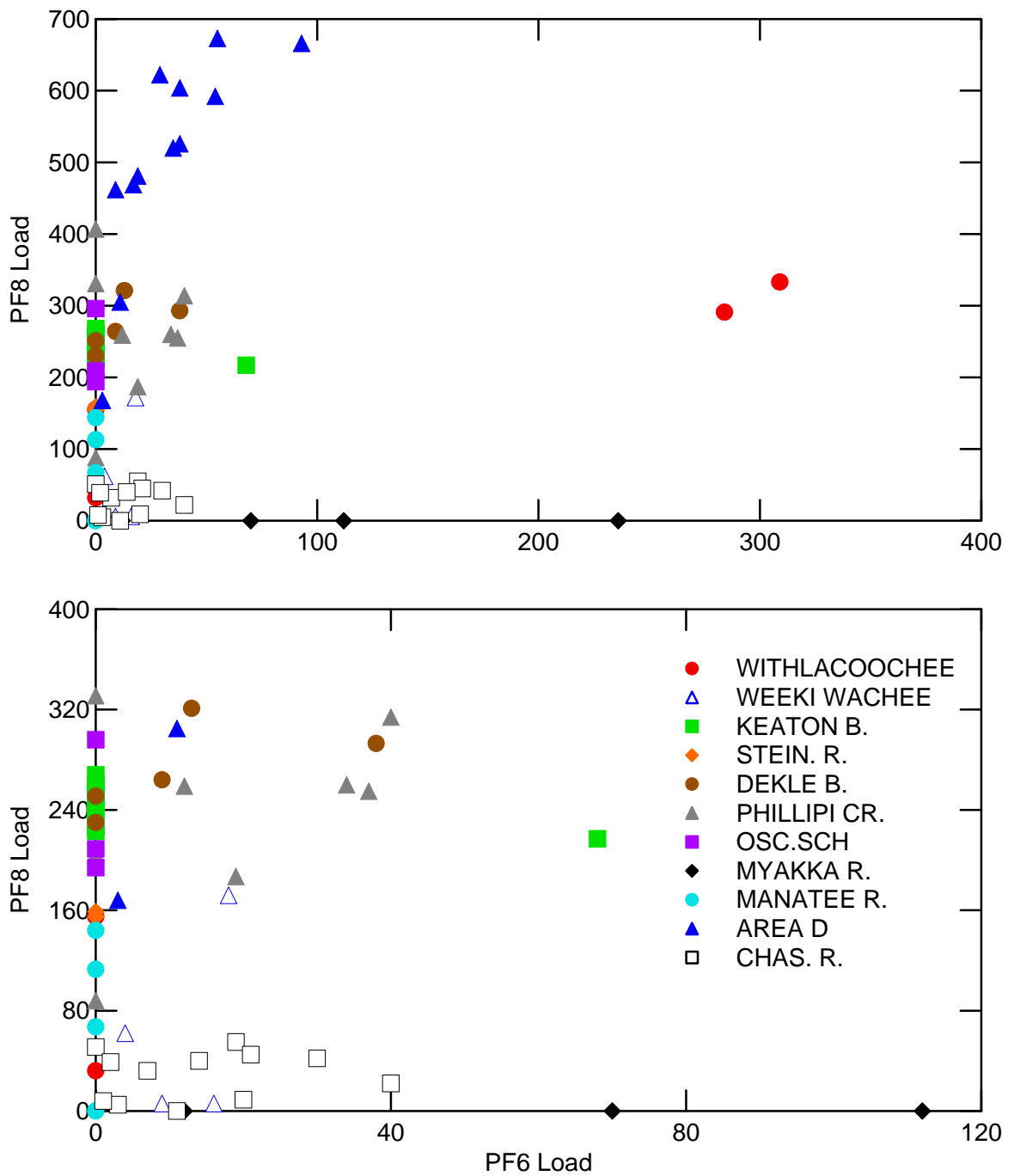
**Figure 19.** Distribution of PARAFAC factor loads, PF1 through PF8, by sample category.

Table C.1, Appendix C, lists all modeled factor loadings for ambient samples and unspiked dilution matrix sample combinations. The loads of PF6 and PF8 are jointly illustrated in **Figure 20** for ambient samples, OSTDS, WWTP and laundry facilities. The factors separate many OSTDS and most laundry samples from the ambient samples, with WWTP samples appearing intermediate. With a few exceptions, the ambient samples appear to have dominant amounts of either PF6 or PF8, but generally not both together. WWTP samples are similarly divided into two dominant relationships. **Figure 21** illustrates the regional distribution of PF6 and PF8 in the ambient samples and indicates that several stations in the Withlacoochee River have loads of both PF6 and PF8, while the Myakka River samples have more PF6 and Area D samples from Phillippi Creek have higher loadings of PF8. A further increase in scale indicates several other systems where slight amounts of both PF6 and PF8 were present.

The range in detergent formulations was emphasized by the fact that PF6 factor loadings for an estimated 100% OSTDS effluent ranged from over 14,000 (Detergent A) to ~2000 for Detergent E, with Detergent I exhibiting little response. The detergent specific PF6 factor loading data were used to transform sample PF6 loadings to a series of estimated %OSTDS effluents (Appendix C, Table C.2). The detergent-specific %OSTDS effluents were then averaged for an approximate %OSTDS effluent value in order to compare stations.



**Figure 20.** Factor loads of PF6 and PF8 by sample category, at two different scales.



**Figure 21.** Factor loads of PF6 and PF8 by region for ambient samples, at two different scales.

### *Conceptual Design of Field Instrumentation – Method 1*

The PARAFAC modeling identified a single spectral component (PF6) which was quantitative with added detergent, was uncorrelated with absorption or CDOM, and was not apparently affected by other known fluorescent components. (Although PF6 should not technically be termed an OB since it does not fluoresce the visible region, the relationship with detergent can provide the same indicator features as OB.) The first approach for conceptual design of a field method for detergent/OB detection takes advantage of the wavelengths indicated by the PF6 factor uncontaminated by CDOM dependence.

PF6 has a maximum fluorescence of <230/288 ex/em with a minor emission near 580 nm (see **Figure 12**, PF6). Although maximum excitation energy is <230 nm, excitation increases dramatically as for all wavelengths below 240nm. A possibly interfering factor in emission mode (**Figure 22**) is PF4, indicative of tyrosine. The overlap, however, indicates that if fluorescence emission can be observed at slightly less than 288 nm, any interference from tyrosine-like fluorescence will be minimized. **Figure 23** illustrates emission spectra from a 235 nm excitation for a detergent in deionized water at 50% typical OSTDS, and an ambient sample, together with a 25% and a 50% OSTDS level spike indicating that amplitude of the selected peak provided adequate sensitivity and freedom from CDOM effects.

If a filter-type fluorometer is the instrument platform of choice, then the narrow wavelength range will require precise filters and a comparatively intense light source to maximize the detected signal. For excitation, a quartz mercury lamp, with a dominant mercury line emission near 254nm, would likely not provide sufficient or suitable excitation energy below 240 nm. A deuterium lamp does provide additional energy in the proper region of the spectrum. A short pass cutoff filter would also be needed to limit excitation wavelengths, preventing interference with emission detection. The cutoff wavelength will be a function of the emission filter and band pass characteristics but likely near 240 nm. A quartz sample cell would be helpful to maximize excitation energy and fluorescence transmission. Fluorescence detectors could employ a photocell provided spectral response is relatively flat over the region of interest. A spectral dispersion device such as a grating or prism would allow a charged coupled device (CCD) detector to be directly without an emission filter, provided fluorescent intensity is sufficient.

The EEM data and PARAFAC model results were queried to produce **Figure 24**. The PARAFAC modeled PF6 loads, which the field method is endeavoring to reproduce, are presented as a function of a single wavelength pair 230/286 ex/em of fluorescence, both before and after correction for absorption. The necessity for absorption correction is demonstrated. As PF6 loads for a 100% OSTDS effluent were approximately 9,500-10,000 units (depending on detergent), the sensitivity of the selected fluorescent pair to PF6, and by extension, to detergents/OB is excellent with variation of less than a few percent of expected OSTDS effluent, provided absorption correction is applied.

An ideal approach for a field instrument would be to measure absorption using the same excitation source (and in the same sample volume or cell) as is used for fluorescence. This has the advantage of not requiring another light source and of measuring absorption very close to the wavelength where it would be applied. Absorption at nearby wavelengths would be estimated using either a classic exponential model (Jerlov, 1976) or more recent formulations (Twardowski, et al., 2004).

If absorption measurements are incorporated directly into the fluorescence instrument, absorption path length could be optimized for expected optical density of samples to be encountered but would likely be 1 cm or less for freshwater and estuarine applications. Light source and optical path would need to be robust and stable, and either calibrated and zeroed frequently (analogous to a single beam spectrophotometer) or additional optics would be required to form a double beam instrument that could correct for lamp fluctuations over time. (The double beam approach would provide additional advantages for normalizing fluorescence data as well.) If absorbing particulates need to be addressed, then an internally reflective sample cell would be needed. Alternatively, an indication of turbidity, perhaps measured as the scattered excitation energy at the primary or secondary Rayleigh lines could alert an operator that biases could exist.

Before recommending the expense and complexity of additional electronics and/or sample path for absorption measurement, we investigated several methods to empirically estimate absorption from some portion of the fluorescence spectrum. Using only ambient samples, successive regressions were performed of raw fluorescence at specific wavelength pairs against measured absorption coefficients at 250 nm. The resulting response surface of correlation coefficients indicated that fluorescence in the region of 370/576 ex/em provided the best estimates of  $a_{250}$  (**Figure 25**). The relationship, although significant ( $r^2 > 0.8$ ), indicated that predictive use would result in errors of up to  $50 \text{ m}^{-1}$  in estimated absorption coefficients (**Figure 26**) with a resulting range in absorption correction factors of over 300%. With inclusion of OSTDS and other source samples, the relationship deteriorated. Prediction of absorption at alternate wavelengths displayed similar variation. It is clear that the relationship between absorptive and fluorescent organic matter is complex and non-uniform.

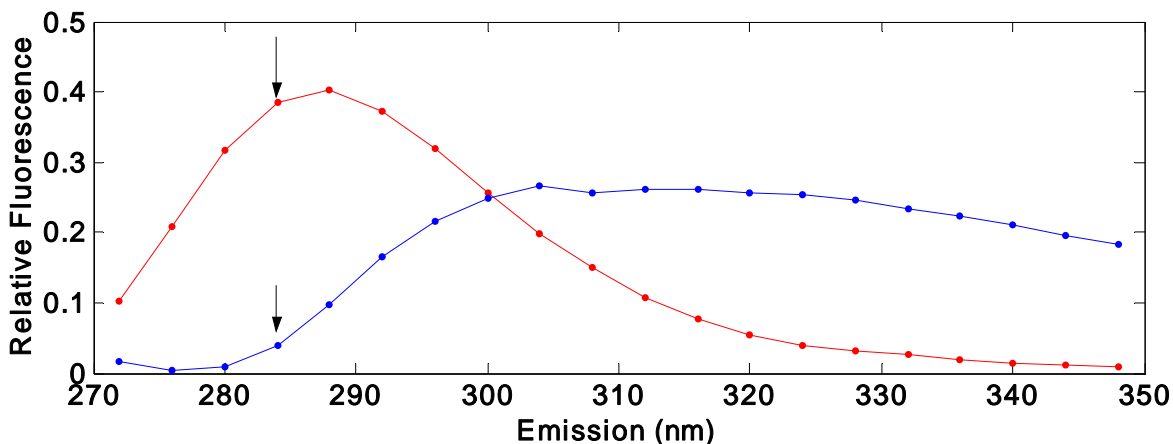


**Figure 22.** Overlap of the emission spectra of PARAFAC factors PF6 (red) and PF4 (blue). Arrows indicate a region of maximal response of PF6 with reduced influence of PF4.

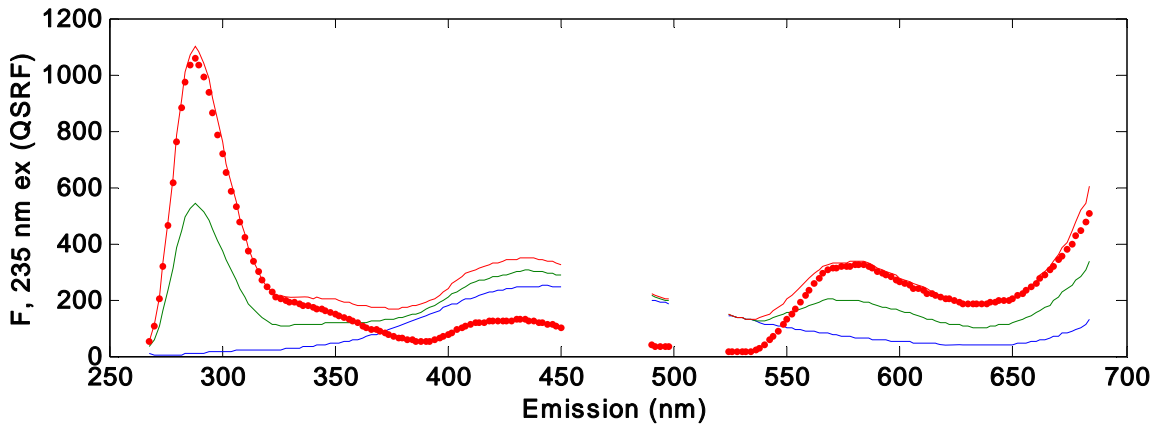


**Figure 23.** Corrected fluorescence emission spectra from 235 nm excitation of a Detergent A at 50% “typical” OSTDS (red dotted), moderate CDOM sample (blue), and sample spikes at 25% (green), and 50% “typical” OSTDS (red).

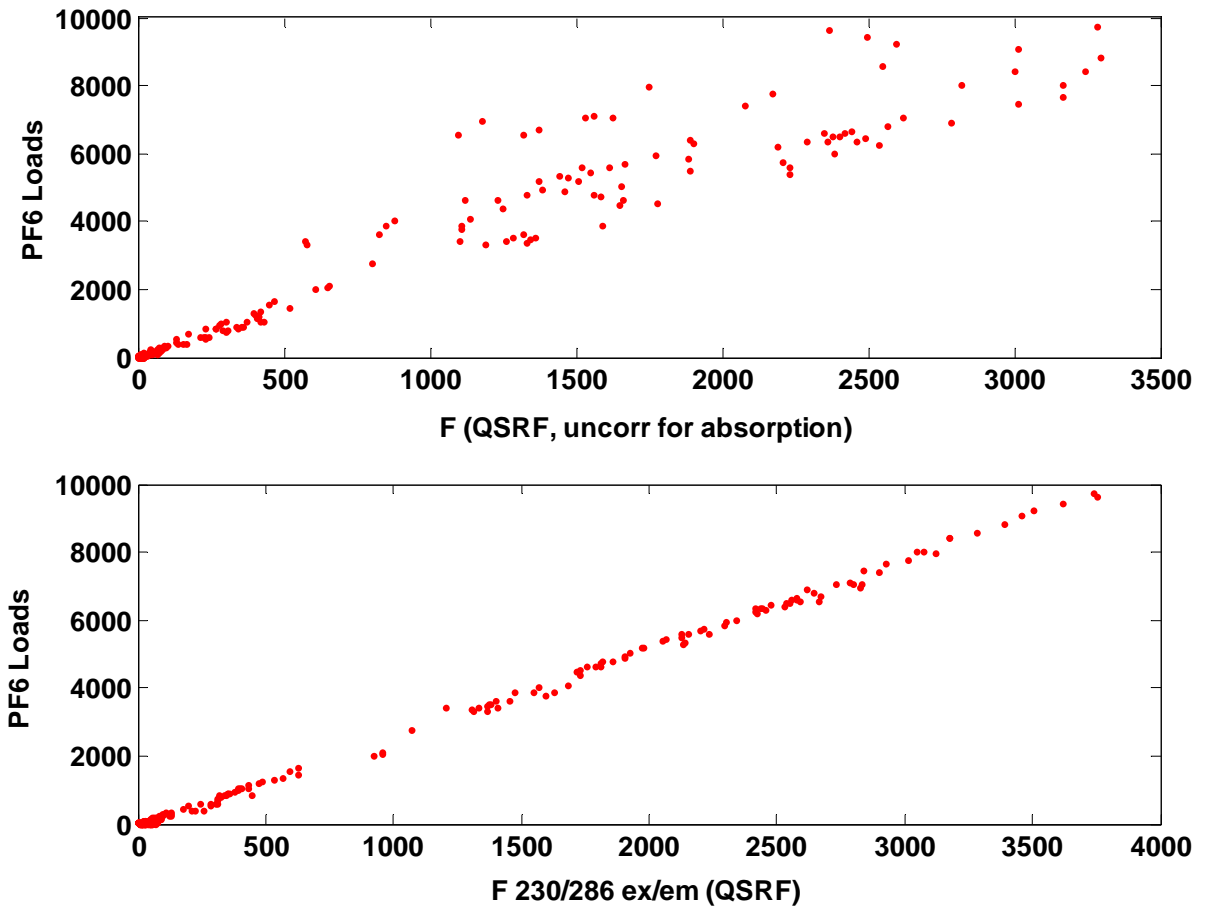


**Figure 24.** Modeled PF6 factor loads as a function of fluorescence, 230/286 ex/em, both uncorrected and corrected for absorption, for ambient, source, and spiked samples.

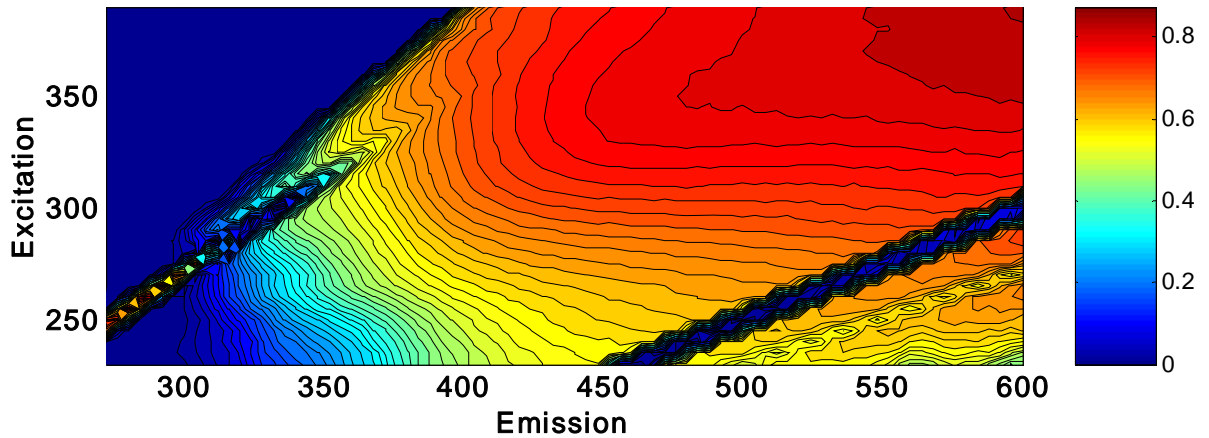


**Figure 25.** Compiled  $r^2$  values of absorption coefficients at 250 nm ( $a_{250}$ ) as a function of fluorescence at individual wavelength pairs. Ambient samples only.

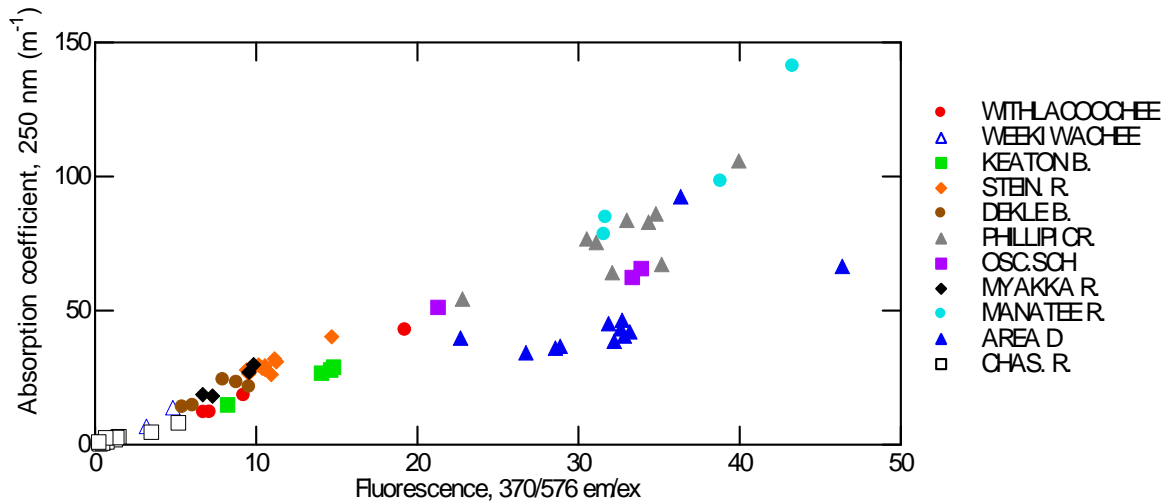


**Figure 26.** Absorption of ambient samples as a function of fluorescence at the most highly correlated ex/em wavelength pair.

There were regional groupings of measured absorption as a function of fluorescence, however (Figure 26, above), with approximately linear relationships for some sites. As a result, absorption along a simple gradient between two end members might be reasonably approximated from fluorescence data with a minimum number of site specific absorption measurements, but other water masses or sources mixing with this gradient would be expected to have very different absorption fluorescence/absorption ratios and would not be accurately corrected for absorption. [This is illustrated by data from Area D, in which a small linear canal (the bulk of the data) was sampled, including the receiving waters (two outliers to the upper right) and a pipe discharging into the canal (outlier to the left).]

As a final attempt to predict absorption coefficients, the spectral shape of PARAFAC factors were used to *a priori* select wavelengths of fluorescence where CDOM factors dominated. As the PF1 factor was the most clearly associated with CDOM, unassociated with OB, and loads of PF1 were correlated with absorption, the shapes of the PF1 spectra were examined to select wavelength pairs with minimal influence from other factors. Fluorescence at 290/540 ex/em fulfilled these criteria, but agreement between absorption and fluorescence for ambient samples did not improve beyond that illustrated above.

Calculation of absorption for multiple wavelengths from measurement at a single wavelength was much more successful than absorption derived from fluorescence. From a single absorption coefficient measured in the UV region ( $a_{250}$  in this example), absorptions can be computed at alternate wavelengths using the mean spectral slope between 250 and 300 nm for all samples (Jerlov, 1976) and 250 nm as a reference wavelength. The formula is:

$$a_{\lambda} = a_{250} * e^{-S * (\lambda - 250)}$$

where S is the spectral slope and for both ambient and source samples averaged 0.0158 for a 250-350 nm wavelength range. (Slopes for a longer wavelength range averaged 0.0183 for a 300-450 nm wavelength range with a 350 nm reference wavelength.) The resulting  $a_{300}$ , modeled from observed  $a_{250}$ , averaged 98.8% of observed  $a_{300}$  (**Figure 27**) and indicated that extension of measured absorption to alternate wavelengths, whether based on a large geographic scale value or more regionally-derived data, can provide the basis for a robust absorption correction of fluorescence. In addition, individual sample slopes and the resulting agreement between modeled and observed absorption indicated no bias from OSTDS, WWTP, other sources of OB, or added detergents.

Lastly, quinine sulfate was used as a fluorescence standard to monitor instrument efficiency and lamp output over time for EEM data collection. If the field instrument is constructed with fluorescence measurements in the UV range alone, then some other standard with fluorescence maximum in a nearby region would be more appropriate. Alternatively, fluorescence should also be measured in the 425-450 nm range where quinine sulfate has sufficient signal at a 230-249 nm excitation to provide daily normalizing data.

### *Conceptual Design of Field Instrumentation – Method 2*

Quantification of OB could also employ some form of fluorescence ratio, targeting two or more wavelength regions where 1) CDOM alone and 2) OB (together with CDOM) fluoresce. (Both in PARAFAC modeling and in empirical examination of spectra, there were no visible regions where the visible region of OB fluoresced and CDOM did not.) The dual wavelength field fluorescence method was employed in the prior project (Anastasiou, 2007) and in other work in which the technique was developed (Dixon et al., 2005; Dixon and Julian, 2005). The dual wavelength method used filters to achieve a 300-400 nm excitation and 440 nm and 550nm emissions, selecting wavelength ranges based on literature and observed values of OB and CDOM fluorescence.

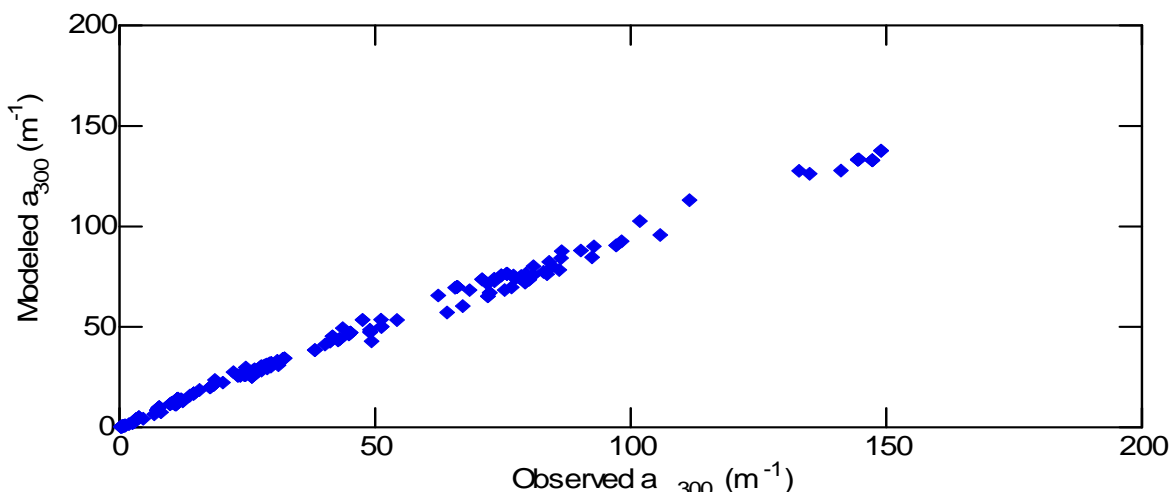


**Figure 27.** Correspondence of modeled and observed absorption coefficients at 300nm ( $a_{300}$ ) for all samples, using measured  $a_{250}$ , a mean spectral slope of 0.0158, and a reference wavelength of 250nm.

**Figure 28** illustrates the dual wavelength concept under varying amounts of CDOM but with fixed amounts of added OB. For a given amount of CDOM fluorescence, the simple ratio  $F_{440}/F_{550}$  will increase from a sample with no OB ( $C/A$  in the upper panel) to the same sample with added OB ( $(C+D)/A$ ). When CDOM is low, however, the ratio increases by a much larger degree for the same amount of added OB (bottom panel), resulting in a depressed ratio response to OB in highly colored waters, and non-linear behavior. The simple  $F_{440}/F_{550}$  ratio is what the dual wavelength method has used previously. A data processing refinement which could be used regardless of wavelengths selected would be to compute an expected fluorescence from CDOM alone based on either compiled data or regionally specific values from an area in which OB are assumed to be absent. The ratio between  $F_{440}/F_{550}$  in a clean area (or the lowest ratio observed for a field survey) would be used to compute all C values from all observed  $F_{550}$  (A). Observed  $F_{440}$  (C+D) would then be reduced by the expected  $F_{440}$  (C), and the calculated quantity (D) would be linear with OB regardless of background CDOM fluorescence. This was termed the adjusted ratio method to distinguish it from the simple ratio of  $F_{440}/F_{550}$ , and is expressed as:

$$OB = F_{440Obs} - \left( \frac{F_{440Clean}}{F_{550Clean}} \right) * F_{550Obs}$$

In addition to the wavelengths previously selected for emission ratios (440nm, 550nm) PARAFAC factors were also examined for improvements in wavelengths for the same conceptual approach. PF2 was identified as a modeled factor, with a quantitative responsive to detergents, that was also correlated with absorption of the samples. Using the PF2 spectra, after correction for CDOM, would be preferable to PF8 in that removal of CDOM fluorescence from PF2 could be conducted optically in real time rather than evaluating tryptophan contributions to correct PF8 loads. The wider range of excitation wavelengths to which PF2 responds, relative to PF6, would also result in less rigorous lamp requirements, greater energy throughput in the sample compartment, and perhaps greater sensitivity than for Method 1, above. Visible emissions of PF2 are in the region specifically identified with OB, both in the literature and in our work. Longer wavelengths for both excitation and emission are in a region of the absorption spectra where change is minimal relative to the shorter UV wavelengths, and may simplify absorption corrections.

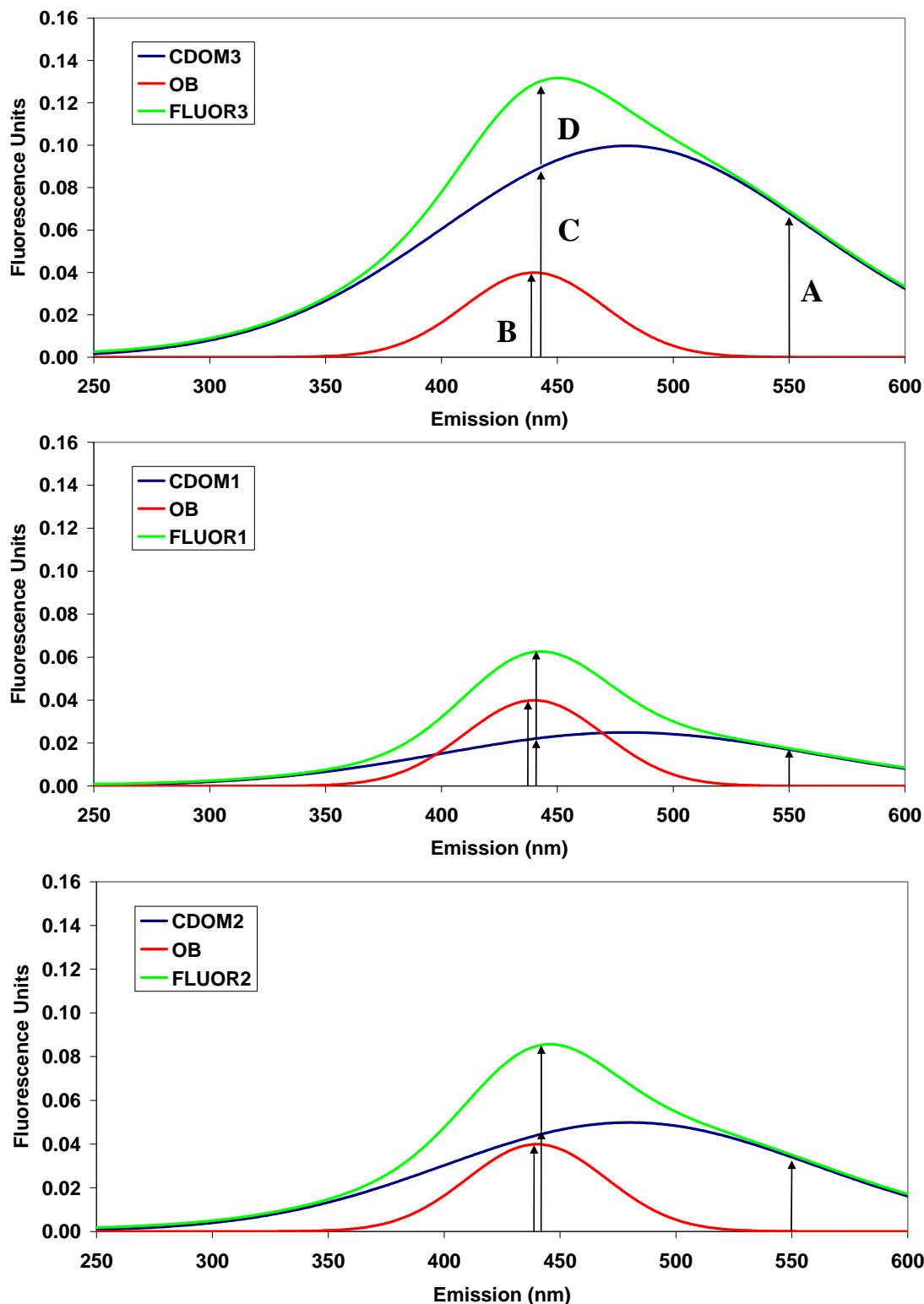


**Figure 28.** Examples of a fixed amount of OB (red) added to samples with varying CDOM (blue) to create a combined spectra (green). Arrows A and C are CDOM fluorescence, arrows B and D are fluorescence due to OB. Spectra are constructed from Gaussian functions for illustration.

To correct for CDOM influence on the levels of PF2, emission spectra of PF1 and PF2 were examined for regions of overlap (**Figure 29**). Loads of PF1 were the most closely correlated with sample absorption coefficients. Fluorescence from wavelengths near 410 nm and 550 nm would have the maximum influence of factors PF2 and PF1, respectively, while minimizing response from the other factor. The illustrated response is proportionally consistent for PF2 and PF1 between a 230-350 nm excitation. Above 350 nm, the response of PF2 declines rapidly relative to PF1, while below 300 nm excitation, a number of other modeled factors would interfere.

A standard mercury vapor fluorometer lamp with a broad emission in the near UV (300-425), coupled with a 350 nm cutoff filter, would provide a suitable source to capture the optimum excitation region. The proposed regions were compared with the previous dual wavelength excitation and emission regions of 440 and 550 nm (**Figure 30**) which used a 300-400 nm excitation filter. The lower wavelength proposed based on PARAFAC modeling (410 nm), will require a restricted excitation range relative to the previous field method to avoid Rayleigh emissions (area A of Figure 30) that would increase with increased turbidity. Inclusion of the Raman region (area B) provides a very minor contribution to the signal for all samples except for deionized water and the clearest ambient samples. If it is anticipated that very clear water will routinely be sampled, then a 325 nm cutoff filter may be needed for the 410 and 550 nm emissions, or a 375 nm cutoff filter for the 440 and 550 nm emissions. The disadvantage to reduced excitation range is a reduction in energy and resultant fluorescence unless the band pass of the emission filters is increased. Limiting excitations to greater than 300 nm will also prevent other turbidity-based secondary Rayleigh emissions (area C of Figure 30).

The necessity of absorption correction was evaluated for the dual wavelength simple ratio approach. **Figure 31** illustrated the  $F_{440}/F_{550}$  ratio from raw fluorescence data as a function of the ratio computed from absorption corrected data, and again for  $F_{410}/F_{550}$  using a 300-350 nm excitation. The relationship between raw and absorption corrected ratios is illuminating in that  $r^2$  are  $>0.997$  and slopes are very near unity. Comparable relationships appear for both  $F_{440}/F_{550}$  and  $F_{410}/F_{550}$ , with  $(RF_X/RF_{550}) = 1.02*(F_X/F_{550}) - 0.1$ , where RF is raw fluorescence and F is fluorescence corrected for absorption. The implication is that for these wavelength pairs, due to the similarity of spectral slopes and the proximity of the wavelengths examined, the ratio of absorption correction is essentially constant, regardless of absorption amplitude, and that the ratio of absorption correction at each wavelength of a pair is very close to one. At wavelengths below 400 nm spectral slopes vary more rapidly and eliminating absorption corrections would generate larger errors. The relationship would allow the dual wavelength ratio method to possibly be conducted without a specific absorption correction, while adding only a small amount of uncertainty. As such, it would be most useful in closed water bodies with relatively constant levels of CDOM, but would not provide quantitative responses to OB under varying CDOM concentrations, as was illustrated in Figure 28, above.

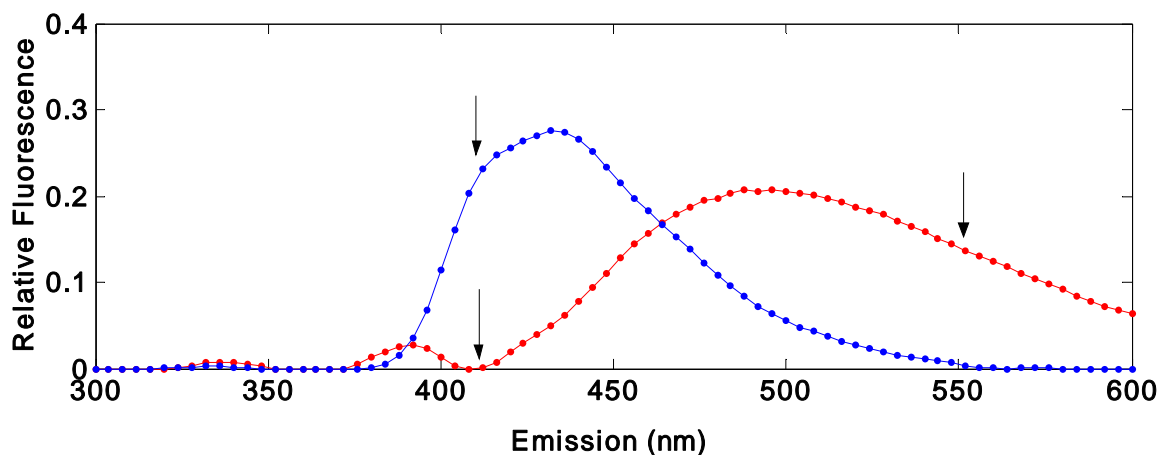


**Figure 29.** Overlap of the emission spectra of PARAFAC factors PF1 (red) and PF2 (blue). Arrows indicate a region of maximal response of PF1 with reduced influence of PF2.

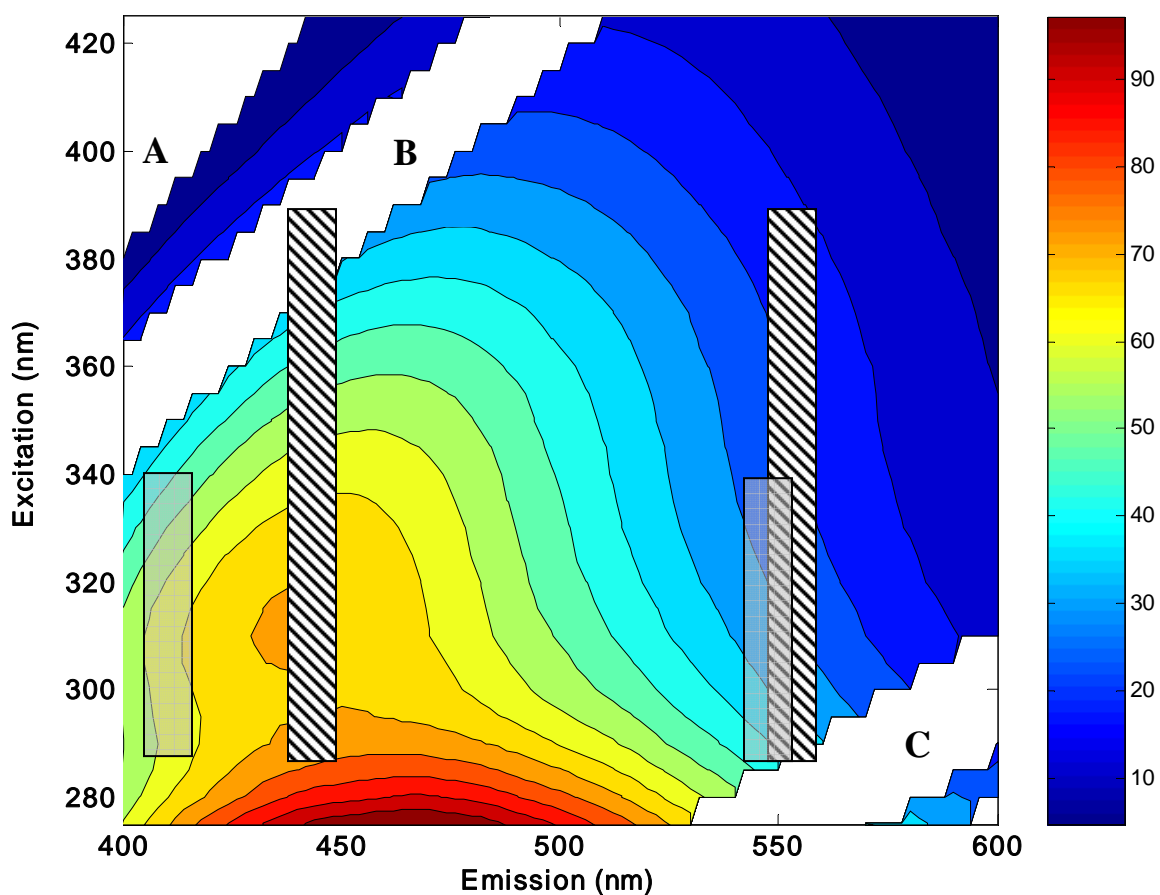


**Figure 30.** Regions of excitation and emission for the dual wavelength method previously used (440 and 550nm, hatched bars) and the proposed method based on PARAFAC factor emission spectra (410 and 550 nm, gray bars). Regions A-primary Rayleigh, B-water Raman, and C-secondary Rayleigh.

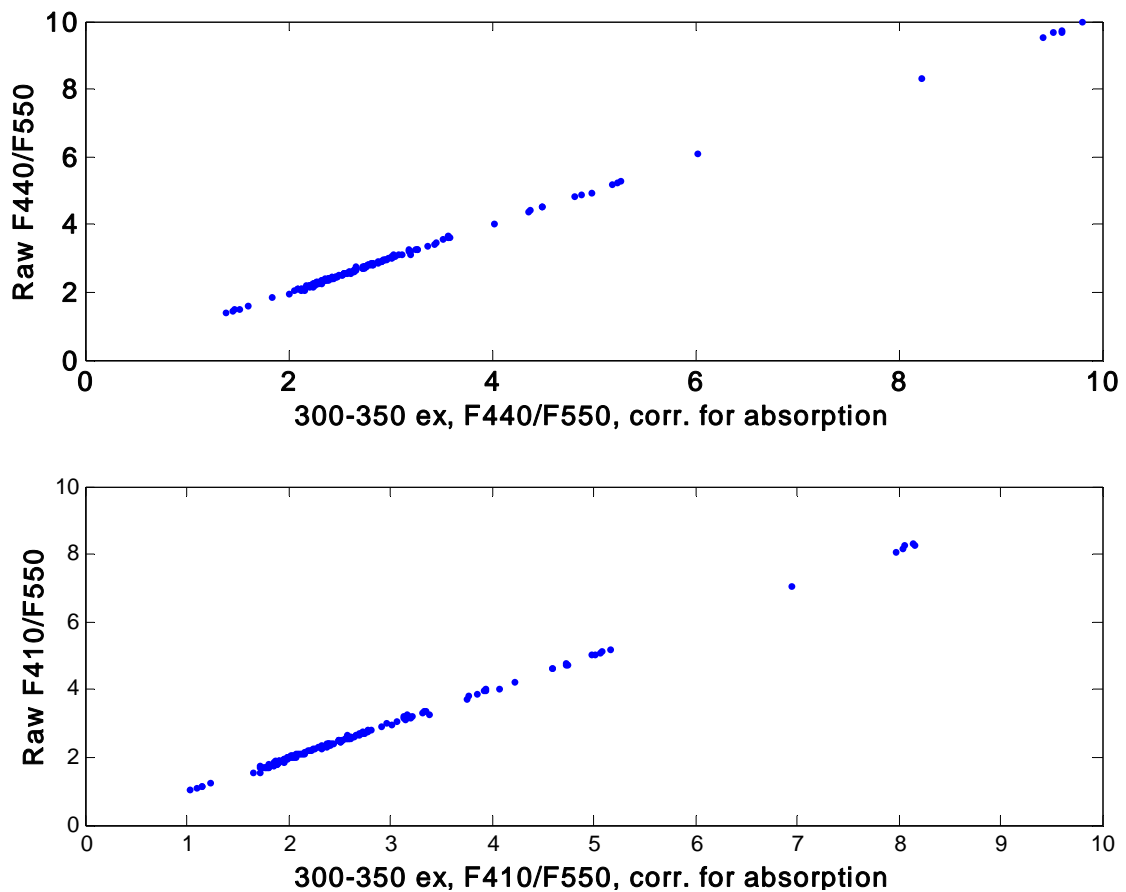


**Figure 31.** Relationship of raw and absorption corrected simple fluorescence ratios for 440/550 and 410/550 emissions. Slopes near unity indicate absorption correction can be neglected for the simple ratio approach.

When absorption corrections are considered explicitly, however, the equation for the adjusted ratio method expands to the following:

$$OB = RF_{440Obs} * CF_{440} - \left( \frac{RF_{440Clean} * CF_{440Clean}}{RF_{550Clean} * CF_{550Clean}} \right) * RF_{550Obs} * CF_{550}$$

With RF = raw fluorescence,  
 CF= ex/em specific absorption correction factor, and  
 ‘Clean’ representing the sample or location where OB is considered to be absent, or where the absorption corrected ratio is at the minimum value.

The non-quantitative, simple ratio method can be approximately applied with no absorption correction. The dual wavelength adjusted ratio method which quantitatively removes CDOM fluorescence contribution from the OB signal retains a dependence on an absorption correction factor and will require at least one absorption determination.

All field methods proposed here neglected the minimal effects of ionic strength (Mobed, et al., 1996). The effects of pH (Mobed, et al., 1996) were also not considered, although the range in pH expected from ambient waters should be captured given the range in ambient and matrix samples evaluated. Effects of temperature were similarly not considered. EEM data were generated at room temperature. While the temperature observed during a field survey may vary, the change is on the order of 0.5% / °C (Patsayeva, et al., 2004) and was considered minimal. Concerns about a temperature effect would be most appropriate for a single wavelength method, as the temperature variation for 440 and 550 nm fluorescence has been shown to be very comparable (Dixon, et al., 2005) and so would affect dual wavelength methods even less.

### *Application of Field Methods to EEM Data*

The following discussion evaluated the success of the various proposed field methods in context of added spikes, and further optimized wavelength selections, querying the EEM data as a surrogate for an additional field study. Lamp spectra (**Figure 32**) were approximated from manufacturer images (Turner Designs, Inc., <http://www.turnerdesigns.com/kb/kb.asp?a=show&ID=106>, Lamp 10-049, and [http://www.msscscientific.de/deuterium\\_lamps.htm](http://www.msscscientific.de/deuterium_lamps.htm)), using either digitized data or modified Gaussian functions. Lamp intensities were both arbitrarily normalized to a relative maximum intensity of 1.0. Cutoff filters (if proposed) were assumed to have a 100% transmission in the passed wavelength region. The band pass of emission filters was similarly taken to be a modified Gaussian function with 80% maximum transmittance, a maximum bandwidth of 20nm, and a bandwidth at half height of 10nm.

After selection of the wavelength ranges for a proposed field method, synthetic or surrogate field data were prepared. Each EEM fluorescence in the excitation and emission range (boxes in Figure 30, above) was matrix multiplied by the relative lamp excitation spectra and averaged by emission wavelength. The resulting vector was multiplied by the emission filter transmittance, and a final average prepared to represent the reading that would be obtained from a filter fluorometer with the described characteristics. The value of the surrogate field data within the ex/em region was much reduced from the EEM values due to the transmission efficiencies and assumed spectral shape of the emission filters.

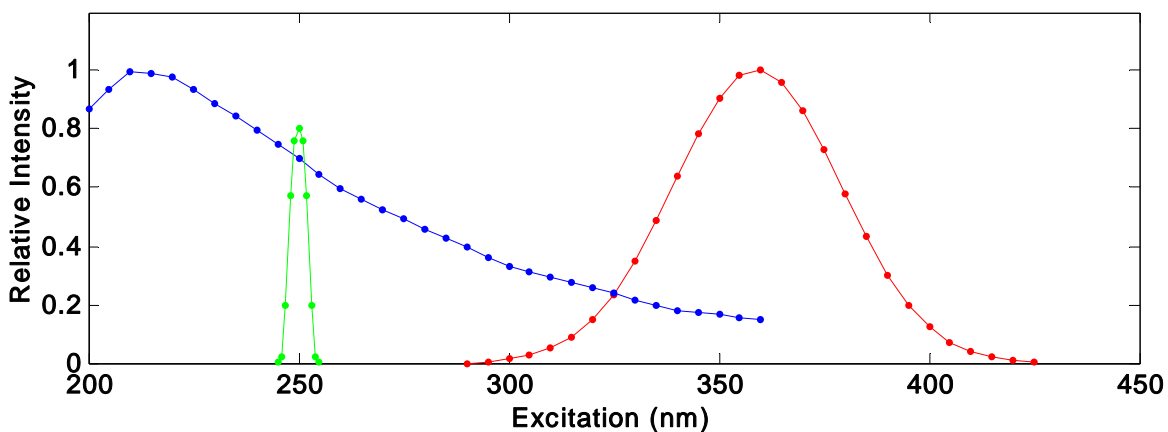


**Figure 32.** Relative intensity of deuterium lamp (blue), mercury vapor lamp (red), and bandpass of an example emission filters at 250 nm (green) used in simulation of field data from EEM data.

The surrogate field data obtained would be proportional to single wavelength pair data from the midpoint of the excitation and emission ranges provided EEM spectra had monotonic slopes in both excitation and emission axes. Where spectra are multimodal or display other strong shape characteristics, the midpoint approximation is not as tenable.

The single wavelength pair method (Method 1), designed to capture the peak identified by PARAFAC factor PF6, was optimized by successive iterations. Absorption corrected results from a 230-240 nm excitation and emission centered at 284 nm resulted in the best correlation between surrogate field fluorescence and PARAFAC modeled PF6 loads for all samples and spikes (**Figure 33**). The slight blue shift from the maximum PF6 emission at 288 nm was apparently more effective at isolating PF6 loads from PF4. Regression results were highly significant ( $r^2=0.9975$ ,  $p<0.001$ ) and the standard error of the estimate was 140. With a 100% OSTDS effluent estimated to be approximately 10,000 PF6 units on average, field detection of the fluorescence peak represented by PF6 loads would be accurate to within 1-2% of typical OSTDS effluent. Surrogate field data were approximately 500 QSRF for 100% of 'typical' OSTDS effluent.

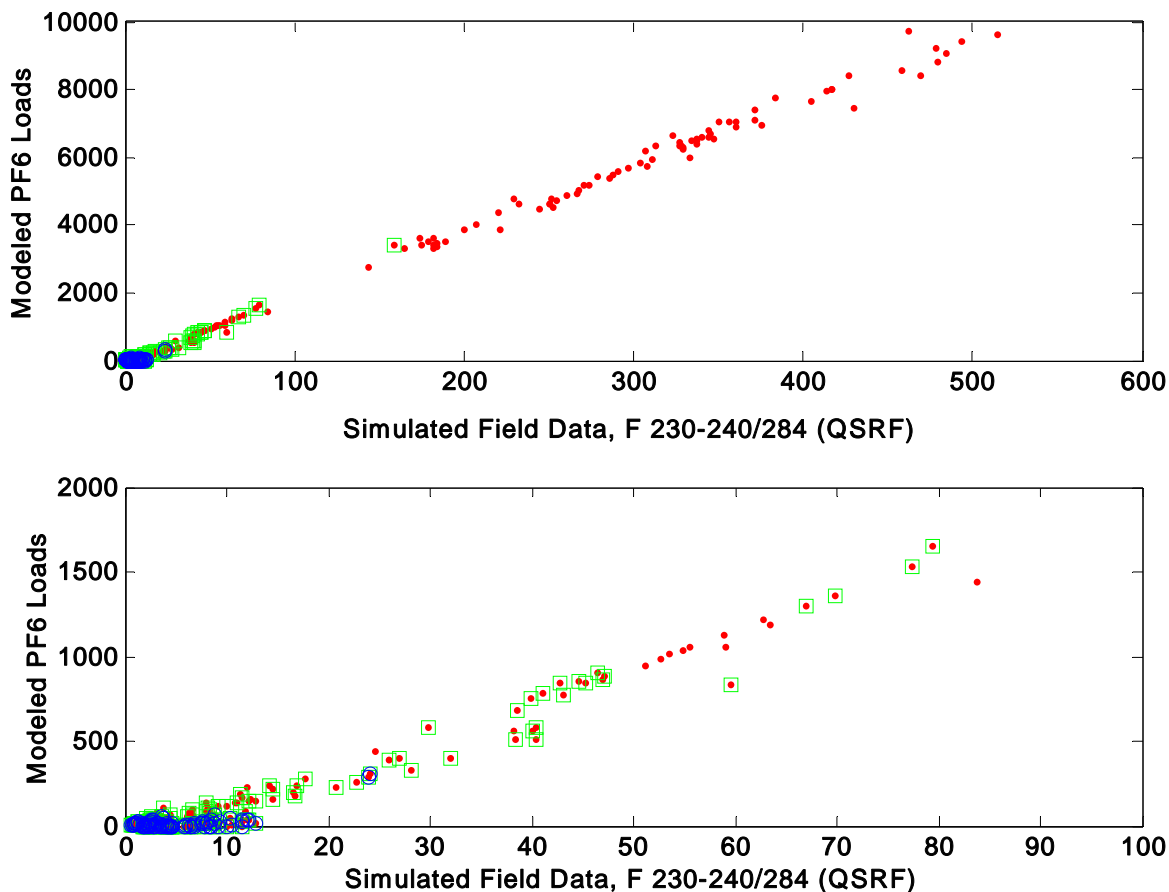


**Figure 33.** PARAFAC modeled PF6 loads as a function of simulated field data with 230-240 nm excitation, and an emission filter centered at 284 nm. Ambient samples (blue open circles); OB sources (green squares); and all samples including spikes (red points). At two different scales.

Spike recoveries of detergents added to ambient, source, and mixture samples (**Figure 34**) were also calculated from the Method 1 surrogate field data, relative to the surrogate detergent fluorescence in deionized water. Recoveries for the single wavelength pair method were very similar to those based on PARAFAC derived PF6 loads (Figure 14, above), and also indicated a depression in spike recoveries due to absorbing particulates during the first project. Detergent I did not contain the UV peak in question and so spike recoveries were not calculated for those spikes.

For the dual wavelength methods (Method 2), the simple ratio was not considered further as it was non-quantitative under varying CDOM conditions. The adjusted ratio dual wavelength method was applied to EEM data in two ways for each of the dual wavelength pairs, 410-550nm and 440-550 nm, to obtain OB quantities. Absorption correction was applied to all data based on a single measured absorption at the lowest wavelength (410 or 440 nm) and a modeled absorption at the higher wavelength (550 nm). The first approach used the lowest ratio of either  $F_{410}/F_{550}$  or  $F_{440}/F_{550}$  from any of the ambient samples to establish a project-wide ‘clean’ ratio. The second approach used the lowest ratio from *each* region (Chassahowitzka, Phillippi Creek, etc.) as a ‘clean’ ratio from which to evaluate all other samples of the region.

In each case, the clean ratio was used to compute the amount of fluorescence at 410 or 440 nm that was due to CDOM based on fluorescence at 550 nm. The first approach would generate only one sample with no OB present, while the second approach would generate at least one sample in each region with no OB present. The first approach may be biased high (computing more OB than actually present) in some regions if the CDOM fluorescence is naturally higher at 410 or 440 nm, i.e varying amounts of PF1 and PF2 in the absence of OB. The second approach may be biased low if the sample from which the clean ratio is selected does indeed contain some amount of OB. Both approaches account appropriately for varying amounts of CDOM (as in Figure 28), but make the assumption that the spectral shape of

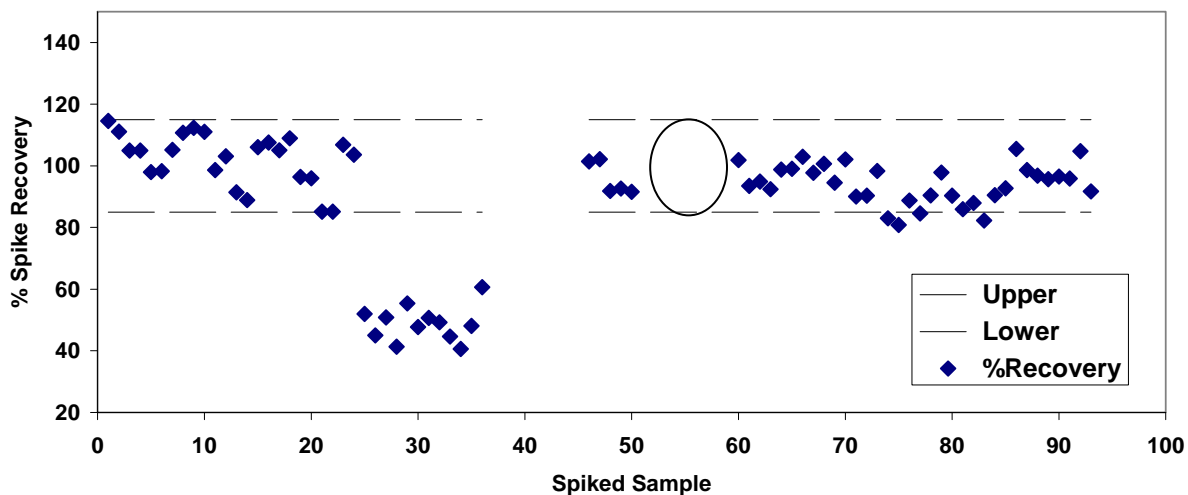


**Figure 34.** Spike recovery from synthesized field data (230-240 / 284 ex/em) relative to fluorescence in deionized water. The UV peak was absent in Detergent I and so no spike recovery was calculated (circled area).

CDOM alone remains constant in proportion (constant  $F_{410}/F_{550}$  or  $F_{440}/F_{550}$ ), even if varying in overall amount or amplitude of fluorescence. Choice of a ratio establishes a somewhat arbitrary baseline against which OB in all samples is quantified. As a result, while the numeric quantity of OB will vary depending on the clean ratio used in calculation, the differences among a group of samples will be similar provided CDOM spectral characteristics remain similar.

To illustrate the removal of the CDOM fluorescence from the 410 or 440 nm readings, the individual surrogate fluorescence values of the 410 and 550 nm dual wavelength methods are illustrated as a function of absorption coefficient (**Figure 35**). As intended, absorption corrected fluorescence at 550 nm (upper panel) was a relatively linear function of absorption although the regional differences noted above were apparent and reflected the regionally variable proportions of different fluorescent materials in the CDOM pool. The relationship between  $F_{550}$  and absorption appeared consistent for both ambient samples and potential OB sources and, more importantly, fluorescence at 550 nm did not increase for spiked samples. In contrast, fluorescence of samples at 410 nm (lower panel) responded to detergent addition, and potential OB sources were generally elevated above the pool of ambient samples. Also as expected, a general relationship of fluorescence at 410 nm with absorption was still apparent.

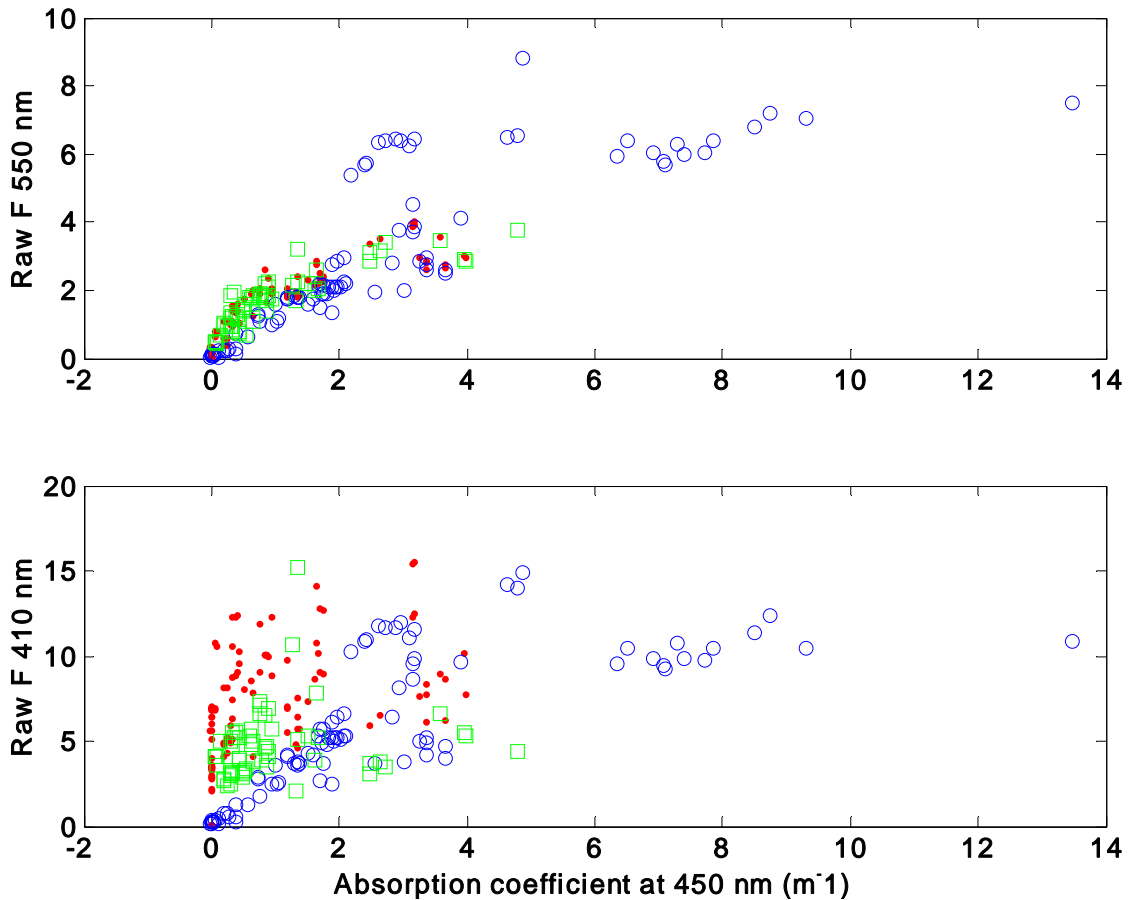


**Figure 35.** Raw fluorescence at 550 and 410 nm as a function of absorption coefficient ( $a_{450}$ ). Ambient samples (blue open circles); OB sources (green squares); and spiked samples (red points)

Values of OB computed by the adjusted ratio dual wavelength method from the absorption corrected surrogate field data (410-550 nm) were also illustrated as a function of measured absorption (**Figure 36**). The lack of correlation, either as a group, or by ambient samples, sources, or detergent additions indicated that the influence of CDOM fluorescence was removed from the computed OB levels. Fluorescent units are in QSRF and a 'typical' 100% OSTDS effluent was expected to have a response of between 7-8 QSRF. Estimates of detection limits for the dual wavelength methods were on the order of 0.1-0.2% of typical OSTDS effluents. While fluorescence amplitude was apparently less sensitive than the PF6 approach above, the fluorescence was in a region where reduced absorption correction, lamp fluctuations, and instrumental noise improved signal to noise and ultimately improved measuring capability. Spike recoveries in ambient, source and mixture samples, relative to detergents in deionized water, using the adjusted ratio dual wavelength method with an overall regional clean value, appear in **Figure 37**. Detergent spike recovery was excellent, with a mean of 99.5% for 410-550 nm and a much reduced sensitivity to absorbing particulates. The method using 440-550 nm emissions was nearly identical in spike

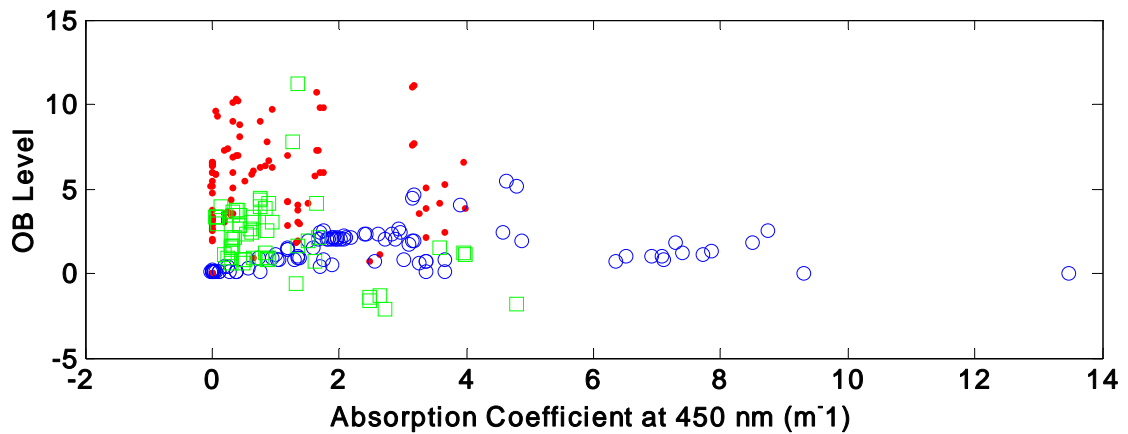


**Figure 36.** OB computed with the adjusted ratio method from 410/550 nm fluorescence as a function of absorption coefficient ( $a_{450}$ ). Ambient samples (blue open circles); OB sources (green squares); and spiked samples (red points).

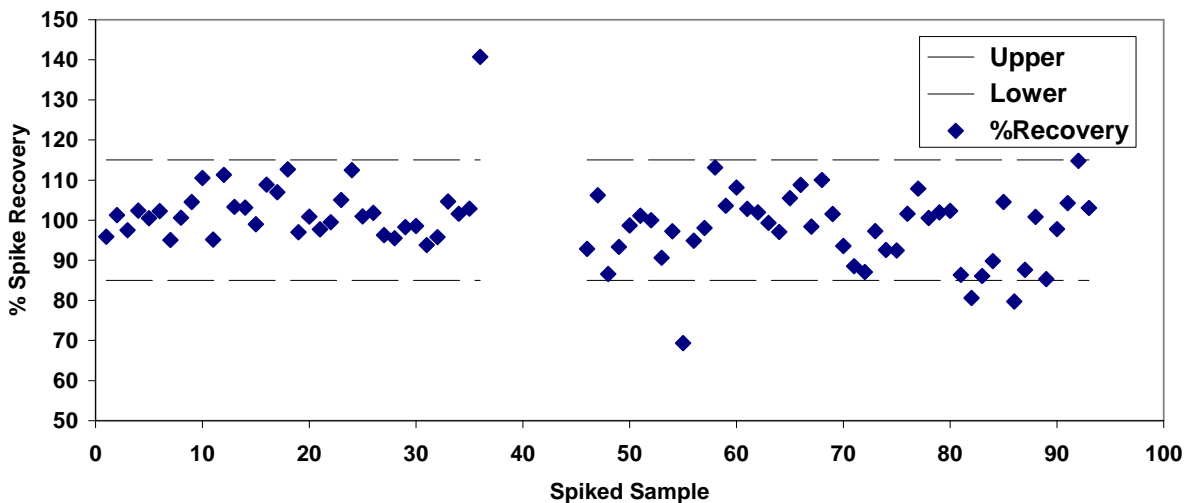


**Figure 37.** Spike recovery from synthesized field data using the adjusted ratio method for 300-350 nm excitation and 410, 550 nm emissions, relative to fluorescence in deionized water.

recovery results (not shown; mean recovery 102.7%). Using regional clean ratios generated similar excellent mean spike recoveries for 410-550 nm and 440-550 nm, 101.1% and 103.8% respectively. Choice between the two dual wavelength methods (410-550nm or 440-550 nm) could be made based on slight reduction in absorption correction at 440 nm or on availability of filters for instrument construction.

For the adjusted ratio methods using either 410-550 nm or 440-550 nm emission, the selection of the clean fluorescence ratio where OB is absent was critical to the numerical output of OB, either in QSRF units or as % typical OSTDS. In the absence of OB, the ratio of  $F_{440}/F_{550}$  was a measure of the spectral shape of CDOM fluorescence. Differing sources, ages, and composition of dissolved organics resulted in a continuum of differing spectral shapes and of  $F_{440}/F_{550}$  ratios. Regional relationships were visible in the spectral shapes, as was also evidenced by the regional relationships of the various PARAFAC factors which displayed a dependence on absorption. Even within a small region, ratios varied widely at the confluence of different waterbodies. In the known presence of OB, the  $F_{440}/F_{550}$  ratio increased due to the peak OB fluorescence at 440 nm. The increased fluorescence in the 440 nm region, however, was superimposed on one of the several CDOM factors (PF2) and there was no unique PARAFAC factor for OB in the visible region. Similarly with the adjusted ratio approach, one could not *a priori* identify an elevated  $F_{440}/F_{550}$  ratio as associated with OB in addition to CDOM, except in extreme cases.

Levels of OB were therefore computed for the adjusted ratio methods using 1) the lowest ratio observed from any ambient sample, or 2) the lowest ratio observed within the geographic region. For the regional calculations, source waters were treated as a group and the lowest of the group used. Otherwise, source waters were referenced to the clean ratios established from all ambient samples. The mean level of computed OB in detergent standards was used to transform results into a percentage of typical OSTDS effluent (Table D.1, Appendix D).

Computed levels of dual wavelength OB, and subsequent estimated %OSTDS effluent varied substantially between regional or overall methods. **Figure 38** illustrates the range in computed %OSTDS for a single region, Area D of Phillippi Creek. The spatial pattern of computed OB is quite consistent between methods, however. For data as a whole, the computed OB of the various dual wavelength methods were linearly correlated with one another, indicating that any of the dual wavelength methods could generate similar results, albeit on different numerical scales. The differences are attributed to the varying baseline established by the choice of the clean ratio.

While the range between the various dual wavelength applications appears large, the highly variable concentration of OB in detergents must be kept in mind. The % typical OSTDS values are based on the mean OB observed in several detergents used in the project. The individual detergents used ranged over three fold in the amount of OB contained, and other detergents not used contained either no OB or OB over 10 times greater than the mean that was used. Use of individual detergent OB amounts to compute % OSTDS would produce results over a similar distribution of that seen for the various dual wavelength methods. It is

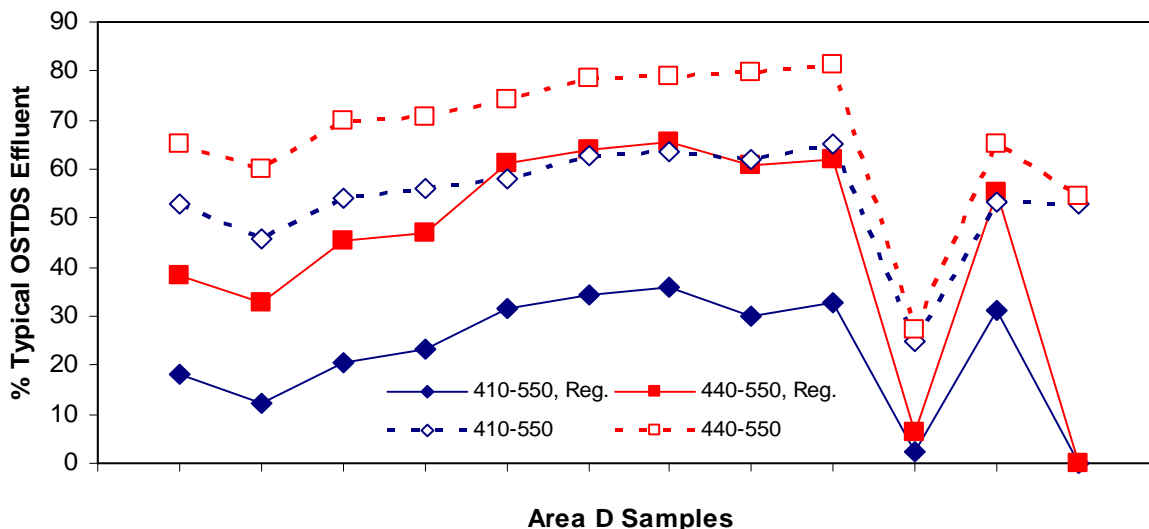


**Figure 38.** Computed OB, as % typical OSTDS effluent, by the various dual wavelength adjusted ratio methods. Samples collected from Area D of Phillippi Creek.

worth restating that due to the varying concentrations of OB in detergents, varying homeowner activities, the varying removal efficiencies of soils, and the varying baselines resulting from the clean ratio selection, that OB detection is not a quantitative loading tool. Instead, OB presence is confirmation that anthropogenic impacts are present, and the spatial distributions observed in semi-quantitative, comparison-based field surveys can provide additional information on source locations.

For all adjusted ratio dual wavelength methods (Method 2), correlation of results with either PF6 loads or results from the 284 nm single wavelength method (Method 1) were not significant. The result was expected, as the OB-UV peak and the visible OB fluorescence in the 400-450 nm range were not uniformly present in all detergents and the two fluorescent regions represent differing classes of compounds. **Figure 39** illustrates the PARAFAC modeled loads of factors PF2 and PF6 in the various detergents tested. (In the case of detergents, with no intrinsic CDOM, PF2 loads are equivalent to OB calculated via the dual wavelength adjusted ratio method.)

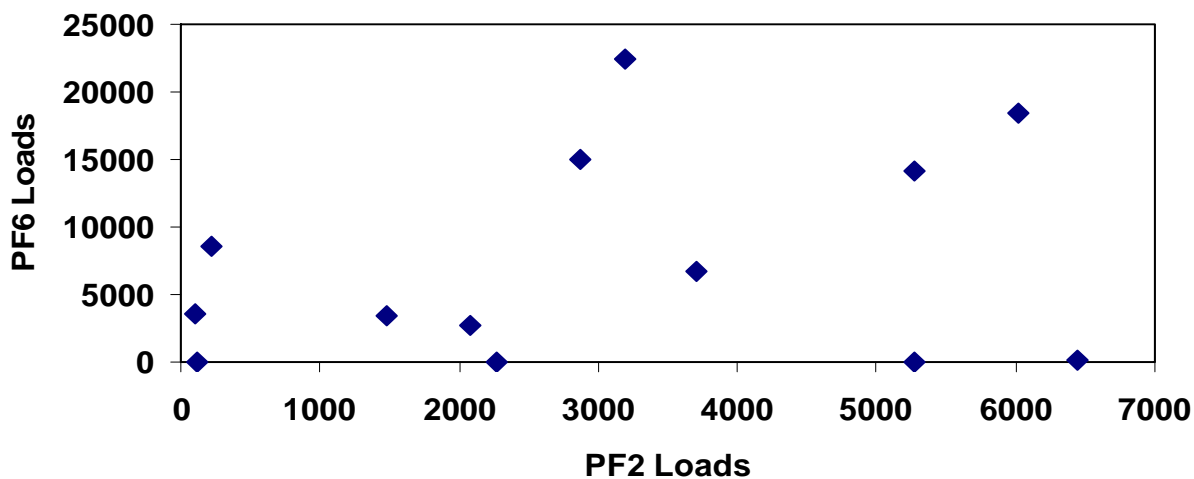


**Figure 39.** Loads of PF6 (OB-UV Peak) and PF2 (visible OB+CDOM) in individual detergents (where CDOM is absent) indicating the variety of manufacturer formulations

### *Remote Sensing Considerations*

Airborne laser induced fluorescence (LIF) techniques have been in use for some time. Excitation sources used in seawater LIF studies include Nd:YAG lasers at 355 nm (Vodacek, et al., 1995), and tunable systems from 320-670 nm (Drozdowska, 2007). A search of laser specifications also indicated tunable systems capable of 220-285 nm output (Sivaprakasam and Killinger, 2003) as well as commonly available discrete outputs at 351, 337, and 308 nm ([www.lexellaser.com](http://www.lexellaser.com)). These wavelengths cover the range of interest determined for the excitation of OB and detergent indicators. Full spectrum detection (400-850 nm; Drozdowska, 2007)) permit post-processing selection of many emission ranges. Multiple emission bands have also been used successfully (Hoge and Swift, 1981). Isolation of sufficient fluorescence signal at 404, 430, and 450 nm (Hoge, et al., 1993), could presumably be expanded to the wavelength ranges identified in the present study.

We have demonstrated the necessity of having accurate absorption coefficients at a minimum of one wavelength in order to produce accurate fluorescence data. Data processing for a number of prior LIF efforts have included the determination of absorption coefficients from the strength of the water raman signal return (Hoge, et al., 1993; Vodacek, et al., 1995; Hoge, 2006), determination of absorption by a time-resolved dual wavelength laser through backscattering (Hoge, 2003; Hoge, 2005), and numerous determinations of CDOM and chlorophyll (Fiorani et al., 2006; Drozdowska, 2007). Multi-wavelength passive remote sensing reflectances have also been used to determine CDOM absorption in a number of empirical band-ratio approaches (Carder, et al., 2003; Mannino, et al., 2008) although the error between algorithm-derived and field validation samples at these low CDOM levels can approach 20-40%.

The LIF work, however, and most passive algorithm development have predominantly been performed in coastal and oceanic settings. Maximum absorption coefficients ( $a_{355}$ ) were on the order of  $1.0 \text{ m}^{-1}$  (Vodacek, et al., 1995) or  $0.1 \text{ m}^{-1}$  for  $a_{400}$  (Carder, et al., 2003). In contrast, the maximum absorption coefficients observed in ambient samples for this project were approximately  $150 \text{ m}^{-1}$  and  $70 \text{ m}^{-1}$  for  $a_{300}$  and  $a_{350}$ , respectively. For the successful use of the water Raman signal to indicate absorption, the Raman peak averaged twice the maximum amplitude of CDOM fluorescence in coastal waters (Hoge, et al., 1993), similar to that observed in samples from spring-fed rivers in this project (**Figure 40**). In most samples from the two projects, however, the Raman of most samples at 355 nm excitation was barely visible (**Figure 41**). Determination of needed absorption coefficients from Raman heights through curve fitting on each side of the Raman region (Hoge, et al., 1993) at 404 nm will be difficult or may require long signal averaging times to reduce noise. Absorption algorithm performance from band ratios of passive reflectance degrade at high CDOM levels (Carder, et al., 2003) and can also be contaminated by bottom reflectance in systems that are not optically deep. Data from hyperspectral sensors can be inverted to determine CDOM absorption, depths, chlorophyll concentrations and other optical properties (Lee, et al., 1998; Lee and Carder, 2004), but the requirements of mounting both a hyperspectral and an LIF instrument package make the combined effort far from inexpensive.

In summary, LIF instrumentation has been used successfully to measure CDOM fluorescence. Lamps and sensors sensitive to the identified excitation and emission

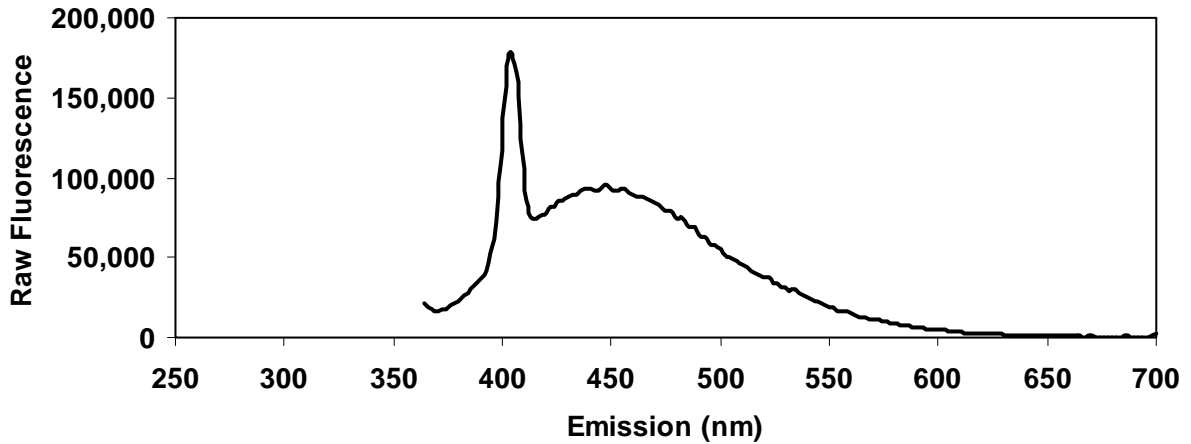


**Figure 40.** Raw fluorescence (355 nm excitation) of a sample with low CDOM. Note water amplitude of Raman signal as a peak at 404 nm.

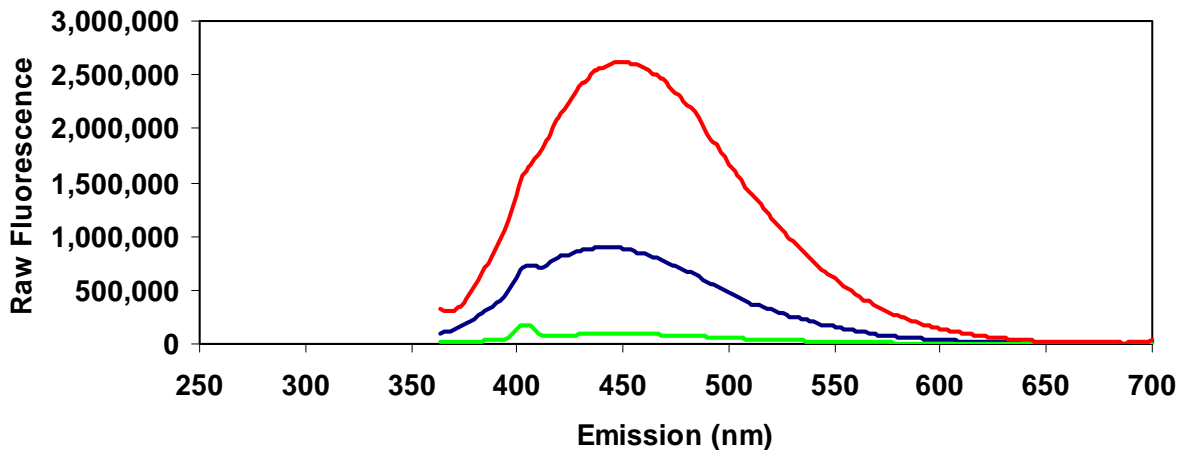


**Figure 41.** Raw fluorescence (355 nm excitation) of samples with low (green), moderate (blue), and high (red) CDOM. Note water Raman signal in all samples as peak or shoulder at 404 nm.

wavelengths are available. Whether ground level or remotely sensed, the separation of CDOM and OB fluorescence would have to be similarly performed via data processing. The accuracy of the absorption coefficient has been shown to be critical for generating accurate fluorescence data. Absorption coefficients have been remotely determined both with fluorescence and with passive reflectance, but in waters that are several orders of magnitude clearer than were observed in our work. The success of remotely determining accurate absorption coefficients by Raman heights appears unlikely. Potential for success using time resolved fluorescence or passive methods are unknown at this time, but could be modeled prior to actual instrument development using radiative transfer models (Hydrolight™). Both Raman and CDOM fluorescence should be explicitly included in the modeling effort, as should bottom reflectance. The existing EEM data base could be readily queried by the developer of a remote sensing platform to validate a planned approach. While others have found oceanic absorption and fluorescence to be linearly related with relatively little spatial differences (Hoge, et al. 1993), our work at much finer spatial scales does indicate regional differences (Figure 26, above) that will require some ground level, site specific calibrations for any remote sensing effort.

## Summary

The ability of fluorescence techniques to detect optical brighteners in the presence of CDOM was investigated by adding or spiking laundry detergents to a wide variety of ambient samples, potential OB sources, and various mixtures. The project was funded by the U.S. EPA through the Florida Department of Health and the Florida Department of Environmental Protection with the intent of developing a field method for the detection of OB as a uniquely anthropogenic indicator of failing OSTDS or other waste discharges. Both laboratory and field methods developed will be semi-quantitative for OSTDS effluent due to the variety of individual OB compounds and the range of concentrations of OB in individual detergents, which together form a highly variable loading source.

Samples likely to be sources of OB were collected from OSTDS, WWTP, and laundries. Ambient samples were collected from 11 distinct geographic regions along the west coast of Florida, and from estuarine to freshwater conditions. The ambient waters experienced a wide range of absorption coefficients, as freshwaters sampled included both spring fed systems and black water rivers high in humic and fulvic acids. Systems also ranged from large surface drainage watersheds to small discrete ditches so that CDOM could be expected to reflect of variety of sources, ages, and degradation states. Samples, prepared mixtures, and spikes were analyzed with EEM fluorescence techniques and were also analyzed for absorption. All measurements were performed under an EPA-approved quality assurance plan. There were instrument-specific limits of linearity for fluorescence and some highly fluorescent samples required dilution. Turbidity of samples did not interfere up to 150 NTU, but some source samples (OSTDS in particular) had turbidities which required centrifugation to reduce particulates. Centrifugation was preferable to dilution to optimize signal to noise ratios.

It was demonstrated that absorption correction of fluorescence data was essential. The correction technique, which employed absorption measurements of filtered samples over the entire wavelength range used for fluorescence, was effective up to 0.65 O.D. or nearly 150  $\text{m}^{-1}$  at 300 nm. Unlike light colored particulates, high levels of darker, absorbing particulates depressed fluorescence such that absorption corrections using CDOM measurements alone were inadequate.

EEM data from ambient samples and detergents were subjected to PARAFAC modeling to isolate the optimum number of fluorophores which could be linearly added to describe the initiating samples. Factors identified would also be used to select a smaller number of optimum wavelengths with which to construct field methods. An eight factor model was confirmed as robust and applied to all data. Based on recovery of spiked samples relative to fluorescence in deionized water, three of the eight factors were identified as associated with detergents or OB. Factor PF2 had a UV excitation and a blue emission, or in the spectral range where OB are reported to fluoresce. The factor, however, displayed a correlation with absorption coefficients indicating a dependence on CDOM, and was also coincident with literature values for CDOM fluorescent peaks. Factor PF8 was also quantitative for detergent recovery, but coincided with literature values for the fluorescence of tryptophan-like compounds. Factor PF6 was a peak with a UV excitation and emission. Although not technically an OB due to the non-visible primary emission wavelengths, the PF6 fluorophore

was quantitative with added detergents and did not coincide with any value of CDOM fluorescence typically reported. PARAFAC modeling, due to the continuum of CDOM sampled, was not successful in identifying a unique OB signal in the visible range, but did identify a useful fluorophore in the UV. The UV peak, due to the spectral shape of CDOM absorption, particularly required absorption correction. Depressed spike recoveries during an initial phase of the study were attributed to absorbing particulates and inadequate absorption correction. There was no reason to expect a correspondence of the UV fluorophore (PF6) and the visible OB element in either samples or in spikes as their presence in detergents exhibited a wide range and varied independently.

The loadings of factor PF6 in all samples was computed and converted to an approximate % of a typical OSTDS effluent, although the individual detergents tested exhibited at least a range of 7X in PF6 concentrations, if present at all. The model-based PF6 loads were considered to be the true value when evaluating the success of the proposed field method which targeted the UV peak. Using the spectral shape of PARAFAC factor PF6 and other identified factors, wavelengths were proposed to reproduce the PARAFAC PF6 results. Proposed wavelength ranges, lamp spectra, and typical emission filter transmission characteristics were applied to the EEM data to create surrogate field data to evaluate the proposed method. Needed absorption corrections at excitation and emission wavelengths were based on a single measurement made at excitation midpoints, with emission absorption modeled from an exponential relationship. At least one measurement of absorption was required as the relationship of fluorescence with absorption did not permit absorption corrections to be estimated from fluorescence alone. Instrument design that measured total absorption with a reflective path would reduce dependence on absorbing particulates and extend the utility of a field instrument.

A single measurement of fluorescence from 230-240 nm excitation and centered at 284 nm emission recreated the levels of PF6 with high correlation. Spike recoveries were also good, again with the exception of the samples high in absorbing particulates. Ability to recreate PARAFAC modeled PF6 loads was estimated to be on the order of 1-2% of typical OSTDS concentrations. While present in almost all detergents tested, the PF6 fluorophore is not an optical brightener, per se, and has not been identified in other environmental studies of water and wastes, although it was observed without comment in work by Westerhoff, et al. (2001). Some additional work is warranted to identify the class of compounds that PF6 represents and to determine parameters such as absorption to soils and sediments, degradation rates, and photobleaching susceptibility.

The interference of CDOM fluorescence with that of OB in the visible range has been previously addressed by the use of a dual wavelength method. Ratios of fluorescence in a region with both OB and CDOM fluorescence, relative to another region where CDOM alone fluoresces, were used to indicate the presence of OB. The technique can be quantitative provided CDOM fluorescence remains unchanged both in amplitude and in spectral shape (as in a lake or similar stable water body), but was demonstrated to be non-linear for gradients of CDOM. A dual wavelength adjusted ratio method was proposed in which OB was computed from fluorescence in the combined OB and CDOM region after subtracting the fluorescence that would be due to CDOM alone. Wavelength pairs selected for analysis included the 440

and 550nm used previously for the simple ratio approach and also 410 and 550 nm based on regions of minimal overlap observed in PARAFAC factors. Excitation ranges were selected to minimize Rayleigh or Raman signals in the resulting data.

Spike recovery of both adjusted ratio methods was excellent, and equivalent results were generated by both sets of wavelengths used. Sensitivity to absorbing particulates was much reduced. The methods were quantitative for OB under varying amplitudes of CDOM fluorescence, but were still based on the underlying CDOM absorption retaining a fixed spectral shape. The spectral shape of bulk CDOM fluorescence, however, can alter with source or age as proportions of humics and fulvics change or more labile compounds are photobleached and degraded. Additionally, the spectral shape of CDOM used to estimate the CDOM component of all samples is ideally determined from a sample with no OB present. Selecting the lowest ratio of a survey is an attempt to ensure this condition.

The approximate levels of OB were computed using both regionally specific minimum ratios and a minimum of all ambient samples to investigate the sensitivity of the method to the ratio selected to represent the absence of OB. Although slopes differed from unity, the OB computed using either overall or regional minimum ratios were all linearly related and indicated that comparable assessments of OB could be performed using any of the ratios or wavelength pairs, although computed concentrations or scale would vary. Given the variable nature of OB loading in OSTDS effluents to begin with, a semi-quantitative, comparative approach was likely more helpful than registering results to a typical OSTDS effluent. The adjusted ratio methods would be the most powerful in a relatively small geographic region, where the age and spectral shape of fluorescing CDOM could be assumed to be relatively constant even if varying in concentration. Caution should be used at the confluence of water masses where this assumption is less tenable.

Transference of the proposed methods to a remote sensing platform benefit from the existence of lasers and instruments operating in the identified wavelength ranges. Remote laser induced fluorescence, however, retains a dependence on absorption correction for accurate assessments, just as the field methods here proposed. While absorption coefficients have been determined remotely, the extreme absorption of the high CDOM waters addressed here may not allow similar determinations due to interfering CDOM fluorescence. Regional relationships between fluorescence and absorption may provide an acceptable approximation but will require some degree of surface truthing. The EEM data set forms a valuable resource to evaluate various remote sensing approaches as has been done here for proposed field instrumentation.

## Literature Cited

Anastasiou, C. 2007. Optical brightener detection for tracking wastewater contributions to coastal, estuarine, and freshwater Systems: Task 2 Summary Report. Florida Department of Environmental Protection, Watershed Management Program, Tampa, FL .

Andersen, C., and R. Bro. 2003. Practical aspects of PARAFAC modeling of fluorescence excitation-emission data. *Journal of Chemometrics*, 17:200-215.

Baker A., D. Ward, S. Lieten, R. Periera, E. Simpson, and M. Slater. 2004. Measurement of protein-like fluorescence in river and waste water using a handheld spectrophotometer. *Water Research*, 38(12):2934-2938.

Baker, A. 2002a. Fluorescence excitation - emission matrix characterization of river waters impacted by a tissue mill effluent. *Environmental Science & Technology*, 36(7):1377-1382.

Baker, A. 2002b. Fluorescence properties of some farm wastes: implications for water quality monitoring. *Water Research*, 36(1):189-195.

Baker, A. 2002c. Spectrophotometric discrimination of river dissolved organic matter. *Hydrological Processes*, 16(16):3203-3213.

Baker, A., and R. Inverarity. 2004. Protein-like fluorescence intensity as a possible tool for determining river water quality. *Hydrological Processes*, 18(15):2927-2945.

Baker, A., D. Ward, S. Lieten, R. Periera, E. Simpson, and M. Slater. 2004. Measurement of protein-like fluorescence in river nad waste water using a handheld spectrophotometer. *Water Research* 38:2934-2938.

Bricaud, A., and D. Stramski. 1990. Spectral absorption coefficients of living phytoplankton and nonalgal biogenous matter: A comparison between the Peru upwelling and the Sargasso Sea. *Limnology and oceanography* 35:562-582.

Carder, K.L., F.R. Chen, Z. Lee, S.K. Hawes, and J.P. Cannizzaro, 2003. MODIS Ocean Science Team Algorithm Theoretical Basis Document ATBD 19, Case 2 Chlorophyll a, Version 7, 30 January 2003. College of Marine Science, University of South Florida, St. Petersburg, Florida.

Cleveland, J., and A. Wiedemann. 1993. Quantifying absorption by aquatic particles: A multiple scattering correction for glass-fiber filters. *Limnology and Oceanography* 38(6): 1321-1327.

Coble, P. 1996. Characterization of marine and terrestrial DOM in seawater using excitation-emission matrix spectroscopy. *Marine Chemistry*, 51(4):325-346.

de Souza Sierra M., O. Donard, and M. Lamotte. 1997. Spectral identification and behaviour of dissolved organic fluorescent materials during estuarine mixing processes. *Marine Chemistry*, 58(1-2):51-58.

Coble, P. C. del Castillo, and B. Avril. 1998. Distribution and optical properties of CDOM In the Arabian Sea during the 1995 southwest monsoon. *Deep-Sea Research Part2*-45:2195-2223.

Dixon, L., and P. Julian. 2005. Phillippi Creek Optical Brightener Investigation for Sarasota County Water Resources. Mote Marine Laboratory Technical Report # 1038. Sarasota, FL.

Dixon, L., H. Taylor, E. Staugler, and J. Scudera. 2005. Development of a fluorescent method to detect optical brighteners in the presence of varying concentrations of fluorescent humic substances: Identifying regions influenced by OSTDS in the estuarine waters of Charlotte Harbor. Mote Marine Laboratory Technical Report # 1045. Sarasota, FL.

Drozdowska, V. 2007. Seasonal and spatial variability of surface seawater fluorescence properties in the Baltic and Nordic Seas: results of lidar experiments. *Oceanologia*, 49(1):59-69.

FDEP. 2006. Quality assurance project plan for assessment of remote sensing techniques using optical brighteners for identifying wastewater contributions to coastal, estuarine, and freshwater systems. Prepared for the EPA-Gulf of Mexico Program and the Florida Department of Health. FDEP, Tampa, FL.

FDEP. 2008. Revision to Quality Assurance Plan: Project description and schedule for the assessment of remote sensing techniques using optical brighteners for identifying wastewater contributions to coastal, estuarine, and freshwater systems. Anastasiou, C.J. Ed. Temple Terrace, FL

Fiorani, L., R. Fantoni, L. Lazzara, I. Nardello, I. Okladnikov, and A. Palucci. 2006. Lidar calibration of satellite sensed CDOM in the Southern Ocean. *EARSeL eProceedings* 5:89-99.

Gauthier, T., E. Shane, W. Guerin, W. Seitz, and C. Grant. 1986. Fluorescence quenching method for determining equilibrium constants for polycyclic aromatic hydrocarbons binding to dissolved humic materials. *Environmental Science & Technology* 20:1162-1166.

Hagedorn, F., M. Saluta, A. Hassall, and J. Dickerson. 2005. Fluorometric detection of optical brighteners as an indicator of human sources of water pollution. Part I. Description and detection of optical brighteners. *Crop and Soil Environmental News*. Virginia Cooperative Extension.

Hoge, F. 2003. Validation of satellite-retrieved oceanic inherent optical properties: proposed two-color elastic backscatter lidar and retrieval theory. *Applied Optics*, 42(36):7197-7201.

Hoge, F. 2005. Oceanic inherent optical properties: proposed single laser lidar and retrieval theory. *Applied Optics*, 44(34):7483-7486.

Hoge, F. 2006. Back attenuation coefficient retrieval by inversion of airborne lidar-induced chromophoric dissolved organic matter fluorescence. *Applied Optics* 45(10):2344-2351.

Hoge, F., A. Vodacek, and N. Blough. 1993. Inherent optical properties of the ocean: Retrieval of the absorption coefficient of chromophoric dissolved organic matter from fluorescent measurements. *Limnology and Oceanography*, 38(7):1394-1402.

Hoge, F., and R. Swift. 1981. Airborne simultaneous spectroscopic detection of laser induced water Raman backscatter and fluorescence from chlorophyll a and other naturally occurring pigments. *Applied Optics*, 20:3197-3205.

Jerlov, N. 1976. *Marine Optics*. Elsevier, New York, NY.

Jiji, R. and K. Booksh. 2000. Mitigation of Rayleigh and Raman Spectral Interferences in Multiway Calibration of Excitation-Emission Matrix Fluorescence Spectra. *Analytical Chemistry*, 72:718-725.

Komada, T., O. Schofield, and C. Reimers. 2002. Fluorescence characteristics of organic matter released from coastal sediments during resuspension. *Marine Chemistry*, 79(2):81-97.

Lakowitz, J. 1983. *Principles of fluorescence spectroscopy*. Plenum Press, New York, N.Y.

Lee, Z.P., K. Carder, C.D. Mobley, R. Steward, and J. Patch. 1998. Hyperspectral remote sensing for shallow waters. 1. a semi-analytical model. *Applied Optics*, 37, 6329-6338.

Lee, Z.P., and K.L. Carder. 2004. Absorption spectrum of phytoplankton pigments derived from hyperspectral remote-sensing reflectance. *Remote Sensing of the Environment* 89(3):361-368.

MacDonald, B., S. Levin, and H. Patterson. 1997. Correction of fluorescence inner filter effects and the partitioning of pyrene to dissolved organic carbon. *Analytical Chimica Acta*, 338:155-162.

Mannino, A., M.E. Russ, and S.B. Hooker. 2008. Algorithm development and validation for satellite-derived distributions of DOC and CDOM in the U.S. Middle Atlantic Bight. *Journal of Geophysical Research* 113, C07051.

Mayer, L., L. Schick, T. Loder. 1999. Dissolved protein fluorescence in two Maine estuaries. *Marine Chemistry*, 64(3):171-179.

McKnight, D., E. Boyer, P. Westerhoff, P. Doran, T. Kulbe, and D. Andersen. 2001. Spectrofluorometric characterization of dissolved organic matter for indication of precursor organic material and aromaticity. *Limnology Oceanography*, 46(1) 38-48.

Mobed, J., S. Hemmingsen, J. Autry, and L. McGown. 1996. Fluorescence characterization of IHSS humic substances: total luminescence spectra with absorbance correction. *Environmental Science & Technology*, 30(10):3061-3065.

Mopper, K. and C. Schultz. 1993. Fluorescence as a possible tool for studying the nature and water column distribution of DOC components. *Marine Chemistry*, 41:229-238.

Mueller, James L., Giulietta S. Fargion and Charles R. McClain, Editors. S. Pegau, J. Ronald, V. Zaneveld, B. Mitchell, J. Mueller, M. Kahru, J. Wieland, and M. Stramska., 2003. *Ocean Optics Protocols For Satellite Ocean Color Sensor Validation, Revision 4, Volume IV: Inherent Optical Properties: Instruments, Characterization, Field Measurements and Data Analysis Protocols*. National Aeronautical and Space Administration NASA/TM-2003-211621/Rev4-Vol.IV

Ohno, T., and R. Bro. 2006. Dissolved organic matter characterization using multiway spectral decomposition of fluorescence landscapes. *Soil Science Society of America Journal*, 70:2028-2037.

Patsayeva, S., R. Reuter, and D. Thomas. 2004. Fluorescence of dissolved organic matter in seawater at low temperatures and during iceformation. *EARSel eProceedings* 3(2):227-238.

Puchalski, M., M. Morra, and R. von Wandruszka. 1991. *Fresenius Journal and Analytical Chemistry*, 340:341-344.

Senesi, N., T. Miano, M. Provenzano, and G. Brunetti. 1991. Characterization, differentiation and classification of humic substances by fluorescence spectroscopy. *Soil Science*, 152(4):259-271.

Sivaprakasam, V., and D. Killinger. 2003. Tuneable ultraviolet laser-induces fluorescence detection of trace plastics and dissolved organic compounds in water.

Stedmon, C., and S. Markager. 2005. Resolving the variability in dissolved organic matter fluorescence in a temperate estuary and its catchment using PARAFAC analysis. *Limnology and Oceanography*, 50(2):686-697.

Stedmon, C., S. Markager, and R. Bro. 2003. Tracing dissolved organic matter in aquatic environments using a new approach to fluorescence spectroscopy. *Marine Chemistry*, 82(3-4):239-254.

Stoll, J., M. Ulrich, and W. Giger. 1998. Dynamic behavior of fluorescent whitening agents in Greifensee: Field measurements combined with mathematical modeling of sedimentation and photolysis. *Environmental Science & Technology*, 32:1875-1881.

Tucker, S., V. Amszi, and W. Acree, Jr. 1992. Primary and secondary inner filtering. *Journal of Chemical Education*, 69(1):A8-A12.

Twardowski, M., E. Boss, J. Sullivan, and P. Donaghay. 2004. Modeling the spectral shape of absorption by chromophoric dissolved organic matter. *Marine Chemistry*, 89:69-88.

U.S. Environmental Protection Agency. 2002. Onsite Wastewater Treatment Systems Manual, EPA/625/R-00/008. Office of Water, Office of Research and Development.

Vodacek, A., F. Hoge, R. Swift, J. Yungel, E. Peltzer, and N. Blough. 1995. The use of in situ and airborne fluorescence measurements to determine UV absorption coefficients and DOC concentrations in surface waters. *Limnology Oceanography*, 40(2):411-415.

Westerhoff, P., W. Chen, and M. Esparza. 2001. Fluorescence analysis of a standard fulvic acid and tertiary treated wastewater. *Journal of Environmental Quality*, 30(6):2037-2046.

Yamashita, Y., and E. Tanoue. 2003. Chemical characterization of protein-like fluorophores in DOM in relation to aromatic amino acids. *Marine Chemistry*, 82(3-4):255-271.

Yentsch, C. 1962. Measurement of visible light absorption by particulate matter in the ocean. *Limnology and Oceanography* 7:207-217.